

**NUMERICAL SIMULATION OF BLOOD
FLOW THROUGH TORTUOUS AND
STENOTIC CORONARY ARTERIES
USING MULTIPHASE APPROACH**

Thesis

Submitted in partial fulfillment of the requirements for the Degree of

DOCTOR OF PHILOSOPHY

By

ABDULRAJAK BURADI



**DEPARTMENT OF MECHANICAL ENGINEERING
NATIONAL INSTITUTE OF TECHNOLOGY KARNATAKA,
SURATHKAL, MANGALORE -575025**

SEPTEMBER, 2019

DECLARATION

I hereby declare that the Research Thesis entitled “**NUMERICAL SIMULATION OF BLOOD FLOW THROUGH TORTUOUS AND STENOTIC CORONARY ARTERIES USING MULTIPHASE APPROACH**” which is being submitted to the **National Institute of Technology Karnataka, Surathkal** in partial fulfillment of the requirements for the award of the Degree of **Doctor of Philosophy in Mechanical Engineering** is a *bonafide report of the research work carried out by me*. The material contained in this Research Thesis has not been submitted to any other Universities or Institutes for the award of any degree.

Register Number: **145019ME14F01**

Name of the Research Scholar: **ABDULRAJAK BURADI**

Signature of the Research Scholar:

Department of Mechanical Engineering

Place: NITK, Surathkal

Date:

C E R T I F I C A T E

This is to certify that the Research Thesis entitled “**NUMERICAL SIMULATION OF BLOOD FLOW THROUGH TORTUOUS AND STENOTIC CORONARY ARTERIES USING MULTIPHASE APPROACH**” submitted by **Mr. ABDULRAJAK BURADI (Register Number: 145019ME14F01)** as the record of the research work carried out by him, *is accepted as the Research Thesis submission* in partial fulfillment of the requirements for the award of the Degree of **Doctor of Philosophy.**

R e s e a r c h G u i d e (s)

Dr. Arun M.

Associate Professor

Department of Mechanical Engineering

National Institute of Technology Karnataka, Surathkal

:

Chairman-DRPC

Date:

ACKNOWLEDGEMENTS

With a deep sense of gratitude, I wish to express my sincere thanks to my supervisor **Dr. Arun M.**, Associate Professor, Department of Mechanical Engineering, National Institute of Technology Karnataka (N.I.T.K), Surathkal, for his excellent guidance and support throughout my research work. I received very useful, encouraging and excellent academic feedback from him, which has helped me in coming up with this thesis. His constant encouragement, help and review of the entire work during the course of the investigation were invaluable. I profoundly thank them.

I take this opportunity to thank **Dr. Shrikantha S. Rao**, Professor and Head, Department of Mechanical Engineering for his continuous and timely suggestions.

I wish to thank all the members of the Research Program Assessment Committee members, **Dr. Anish S.**, Assistant Professor, Department of Mechanical Engineering and **Dr. Vishwanath K. P.**, Assistant Professor, Department of Mathematical and Computational Sciences for their appreciation and valuable suggestions for this research work.

I wish to express my sincere gratitude to all the faculty members of the Department of Mechanical Engineering, N.I.T.K Surathkal for their help, encouragement and support all through this research work.

I wish to express my sincere gratitude to **Prof. M. B. Patil**, Senior Grade Lecturer, Department of Electronics & Communication Engineering, Government Polytechnic, Kalaburagi, and their family members for their continuous support, help, encouragement, motivation, and timely suggestions for this all success.

My sincere thanks to all my lab mates Abdul Raouf Tajik, Srinivas Rao, Tippeswamy L R, Anil Kadam, Venkatesh Lamani, Parashuram Bedar, Parashuram Chitragar, Sreebash Kutty, Girish Kini, Udhav Gawandalkar, Shrijeeth BK, Suhas BG, Harsha Kumar, Prashantha B, Deepak Kumar Kolke, G. Narendran, Madagonda Biradar, Nuthan Prasad, Vashista, Vishweshwara P S, Srivathsa T, Praveen T R, Shashikumar

CM, Banjara Kotresha, Tabish Wahidi, Sreevatsa T, Ashok Kumar K, Shankar Kodate, Kiran Kumar D, Sumant Morab, Isaac Rajan, Varun Kalkur, Srinivasa N, for their help and support to carry out this dissertation work.

I am indebted to my batch mates Bala Narasimha G, Gorantla Kirankumar, Shaik Sharmas Vali, Jagadish C, Jayavardhana ML, Kevin Amith Mathias, Mahantayya Mathapati, Mallikarjuna, Praveen Shenoy, Susheel Kumar N, Vasu M, Veeresh Nayak, Vipin Allien, Mohammed Sohail Bakshi, Ajmal T. S, Mohammed Khalifa, Prakash Pawar, Bheemappa Halavar, Chetan Srinidhi and my MTech project supervisors Dr V.V. Katti and Dr B.M. Angadi for their constant help and encouragement during the entire research work.

Finally, and most importantly I would like to thank my parents, relatives and my family members who have trusted me throughout my life. I would like to share this moment of happiness with my wife Sabiha Bhanu, brothers Ameen and Altaf, and sisters Parveen Bhanu and Afreen Bhanu for their love, motivation, patience, sacrifices and constant encouragement all the time. I will be forever indebted to the courage, understanding and dedicated support shown by my wife Sabiha Banu and my father and mother in law.

Abdulrajak Buradi

*Dedicated to My Beloved Parents, Relatives and
Teachers*

*Without Their Support This Would Not Have
Been Possible*

ABSTRACT

The cardiovascular pathologies such as atherosclerosis and thrombosis are vascular diseases involving fluid-dynamical, mechanical, and biological factors. In past few years, the study of numerical blood flow dynamic studies within anatomically complex arteries has garnered great interest among cardiologists, clinicians and biomedical engineers. The evolution in computational fluid dynamics (CFD) and high computing performance have helped us to identify the probable arterial regions for the presence of cardiovascular diseases (CVDs) and to understand and predict how this disease may develop. The presence of tortuosity and stenosis in coronary artery (CA) disturbs the local wall shear stress (WSS) which is considered as an influential hemodynamic descriptor (HD) for the growth of atherosclerotic sites. Different WSS based HDs have been formulated over the years to understand the hemodynamic flow conditions as predictors of endothelial wall dysfunction which is precursor for all CVDs. In general, these HDs have been numerically determined using ‘single phase’ approach. In single phase approach, the flow-dependent cell transport and their interactions with the carrier fluid are generally ignored by considering blood as a single phase fluid.

In the present work, numerical investigation of two phase blood flow through stenotic and tortuous left coronary arteries (LCAs) was performed using Eulerian multiphase mixture theory model for the modeling of blood flow in multiphase mixture model, plasma is modeled as continuous liquid phase and Red Blood Cells (RBCs) as the dispersed phase. The model of interest is first validated and the results of multiphase and single phase modeling of blood were compared with experiment results in order to evaluate the performance of multiphase mixture model for blood flow. The multiphase mixture theory approach performed better than single phase approach and showed good agreement with the experimental results. With the confidence gained, the mixture theory multiphase approach is then used for pulsatile blood flow simulations through four idealized CA geometries having varying degrees of stenosis (DOS) severities viz., 30, 50, 70, and 85% diameter reduction stenosis and through several tortuous artery models by varying three morphological indices namely,

curvature radius (CR), distance between two bends (DBB) and the angle of bend (AoB). The geometric models of both stenosed and tortuous idealized LCAs were designed in the commercial program SolidWorks and the CFD simulations were carried out with the use of commercial program Ansys Fluent (V14.5).

The aim of this study was to understand the effect of stenosis and tortuosity in coronary artery hemodynamics. This interaction between artery geometry and flow is examined in two ways; initially by investigating the influence of stenosis severity and tortuosity parameters on various WSS based hemodynamic descriptors and then on RBC concentration. In addition, a detailed hemodynamic study was performed to determine the influence of the stenosis severity and tortuosity on flow and vice versa.

In large blood vessels (millimeter to centimeter size) such as in coronary and carotid arteries, the RBCs shear induced migration affects the transport of oxygen to the arterial endothelial cells (ECs). Hence, in this work we also investigated the locations where hydrodynamic diffusion of RBCs occurs and the effects of stenosis severity on shear induced diffusion (SID) of RBCs, concentration distribution and WSS. For the first time, multiphase mixture theory approach along with modified Phillips shear-induced diffusive flux model and coupled with Quemada non-Newtonian viscosity model has been applied to numerically simulate the RBCs macroscopic behavior in four different degrees of stenosis (DOS) geometries viz. 30, 50, 70, and 85%. The capability to describe the blood flow through a stenosed and tortuous artery for varying degrees of stenosis (DOS) severity and tortuosity morphological indices combined with imaging modalities provides the medical practitioners the ability to diagnose the severity of disease with high accuracy in its early stages and the opportunity of treatment before the ailment becomes fatal.

Keywords: Multiphase blood flow; Stenosis; Wall shear stress; Coronary artery; Oscillatory shear index; Atherosclerosis; Red blood cell; Shear-induced diffusion.

CONTENTS

DECLARATION	
CERTIFICATE	
ACKNOWLEDGEMENTS	
ABSTRACT	
LIST OF CONTENTS	i
LIST OF FIGURES	v
LIST OF TABLES	ix
NOMENCLATURE	xi
ABBREVIATIONS	xv
1 INTRODUCTION	1
1.1 INTRODUCTION	1
1.2 HEMODYNAMICS OF ARTERIAL STENOSIS	3
1.3 OUTLINE OF THE THESIS	6
2 LITERATURE REVIEW	9
2.1 INTRODUCTION	9
2.2 BLOOD AND ITS COMPOSITION	10
2.3 BLOOD VISCOSITY	12
2.4 COMPUTATIONAL NON-NEWTONIAN RHEOLOGICAL MODELS IN BLOOD FLOW STUDY	13
2.5 MULTIPHASE NATURE OF BLOOD	16
2.6 INHOMOGENEITY OF BLOOD CELLS IN BLOOD VESSELS	17
2.7 MODELING OF MULTIPHASE BLOOD FLOW	18
2.8 HEMODYNAMIC DESCRIPTORS BASED ON WALL SHEAR STRESS AND THE DEVELOPMENT OF ATHEROSCLEROSIS	19
2.8.1 Steady or Instantaneous WSS	19
2.8.2 Time-Averaged WSS (TAWSS)	20

2.8.3	WSS Gradient (WSSG)	21
2.8.4	Oscillatory Shear Index (OSI)	22
2.8.5	Relative Residence Time (RRT)	24
2.9	SHEAR INDUCED MIGRATION	26
2.10	SHEAR INDUCED MIGRATION OF RBCs	28
2.11	SUMMARY OF LITERATURE	29
2.12	MOTIVATION	29
2.13	OBJECTIVES OF THE PRESENT STUDY	30
3	EFFECT OF STENOSIS SEVERITY ON WALL SHEAR STRESS BASED HEMODYNAMIC DESCRIPTORS USING MULTIPHASE MIXTURE THEORY	33
3.1	INTRODUCTION	33
3.2	MATERIALS AND METHODS	35
3.2.1	Geometry Representation and Computational Mesh Generation	35
3.2.2	Multiphase Blood Flow Model	37
3.2.2.1	<i>Continuity Equation</i>	37
3.2.2.2	<i>Momentum Equation</i>	38
3.2.2.3	<i>Slip and Drift Velocity</i>	38
3.2.2.4	<i>Constitutive Model</i>	40
3.2.3	Boundary Conditions	42
3.2.4	Numerical Scheme	43
3.2.5	WSS Based Hemodynamic Descriptors	44
3.2.5.1	Time-Averaged Wall Shear Stress (TAWSS)	44
3.2.5.2	<i>Time-Averaged Wall Shear Stress Gradient (TAWSSG)</i>	45
3.2.5.3	<i>Oscillatory Shear Index (OSI)</i>	45
3.2.6	Model Validation	45
3.2.6.1	<i>Blood Flow and Velocity Distribution Study</i>	45

3.2.7	Model Verification	47
3.2.7.1	<i>Grid Independence Study</i>	47
3.3	RESULTS	48
3.3.1	Distribution of WSS and WSS Based HDs	48
3.3.1.1	<i>WSS Distributions in Stenosed Arteries</i>	49
3.3.1.2	<i>TAWSS Distributions in Stenosed Arteries</i>	50
3.3.1.3	<i>TAWSSG Distributions in Stenosed Arteries</i>	51
3.3.1.4	<i>OSI Distributions in Stenosed Arteries</i>	51
3.4	DISCUSSIONS	52
3.4.1	Limitations of the Study	55
3.5	SUMMARY	56
4	IMPACT OF CORONARY TORTUOSITY ON THE ARTERY HEMODYNAMICS	57
4.1	INTRODUCTION	57
4.2	MATERIALS AND METHODS	59
4.2.1	Geometric Model of the Idealized Tortuous Coronary Artery	59
4.2.2	Governing Equations	60
4.2.3	Computational Modelling	60
4.2.3.1	<i>Computational Mesh Generation and Mesh Independence Study</i>	60
4.2.3.2	<i>Boundary Conditions</i>	62
4.2.3.3	<i>Computational Fluid Dynamics Simulation Settings</i>	63
4.2.4	WSS Based Hemodynamic Descriptors	63
4.2.5	Multiphase Eulerian and Mixture Theory Models	64
4.3	RESULTS	66
4.3.1	Effect of CR on HDs	66
4.3.2	Effect of DBB on HDs	76

4.3.3	Effect of AoB on HDs	86
4.4	DISCUSSION	87
4.4.1	Limitations of the Study	88
4.5	SUMMARY	89
5	EFFECT OF STENOSIS SEVERITY ON SHEAR INDUCED DIFFUSION OF RED BLOOD CELLS IN CORONARY ARTERIES	91
5.1	INTRODUCTION	91
5.2	MATERIALS AND METHODS	93
5.2.1	Governing Equations	93
5.2.1.1	<i>Convection – Diffusion Equation for RBCs</i>	94
5.2.2	Numerical Methodology	95
5.2.3	Model Validation	96
5.3	SIMULATION OF SID OF RBCs IN AXISYMMETRIC STENOSED CORONARY ARTERIES	99
5.3.1	Problem Description and Computational Mesh	99
5.3.2	Boundary Conditions	100
5.4	RESULTS AND DISCUSSIONS	101
5.4.1	Velocity Distribution	101
5.4.2	Particle Concentration Distribution	104
5.4.3	WSS Distribution	107
5.5	SUMMARY	109
6	SUMMARY, CONCLUSIONS AND FUTURE SCOPE	113
6.1	SUMMARY	113
6.2	CONCLUSIONS	114
6.3	SCOPE OF FUTURE WORK	115
	REFERENCES	117
	LIST OF PUBLICATIONS BASED ON PHD RESEARCH WORK	143
	BIODATA	145

LIST OF FIGURES

Figure No.	Description	Page No.
Figure 1.1	Atherosclerotic plaque formation and its development in the endothelium (Loscalzo et al. 2003)	1
Figure 1.2	Hemodynamics of Arterial Stenosis	4
Figure 2.1	Artery with cellular components	10
Figure 2.2	Blood Viscosity and Shear Rate	13
Figure 2.3	Two solid spheres interaction in a simple shear flow, before interaction (a) and after interaction (b) (Leighton and Acrivos 1987a)	26
Figure 2.4	A Suspension microscopic flow behaviour depend on the dynamics at micro structure level (Krishnan 2010)	27
Figure 3.1	Ideal stenosed vessel geometry with dimensions showing the boundary conditions and region of interest where four different stenosis geometries are simulated to demonstrate hemodynamic variations	36
Figure 3.2	Idealized stenosis vessel geometries for different DOS severity, a). 30%, b). 50%, c). 70%, and d). 85% stenosis	36
Figure 3.3	Computational grid. (a) 3-D computational grid for idealized CA with 50% diameter reduction stenosis, (b) Zoomed view of inlet grid presenting the prism layer to capture the flow near wall	36
Figure 3.4	Inlet pulsatile coronary velocity profile for blood (plasma and RBC) along the time of the cardiac cycle (Berne and Levy, 1967). End of diastole (0.275s), reversed flow in early systole (0.30s), local maximum systole (0.4s), local minimum systole (0.5s), and maximum flow at beginning of diastole (0.55s)	43

Figure 3.5	Micro-channel rectangular flow system, with 100 μm depth in z-direction (Patrick et al. 2011)	46
Figure 3.6	Comparison of present numerical (Single phase and Multiphase) and experimental results (Patrick et al. 2011) of RBC velocity distribution along stream-wise direction (x) as a function of the wall distance (y) at the depths $z = 8 \mu\text{m}$ and $z = 16 \mu\text{m}$	46
Figure 3.7	Axial velocity profiles measured at distances 1D and 2D, before the stenosis region for different grid elements	48
Figure 3.8	WSS distributions in idealized CA for different DOS severity models for one cardiac cycle at 0.55s	49
Figure 3.9	TAWSS distributions in idealized CA for different DOS severity models averaged over one pulsatile cycle	50
Figure 3.10	TAWSSG distributions in idealized CA for different DOS severity models over one cardiac cycle.	51
Figure 3.11	OSI distributions in idealized CA for different DOS severity models and averaged over one pulsatile cycle	52
Figure 4.1	Geometry of the tortuous CA. (a) Idealized tortuous artery model with three different morphological indices: the CR, the AoB, and the DBB. (b) Artery model with 150° AoB, 6mm CR and 3 mm DBB showing the different boundary conditions and region of interest	60
Figure 4.2	Computational mesh model with prism layers to capture flow effects near the wall	61
Figure 4.3	In-flow velocity profile for blood (plasma and RBC) during one pulsatile cycle (Berne and Levy 1967)	62
Figure 4.4	Figure 4.4 Rectangular micro-channel flow system, with depth 100 μm in z-direction (Patrick et al. 2011)	64
Figure 4.5	RBC velocity distribution comparison between present multiphase Eulerian, multiphase mixture model and	65

	experimental (Patrick et al. 2011) results along x-direction as a function of the wall distance (y) at $Z=8 \mu\text{m}$ and $16 \mu\text{m}$ depth	
Figure 4.6	Spatial distributions of the velocity contours obtained at maximum flow rate ($t=0.55\text{s}$) for different CRs and AoBs with constant DBB= 0 mm	70
Figure 4.7	Spatial distributions of the TAWSS contours for different CRs and AoBs with constant DBB= 0 mm	71
Figure 4.8	Spatial distributions of the TAWSSG contours for different CRs and AoBs with constant DBB= 0 mm	72
Figure 4.9	Spatial distributions of the OSI contours for different CRs and AoBs with constant DBB= 0 mm	73
Figure 4.10	Spatial distributions of the RRT contours for different CRs and AoBs with constant DBB= 0 mm	75
Figure 4.11	Spatial distributions of the ECAP contours for different CRs and AoBs with constant DBB= 0 mm	76
Figure 4.12	Spatial distributions of the velocity contours obtained at maximum flow rate ($t=0.55\text{s}$) for different DBBs and AoBs with constant CR=6 mm	79
Figure 4.13	Spatial distributions of the TAWSS contours for different DBBs and AoBs with constant CR= 6 mm	81
Figure 4.14	Spatial distributions of the TAWSSG contours for different DBBs and AoBs with constant CR= 6 mm	82
Figure 4.15	Spatial distributions of the OSI contours for different DBBs and AoBs with constant CR= 6 mm	83
Figure 4.16	Spatial distributions of the RRT contours for different DBBs and AoBs with constant CR= 6 mm	85
Figure 4.17	Spatial distributions of the ECAP contours for different DBBs and AoBs with constant CR= 6 mm	86
Figure 5.1	Velocity profiles for (a) 30% average particle VF, (b) 40% average particle VF, (c) corresponding particle concentration	98

	profile for 30% average particle VF and (d) 40% average particle VF	
Figure 5.2	The geometry of ideal stenosed artery with dimensions showing the boundary conditions and region of interest	99
Figure 5.3	Idealized stenosis coronary artery models having different DOS severities	100
Figure 5.4	Computational grid: (a) 3-D computational grid for an idealized artery with 50% diameter reduction stenosis. (b) Cross section grid presenting the prism layers to acquire the flow near the wall	100
Figure 5.5	Inlet pulsatile coronary velocity profile for blood (plasma and RBC) during a single cardiac cycle (Berne and Levy 1967)	101
Figure 5.6	Comparison of lateral velocity profiles at different axial positions with and without consideration of SID of RBCs for 70% DOS (a) $Z/L=-1D$, (b) $Z/L=0D$, (c) $Z/L=1D$, and (d) $Z/L=2D$	102
Figure 5.7	Effect of DOS severity on velocity profiles at different axial positions (a) $Z/L=-1D$, (b) $Z/L=0D$, (c) $Z/L=1D$, and (d) $Z/L=2D$ in the lateral direction	103
Figure 5.8	RBC VF contour maps at the midplane for different DOS severities obtained at maximum blood flow	104
Figure 5.9	Comparison of the RBCs VF profiles at different axial positions (a) $Z/L=-1D$, (b) $Z/L=0D$, (c) $Z/L=1D$, and (d) $Z/L=2D$ for different DOS	106
Figure 5.10	Wall shear stress contour for different DOS severities obtained at maximum blood flow at the beginning of diastole ($t=0.55s$)	107
Figure 5.11	Average WSS (WSS_{avg}) versus time for one cardiac cycle with and without SID model, (a) 30%, (b) 50%, (c) 70% and (d) 85% DOS	108

LIST OF TABLES

Table No.	Description	Page No.
Table 2.1	Composition of blood and its cells dimension (Caro 1978)	11
Table 2.2	Properties of RBC and Plasma at 37 ⁰ C (Bronzino 1999, Burton 1965, Caro et al. 1978)	11
Table 3.1	Maximum peak velocity and percentage error between single phase and multiphase model compared to experimental data at the depths $z = 8 \mu\text{m}$ and $z = 16 \mu\text{m}$	47
Table 3.2	Maximum WSS and WSS based HDs and their % increase for different DOS severities	54
Table 3.3	Average WSS and WSS based HDs and their % increase for different DOS severities	54
Table 4.1	Number of mesh elements and grid independence study results	61
Table 4.2	Comparison of peak velocity and percentage error between present multiphase Eulerian, mixture models and experimental (Patrick et al. 2011) data along at $Z=8 \mu\text{m}$ and $16 \mu\text{m}$ depth	66
Table 4.3	The maximum WSS based HDs for different CRs and AoBs (DBB= 0 mm)	67
Table 4.4	Average variation of WSS based HDs for different CRs and AoBs (DBB= 0 mm)	68
Table 4.5	The maximum HDs for different DBBs and AoBs (CR= 6 mm)	77
Table 4.6	Average HDs for different DBBs and AoBs (CR= 6 mm)	77
Table 4.7	The maximum HDs for different AoBs (DBB= 6 mm and CR= 6 mm)	87
Table 5.1	Simulation parameters considered for validation	97

NOMENCLATURE

Symbols	Description
a	Radius of particle
u	Fluid velocity
y	Spatial coordinate of the fluid position
C	Empirical constant in rheological models of blood
h	Power law model empirical constant
N_c	Particle flux due to particle interaction frequency
N_μ	Particle flux due to spatially varying viscosity
R_e	Reynolds number
W_o	Womersley number
U_0	Average inlet velocity
T	Time period of one cardiac cycle
k_∞ and k_0	Semi-empirical intrinsic viscosities in Quemada model
x and r	Axial and radial coordinates
R and D	Radius and diameter of the geometry
\vec{v}_m	Mass-averaged velocity
d_{rbc}	Diameter of RBC
C_D	Coefficient of discharge
n	Number of phases
\vec{F}	Body force
d_p	Diameter of particle
\vec{a}	Acceleration of secondary phase particles
$\vec{v}_{dr,k}$	Secondary phase drift velocity
\vec{v}_p	Secondary phase velocity
\vec{v}_q	Primary phase velocity
\vec{v}_{pq}	Slip velocity or relative velocity

c_k	Mass fraction of any phase
f_d	Drag force
u_{plasma}	Plasma velocity
u_{rbc}	RBCs velocity
c_{rbc}	Phases momentum exchange coefficient
\vec{v}	Velocity vector
τ_p	Particle relaxation time
ε_{rbc}	RBCs volume fraction
Re'_p	Reynolds number of particle
$\dot{\underline{\gamma}}$	Strain rate tensor
$\underline{\underline{\tau}}$	Viscous stress tensor
$\nabla\vec{v}$	Velocity gradient tensor
Π	Second invariant of a stress tensor
μ_m	Mixture viscosity
μ	Fluid dynamic viscosity or blood viscosity
τ_w	Wall shear stress
ρ	Suspended fluid density
Γ	Shear induced diffusion coefficient
$\dot{\gamma}_{nl}$	Non-local shear rate
ϕ_{max}	Particles maximum packing volume fraction
μ_{eff}	Effective viscosity of the power law model
μ_∞	Infinite or asymptotic viscosity at high shear rate
μ_0	Zero viscosity at low shear rate
$\dot{\gamma}$	Shear rate
τ_y	Yield stress
ϕ	Volume concentration of particle
μ_F	Suspending fluid viscosity

$\dot{\gamma}_c$	Critical shear rate
μ_{eff}	Effective viscosity of the power law model
μ_∞	Infinite or asymptotic viscosity at high shear rate
ρ_m	Mixture density
ε_k	Hematocrit or volume fraction of phase k

ABBREVIATIONS

2D	Two dimensional
3D	Three dimensional
AoB	Angle of bend
BAECs	Bovine aortic endothelial cells
BS1	Bend section 1
BS2	Bend section 2
CA	Coronary artery
CAD	Coronary artery disease
CFD	Computational fluid dynamics
CHD	Coronary heart disease
CR	Curvature radius
CT	Computed tomography
CT	Coronary tortuosity
CVD	Cardiovascular diseases
CVS	Cardiovascular system
DBB	Distance between bends
DFM	Diffusive flux model
DI	Diagnostic indicators
DOS	Degrees of stenosis
EC	Endothelial cells
ECAP	Endothelial cell activation potential
eNOS	Endothelial nitric oxide synthase
FVM	Finite volume method

HD	Hemodynamic descriptor
HUVECs	Human umbilical vein ECs
IBM	Immersed boundary method
IH	Intimal hyperplasia
IVUS	Intravascular ultrasound
LAD	Left anterior descending artery
LBM	Lattice Boltzmann method
LCA	Left coronary artery
LDL	Low density lipoprotein
MRI	Magnetic resonance imaging
NO	Nitric oxide
OSI	Oscillatory shear index
PDE	Partial differential equation
PRESTO	Pressure staggering option
RBC	Red blood cells
RCA	Right coronary artery
RRT	Relative residence time
SCAD	Spontaneous coronary artery dissection
SI	Shear induced
SID	Shear induced diffusion
SIM	Shear induced migration
SMCs	Smooth muscle cells
SWSSG	Spatial wall shear stress gradient
TAWSS	Time-averaged wall shear stress
TAWSSG	Time averaged wall shear stress gradient

TWSSG	Temporal wall shear stress gradient
UDF	User-defined function
VF	Volume fraction
WBC	White blood cells
WHO	World health organisation
WSS	Wall shear stress
WSSG	Wall shear stress gradient

CHAPTER 1

INTRODUCTION

1.1 INTRODUCTION

One of the leading causes of death in all the developed and developing countries is cardiovascular diseases (CVD). According to the world health organisation, an estimated 17.9 million people died from CVD in 2016 which represents 31% of all global deaths (WHO 2016). Atherosclerosis is a common form of CVD which involves the accumulation of fats on the inner layer of the arterial wall. This accumulation of fat grows in the areas of disease and is called plaque or atherosclerotic plaque. The atherogenesis is the beginning of atheromatous plaque formation inside the arterial walls and starts with the vascular endothelium dysfunction. The early stages that precede the formation of atherosclerotic plaque and its development that take place in the endothelium are represented in Fig 1.1.

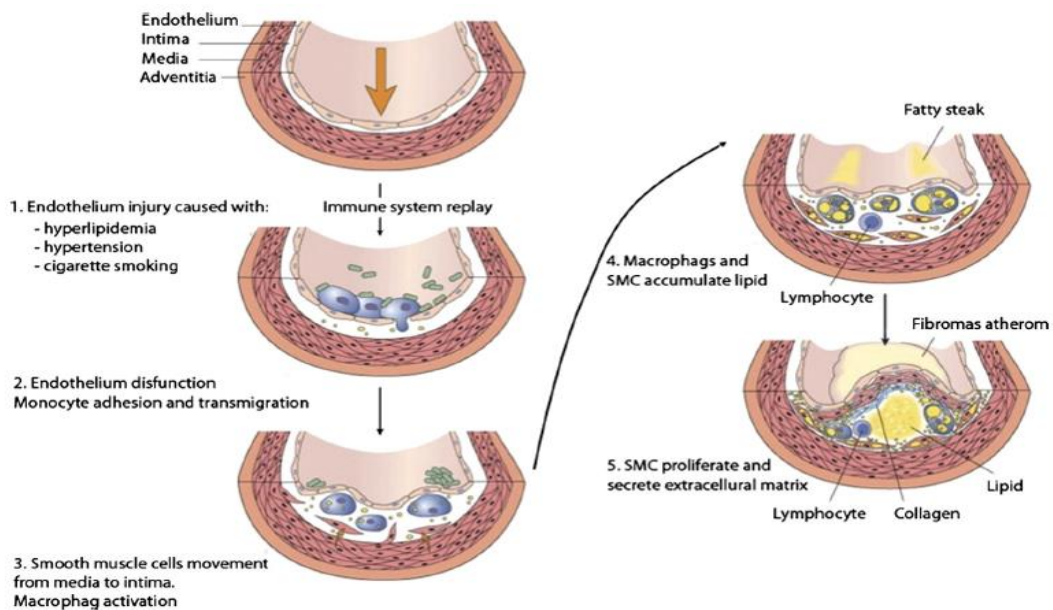


Figure 1.1 Atherosclerotic plaque formation and its development in the endothelium
(Loscalzo et al. 2003)

The branches and junction points are more prone to endothelial cells (ECs) injury (Ross and Glomset 1976). As the plaque increases, the arterial wall loses its elasticity and the wall inner layer thickens which narrows down the lumen size. These atherosclerotic plaques are generally present in sites where complex flow patterns can be expected such as recirculation zones, inner curvatures, bends, junctions and bifurcations.

The narrowed condition of the artery due to the accumulation of fats at the inner layer of wall is known as local stenosis, and generally is not detected until a clot forms or blood flow is restricted severely. Consequently, a build-up of atherosclerotic plaque in coronary arteries (CAs) which supply oxygenated blood to the muscles of the heart may further develop into coronary artery disease (CAD) or coronary heart disease (CHD).

For cardiologists, the diagnosis of local stenosis and its severity in CA has long been a challenging task. Also, the mechanisms and biological processes leading to local stenosis are not understood fully yet. In current clinical settings, to treat the CA stenosis many diagnostic methods have been adapted effectively. In order to evaluate the functional significance of the local stenosis, many diagnostic practices have been developed from fluid dynamic principles. Computational fluid dynamics (CFD) is an emerging area useful in the diagnostic management of the cardiovascular (or circulatory) system (CVS).

In fluid mechanics many researchers have widely investigated the flow behavior associated with vascular diseases and suggested several relationships between growth of plaque and wall shear stress (WSS) in the arterial wall. WSS is the tangential stress produced by flowing blood on the vessel wall and other hemodynamic parameter such as shear rate play a key role in the development and progression of atherosclerosis and other arterial diseases.

The low WSS, reversed flow, flow recirculation zones and stagnation point have been identified as key hemodynamic elements responsible for the development of atherosclerosis and thrombosis. In large arteries, the distribution of WSS is believed

to be one key factor in the development of atherosclerosis, however it is difficult to measure WSS parameter experimentally. Both low and high WSS areas have been projected as being dangerous and proposed as preferential sites for atherosclerosis development. The observed relationship between WSS and the regions where atherosclerosis develops has been a key motivation in the current research on arterial blood flow. The speedy changes in WSS are more likely to be observed in places where the arteries are branched and curved, or near any sudden changes in the artery geometry or in the flow direction.

In the present study, the influence of anatomical factors such as tortuosity, stenosis severity, angle of bend (AoB), curvature radius (CR), and distance between two bends (DBB) of an artery on the physiological significance of the CA blood flow were analyzed using CFD technique by considering blood as multiphase fluid. The blood flow behavior in the downstream and upstream regions of stenosis and curvatures has been studied by modelling blood flow using through different axi-symmetrical stenosis and tortuosity CA geometries.

1.2 HEMODYNAMICS OF ARTERIAL STENOSIS

In arteries, the stenosis is formed as a result of the accumulation of fatty substances (lipids). This accumulation of lipids eventually lessens the cross-sectional area of lumen and hinders the incoming upstream blood flow. In the downstream of the stenosis, a moderate to severe flow disturbances can occur depending upon the severity of the stenosis and the upstream blood flow conditions. In arteries the presence of stenosis alters the movement of blood or hemodynamics. Consider an artery with 70% decrease in its area as shown in Fig 1.2. The area of artery where the lumen diameter is minimum is known as the throat. Downstream of the throat is known as diverging section of the artery and upstream of the throat is known as converging section of the artery.

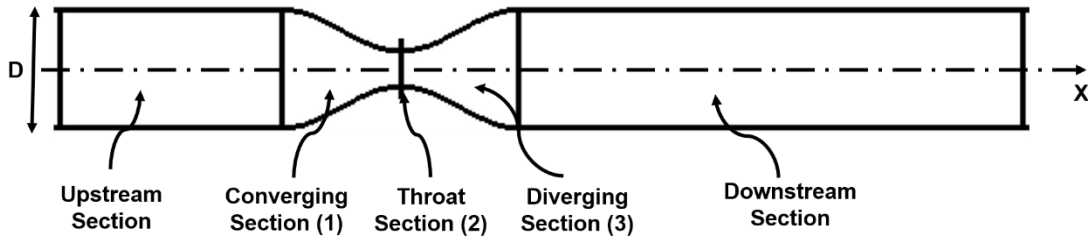


Figure 1.2 Hemodynamics of Arterial Stenosis

In CVS, the WSS is known as the tangential force emanating from the resistance of the blood flowing on the endothelial cells (ECs) surface of the vessel wall. The shear stress mainly depends on the blood viscosity and the spatial gradient of the blood velocity from the artery wall. It is defined as:

$$\tau(y) = \mu \frac{\partial u}{\partial y} \quad (1.1)$$

where μ is the fluid dynamic viscosity, u is the fluid velocity at a height y and y is the spatial coordinate of the fluid position.

The WSS is an important fluid dynamics parameter in the mapping of atherosclerosis. There are two challenging mechanisms that have been found accountable for the atherosclerosis: the shear-dependent mass transport mechanism suggested by Caro et al. (1971) and high WSS suggested by Fry (1968). The hypothesis of shear-dependent mass transport is based on accumulation of lipids in the arterial wall and the mass transport of necessary biological substances (Caro et al. 1971). In the high WSS theory, it is hypothesized that elevated values of this stress can cause direct potential damage to the EC layer and thus initiating atherosclerosis (Fry 1968). In a healthy human artery, it is very necessary to maintain proper diffusion of necessary biological substances between the blood and arterial wall, and vice versa (Caro et al. 1971). Caro et al. suggested that the shear rate near the wall of the artery is the one that influences this mass transport process greatly (Caro et al. 1971). Accumulation of lipids in the faster-moving fluid is carried away with it, but it is not so for the slower-moving fluid. On the contrary, mass transport of the necessary biological substances between the blood and arterial wall is disturbed for the slower-velocity fluid, and consequently,

a higher accumulation of lipid concentration is found to exist near the vessel wall in the low WSS region. Thus the region is susceptible to atherosclerosis as a result of increased particle residence time of the accumulation of lipid. Moreover, the effect of atherosclerosis is endorsed in the region of low WSS or high oscillatory WSS owing to the atherogenic blood particles reported in these regions, and therefore, these regions are more susceptible to atherosclerosis over time.

Several researches have correlated WSS quantities to endovascular diseases such as atherosclerosis, aneurysm, thrombosis and stenosis formation. Variations in shear stress; especially oscillating and low shear stress and the zones of flow reversal, play a greater role on endothelium dysfunction. The continuous exposure of vascular endothelium to shear stresses and shear forces in the normal value range stimulates ECs to release vasoactive substances (Papaioannou and Stefanadis 2005). In vascular system, the arteries are generally adapting to a long-term decreases and increases in WSS to maintain the normal functioning of the vascular system. That is, in the presence of increased WSS, the arteries attempt to reestablish a normal WSS by dilating and subsequently remodeling to a larger diameter and in the presence of decreased WSS, arteries are attempt to thickening of the intimal layer or remodeling to a smaller diameter (Ku 1997). If local disturbed flow patterns persist, such as zones of low WSS then an uncontrolled and excessive intimal thickening response may occur (Ku et al. 1985).

The steady laminar WSS in laminar blood flow pattern promotes the release of factors (Nitric oxide (NO)) from ECs that impede migration of white blood cells (WBCs), smooth muscle cells (SMCs) proliferation, and blood coagulation while simultaneously promoting survival of EC (Traub and Berk 1998). On the contrary, if the flow tends to depart from a laminar pattern then low and oscillating shear stresses will occur at that particular site and it will favor the opposite effects. Consequently, it will contribute to the development of atherosclerosis.

Considering all the above stated localization occurrences and biological indications to account the significance of study of hemodynamics, and hemodynamic descriptors (HDs) in specific becomes more obvious. Investigating the CAs hemodynamics is

important to envisage the CAD in advance by studying the WSS patterns and it can be also employed as a corresponding approach of treatment to areas of lesions with higher risk (Stone et al. 2003b, Stone et al. 2012, Rikhtegar et al. 2012). Hence, it is of great significance to investigate the hemodynamics of stenotic and tortuous CAs to investigate the importance of WSS, WSS based HDs and its part on prognosis of clinical results such as thrombosis and restenosis.

1.3 OUTLINE OF THE THESIS

The present numerical study is focused on the effect of stenosis severity and coronary tortuosity morphological indices on the flow field and on the different HDs of WSS in stenotic and tortuous CAs. Also, the study focuses on the effect of stenosis severity on shear induced diffusion of red blood cells (RBCs) in stenotic CAs. In this thesis there are totally six chapters. The brief of summary of each chapter is discussed below.

Chapter 1 provides the basic introduction to the blood flow and an overview of the atherosclerosis disease process. It also explains in brief about cardiovascular biomechanics, importance of hemodynamics in arterial stenosis and WSS hypothesis linking various WSS based HDs to clinical pathology.

Chapter 2 provides the state of art of literature reviews on blood flow and its composition, blood viscosity, computational non-Newtonian rheological models in blood flow study, multiphase nature of blood flow, inhomogeneity of blood cells in blood vessels, cellular distribution and atherosclerosis, RBCs and its effects, modelling of multiphase blood flow, wall shear stress based HDs that are related to the development of atherosclerosis, and shear induced migration of RBCs.

Chapter 3 explains the use of numerical multiphase mixture theory approach to model and study the effect of stenosis severity on WSS based hemodynamics descriptors. In this chapter four degrees of stenosis (DOS) severities namely 30%, 50%, 70% and 85% diameter reduction idealized artery models were considered. The effect of these stenosis severities on artery blood flow behavior and different WSS based hemodynamic parameters were presented.

Chapter 4 presents the use of multiphase mixture theory model to study the impact of coronary tortuosity on the artery hemodynamics. In this chapter the tortuous idealized CA models were generated for different coronary tortuosity morphological indices namely angle of bend, curvature radius and distance between the bends. Also, the effect of these morphological indices on velocity field and different WSS based HDs are investigated.

Chapter 5 presents the modeling and use of a modified version of Phillips model (Phillips et al. 1992) to study the effect of stenosis severity on shear induced diffusion of RBCs in idealized CA models. In this chapter the Philips model has been chosen to represent the behavior of RBC transport in blood flows. Also, Quemada non-Newtonian model that describes the viscosity behavior of blood has been used to calculate blood viscosity in the Phillips model.

Chapter 6 presents the important conclusions of the present investigation and scope for future study.

CHAPTER 2

LITERATURE REVIEW

2.1 INTRODUCTION

According to the National Heart, Lung, and Blood Institute, peripheral vascular disease affects 8 to 12 million people in the United States alone, which is around 12% of the adult population (NHLB 2011). These diseases are associated with plaque formation and atherosclerosis. The study of the evolution and development of these diseases involve many disciplines such as medicine, mechanics and biology. It has been notably shown that endothelial dysfunction was one of the key factors for the development of atherosclerosis. Clinical indications have constantly permitted us to pinpoint the probable arterial areas for the presence of CVDs and to envisage how these ailments may progress. These clinical indications are generally based on anatomical indicators or biological pointers. The factors such as WSS, pressure drop, flow patterns, velocity, secondary flow, vorticity and vortex flow, and so on, have become an important clinical indices or diagnostic indicators (DIs), especially for CVD.

Hitherto, simulations using patient-specific models remained typically used for predicting the progressed stages of disease. Subsequently from a medical perspective this diagnosis is considered to be time-intensive and ineffective. However, in patient-specific artery geometry the arterial lumen topology is highly irregular and unique for each patient. The simulations with patient-specific artery geometry create difficulties in separating out and identifying the effect of any single parameter on the blood flow behaviour. In that sense, in recent years, CFD has emerged as a reliable and convenient tool to study the characteristics of 3D blood flow and estimate the various diagnostic indicators (DIs) as well as its spatial and temporal variations in complex arterial geometries and play a crucial part in the understanding of CVD hemodynamics. Hence, it is necessary for the medical community to have the precise

knowledge and understanding of computational hemodynamics which is a convergence of CFD, medical imaging and cardiovascular physiology.

2.2 BLOOD AND ITS COMPOSITION

Blood is a fluid element of the circulatory system and is essential for the control of the body's condition. The important role of the blood is to transport oxygen, nutrients, carbon dioxide and other necessary components to the body. The whole blood is a multiphase fluid mainly consisting of plasma and concentrated suspended blood cell elements include RBCs, WBCs and platelets. In blood vessels it has been shown that blood exhibits a thixotropic and viscoelastic behaviour caused by the development of RBC microstructures that split-up at higher velocities (Chien 1970, Thurston 1979, Thurston 1994). A schematic of blood vessel with cellular elements is illustrated in Fig. 2.1. The detailed composition of blood and its cell dimensions are listed in Table 2.1.

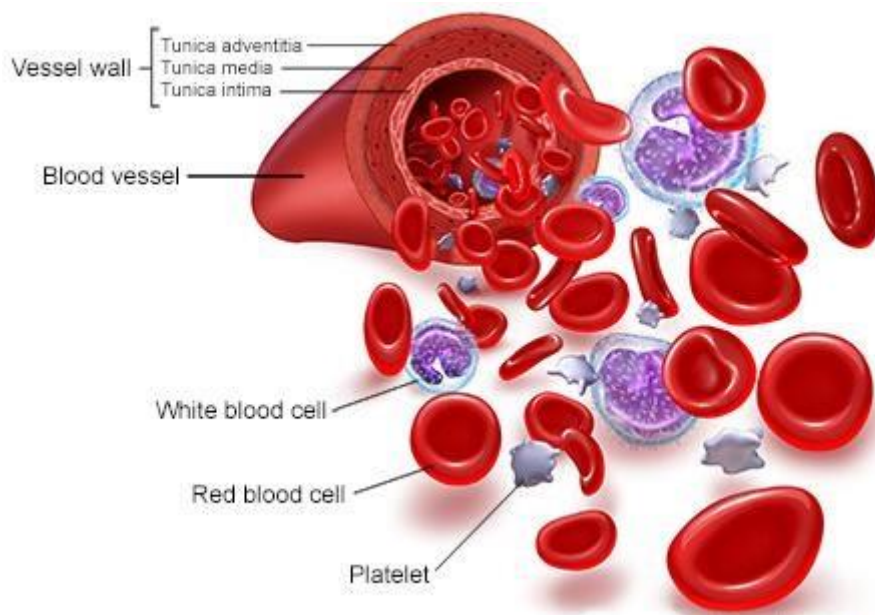


Figure 2.1 Artery with cellular components

(<https://www.myvmc.com/anatomy/blood-function-and-composition/>)

Table 2.1 Composition of blood and its cells dimension (Caro 1978)

Blood components	Number of cells per mm³	Cell dimension and unstressed shape (µm)	Volume fraction
Plasma (Constituents: Proteins, water, hormones, salts, metabolites, nutrients, glucose)	-	-	54%
Erythrocyte or RBCs	4-6 millions	Diameter: 8 µm, Thickness: 1-3 µm, Bi-concave disc	45%
Leukocytes or WBCs (Lymphocytes, Monocytes and Granulocytes)	4-11 thousands	Diameter: 7-22 µm, Roughly spherical	
Thrombocytes or Platelets	250-500 thousands	Diameter: 2-4 µm, Oval or circular	1%

Table 2.2 Properties of RBC and Plasma at 37⁰C (Bronzino 1999, Burton 1965, Caro et al. 1978)

Properties	Plasma		RBC	
Constituents: (Mass fraction) (%)	Water	92	Water	65
	Proteins	7	Membrane components	3
	In organic salts	1	Haemoglobin	32
Dynamic viscosity (mPas)	1.32		-	
Density (kg/m ³)	1025		1100	

Normally, in each adult human the existing volume of blood is between 4 to 6 litres, with an approximate density of 1060 kg/m³ in a homogeneous state (Brooks et al. 1970). On average the RBCs themselves constitute approximately 45% of total blood volume (Bronzino 1999, Lowe et al. 1993). The RBCs volume fraction in total blood

is also called as the haematocrit level. The WBCs and platelets constitute only 1% of the total volume concentration. When all suspended blood cells are removed then the remaining volume of blood consists of plasma and makes up 54% (about 90-92 % of water and 7% of proteins) of the total blood volume which is mainly an aqueous solution containing inorganic and organic materials in low concentration. The properties of RBC and plasma are tabulated in Table 2.2.

2.3 BLOOD VISCOSITY

In general, the viscosity is used to describe the rheology of fluid. The viscosity represents the internal resistance between the layers of fluid and is the ratio of shear stress (force that moves fluid layers) to the gradient of velocity in the fluid (Baskurt and Meiselman 2003). The viscosity of blood mainly depends on the deformability of the blood cells, protein concentration of the plasma, and the blood cells tendency to aggregate (Fung 1993). In blood the suspended cells mainly RBCs strongly influence the apparent viscosity and occupy the maximum blood volume. The blood plasma behaves like a Newtonian fluid with a constant density and viscosity of 1.2 mPas (Fung 1993). However, apparent viscosity of the blood is not constant in the presence of cellular components therefore the rheological behaviour of the blood is non-Newtonian.

The whole blood shows a shear thinning property in viscometer measurements. The viscosity of human blood at 37⁰C, at low shear rate of 23 s⁻¹ is in the range of 8.4 to 5.6 mPas, and at higher shear rate of 230 s⁻¹ is in the range of 5.1 -3.8 mPas (Wells and Merrill 1962). At low shear rate (< 10 s⁻¹), RBCs aggregate and form rouleaux that lead to high blood viscosity (Levick 2003). RBCs disaggregate and deform at high shear rates which above around 50 s⁻¹ (Pries et al. 1992). As the blood shear rate is increased the rouleaux formation breaks down progressively in size by shearing and stretching forces acting during their rotation and deformation that leads to decrease in viscosity. When shear rate reaches to 1000 s⁻¹, an asymptotic viscosity of 3.5 mPas is reached and the blood behaves as Newtonian fluid (Nichols and O'Rourke 2005). Therefore, it is well recognized that at high shear rates blood can be considered as Newtonian and at low shear rates as non-Newtonian fluid (Nerem et al. 1992). The

variation of viscosity and the presence of RBCs in the suspension of blood demonstrate the importance of cellular components on rheology of blood. The Fig. 2.2 describes the shear thinning behaviour of blood.

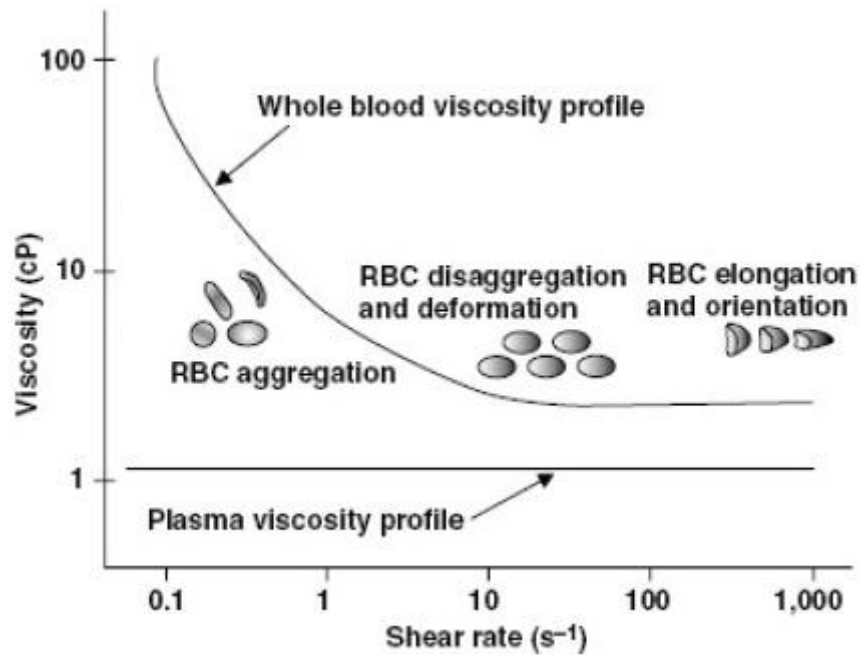


Figure 2.2 Blood Viscosity and Shear Rate
<http://www.yashagrawal.com/2008/01/serum-orwhole-blood-viscosity.html>

2.4 COMPUTATIONAL NON-NEWTONIAN RHEOLOGICAL MODELS IN BLOOD FLOW STUDY

To simulate the blood flow in arteries various CFD models have been developed. In CFD, the Newtonian (Beech-Brandt et al. 2005, Stroeve et al. 2007) and non-Newtonian models (Neofytou and Drikakis 2003, Longest et al. 2004, Hyun et al. 2004) have been employed extensively for hemodynamic studies. In Newtonian blood flow study, the viscosity of blood is considered as a constant value thus ignoring the blood shear-thinning behaviour. The Power Law, Cross, Casson and Quemada models are employed as the common non-Newtonian blood flow constitutive equations (Buchanan et al. 2000, Longest and Kleinstreuer 2003a, Longest and Kleinstreuer 2003b).

A power law model is a non-Newtonian model derived by Walburn and Schneck (1976) to model the blood flow. This model describes the shear-thickening or shear-thinning fluid behaviour for a fixed region of strain rates. It is described as;

$$\tau = C\gamma^h = C\left(\frac{\partial u}{\partial y}\right)^h \quad (2.1)$$

where, h and C are the constants of power law model. The h is the measure of the non-Newtonian behaviour, and C is the measure of fluid consistency. When $h = 1$ then C represents the viscosity of fluid. The effective or apparent viscosity of the power law model can be described as;

$$\mu_{eff} = C\left(\frac{\partial u}{\partial y}\right)^{h-1} \quad (2.2)$$

where μ_{eff} is the effective or apparent viscosity of the non-Newtonian fluid as function of shear rate. If, $h > 1$, the obtained fluid is known as shear-thickening fluid which means with increasing shear rate the apparent or effective viscosity increases. If $h < 1$, the obtained fluid is known as shear-thinning fluid which means with increasing shear rate the apparent or effective viscosity decreases. For blood with 45% haematocrit at 37°C, $h = 0.7755$ and $C = 14.67$ Pas. Though, the use of power law model has a disadvantage while describing the non-Newtonian fluids in both very high and very low shear rate regions and this model application is limited to $0.031\text{s}^{-1} - 120\text{s}^{-1}$ shear rates (Easthope and Brooks 1980). Besides, the power law model does not have the ability to handle the yield stress.

To overcome the disadvantages of power law model, Chien (1970) suggested a Cross model that can be given as;

$$\tau = \frac{\partial u}{\partial y} \left(\mu_{\infty} + \frac{\mu_0 - \mu_{\infty}}{1 + m\left(\frac{\partial u}{\partial y}\right)^n} \right) \quad (2.3)$$

where μ_∞ and μ_0 are the corresponding viscosities at infinite (high) and zero (low) shear rates.

The Casson model (Ferziger and Peric 1999) is a non-Newtonian fluid model with yield stress which is usually employed for blood flow modeling in narrow arteries. It is described as;

$$\begin{aligned} \sqrt{\tau} &= \sqrt{\tau_y} + \sqrt{\mu_\infty \dot{\gamma}}, & |\tau| > \tau_y \\ \dot{\gamma} &= 0 & |\tau| < \tau_y \end{aligned} \quad (2.4)$$

where $\dot{\gamma}$, μ_∞ and τ_y represents respectively the shear rate, asymptotic viscosity and the yield stress. It is difficult to apply of Casson equation for blood flow modelling due to its discontinuous character. Therefore, numerous improved Casson equations have been suggested, to represent the whole range of shear stress by single equation (Ishikawa et al. 1998, Papanastasiou 1987).

The shear rate in Quemada non-Newtonian model (Quemada 1978) is derived from the dependency of viscosity on haematocrit and shear rate in an intense disperse system. The Quemada model has been found to be a more precise in calculating the shear-thinning effect of blood and fits the complex blood rheology for a broader range of shear rates. Compared to Power Law and Casson model the Quemada model extends to a higher maximum shear rate of $256.7s^{-1}$ (Buchanan et al. 2000). The correlation of Quemada model is described as;

$$\tau = \mu_F \left(1 - \frac{1}{2} \frac{k_0 + k_\infty \sqrt{\dot{\gamma}/\dot{\gamma}_c}}{1 + \sqrt{\dot{\gamma}/\dot{\gamma}_c}} \phi \right)^{-2} \dot{\gamma} \quad (2.5)$$

Where ϕ , μ_F and $\dot{\gamma}_c$ represents respectively the particle volume concentration, viscosity of suspending fluid medium and the critical shear rate related with relaxation time. In hemodynamics, the particle volume concentration refers to the blood hematocrit and plasma refers to the suspending fluid medium. The k_∞ and k_0 represents the semi-empirical intrinsic viscosities at $\dot{\gamma}_r \gg 1$ and $\dot{\gamma}_r \ll 1$, respectively,

where $\dot{\gamma}_r = \dot{\gamma}/\dot{\gamma}_c$. For blood flow at 45% haematocrit, the values of $\mu_F = 1.2$ mPas, $c_0 = 4.33$, $c_\infty = 2.07$ and $\dot{\gamma}_c = 1.88$ s⁻¹ (Neofytou 2004).

The other non-Newtonian models include Herschel-Bulkley (Sankar and Lee 2008), Cross (Chien 1970) and Carreau-Yasuda (Cho and Kensey 1991). The detail explanation of these shear-thinning models used in arterial blood flows is concise by O'Callaghan et al. (2006) and Johnston et al. (2004).

2.5 MULTIPHASE NATURE OF BLOOD

Blood is a multiphase fluid composed of mixture of RBCs or erythrocytes, platelets or thrombocytes, and WBCs or leukocytes suspended in watery plasma. Until very recently, it has been modelled as a single disperse phase fluid. The presence of cell suspension in whole blood is the main factor responsible for its non-Newtonian behaviour (Pal 2003). In whole blood, the blood cells are elastic and their properties are insensitive to the WSS and velocity profile distribution in arterial geometries (Gijssen et al. 1998, O'Callaghan et al. 2006). Hence, blood cells can be treated as solid spherical particles. Blood flows through vessels (arteries, veins, and capillaries) transports, oxygen, carbon dioxide, food molecules (glucose, lipids, amino acids), ions (Na⁺, Ca²⁺, HCO₃⁻, etc.), wastes (urea, etc.), hormones and heat. Most CVDs are associated with some form of abnormal blood flow in arteries. The study of blood flows during disease, as well as under normal physiology conditions, has made significant contributions in medical applications. Many researchers concluded that local hemodynamic factors play an important role in the atherosclerosis location, initiation, and progression (Caro et al. 1971, Fry 1968, Berger and Jou 2000, Nerem 1993, Stone et al. 2003).

In recent years, single-phase CFD techniques, combined with non-invasive medical imaging have been used increasingly by researchers seeking to better understand hemodynamic factors (Berthier et al. 2002, Steinman 2002, Zeng et al. 2003, Gijssen et al. 1999, He and Ku 1996, Hoi et al. 2004). The dense particulate nature of blood and its heterogeneous distribution observed through experiments (Reinke et al. 1987, Stadler et al. 1990, Haynes 1960) require multiphase model to explain its complex

behaviour. Jung et al. (2006a, 2006b) modelled an idealized and two realistic right coronary artery (RCA) using a two phase model with an empirical viscosity input whose parameters were determined by rheology experiments.

2.6 INHOMOGENEITY OF BLOOD CELLS IN BLOOD VESSELS

The RBCs in tube flow tend to move near the tube axis by leaving a cell free plasma marginal layer. This plasma layer is relatively devoid of suspended particles. The plasma layer is a very thin layer of plasma and has a significant impact of blood flow dynamics (Fung 1993). In blood flow simulation Butler et al. (1998) enforced a cell-free plasma layer near the vessel wall that containing the scavenging effect of RBCs on NO created from endothelium, indicating that a cell-free plasma layer was essential for NO to have a vasodilator effect as is identified to occur in arteries. The experimental investigations carried out by Aarts et al. (1988) is also revealed that platelets suspended in briny are radially move and concentrate at half way between the vessel wall and the vessel centre. Though, when they suspended in a suspension of RBC ghosts at physiologic haematocrit (40%) the platelets were accumulated almost solely near the vessel wall.

The behaviour of solid spheres and blood cells flowing in the zone that separates flow streamlines are studied by Karino and Goldsmith (1977) in a sudden expansion capillary sized blood vessel. The results revealed that solid spheres and blood cells with less than 20 μ m diameter migrated out of the centre of vortex whereas the sphere and larger cells are remained in the flow recirculation region. The study carried out by Lima et al. (2008) investigated that the distribution of RBCs in glass straight capillaries leads to unequal dispersion of cells depending on the vessel diameter and cell volume fraction. Similar conclusions were attained by Jung and Hassanein (2008) in small arteries, stated that compared to average RBCs volume fraction (VF) of 45% in the lumen, the RBCs VF near the vessel wall is reduced to 5%. These observations reinforced the fact that the blood cellular content varies over wide ranges at different levels of blood circulatory system (Baskurt and Meiselman 2003). All the above works confirm that blood cells inhomogeneity occurs in blood vessel and its microcirculation.

2.7 MODELING OF MULTIPHASE BLOOD FLOW

Blood is a multi-constituent unique fluid whose structure affects the rheological properties that are accountable for its various biological functions. In summary, it is obvious that blood flow at micro-scale shows additional intricate performance and behaves as a multi-constituent fluid, which cannot be explained by single phase fluid models. Inspired by the study of the plasma-skimming phenomenon, numerous multiphase models for blood flow have been established. Such as the Immersed Boundary Method (IBM) joint with the Lattice Boltzmann Method (LBM) is a suitable method for examining the intricate blood behavior in micro-scale flows, predominantly owing to the deformation, cluster formation and collisions of the RBCs (Aidun and Clausen 2010, Dupin et al. 2007, Zhang et al. 2009). Although the IBM-LBM method has been very useful in displaying the complex behavior of blood, it is prohibitive for many practical problems due to its high computational cost. In the literature, for the two-phase formulations, two methods based on continuum mechanics have been used widely: The Averaging Method (Ishii 1975, Ishii and Hibiki 2010, Gidaspow and Huang 2009, Huang et al. 2009) and the Mixture theory (Rajagopal and Tao 1995, Rajagopal 2007). The mixture theory is a homogenization method within the frame work of continuum mechanics, first presented by Truesdell (1984), in which the phenomenon of combination, dissociation, chemical reaction, and diffusion in the broadest sense can be represented. For the detail basics, applications, and historical development of the theory the readers is directed to review few articles by Atkin and Craine (1976a and 1976b), Bowen (1976), Bedford and Drumheller (1983), Massoudi (2008 and 2010) and the book by Rajagopal and Tao (1995) and Truesdell (1984).

In this work, the mixture theory is used as a basis for obtaining a two-phase model of blood, was previously presented by Massoudi and Antaki (2008), and further detailed in Wu et al. (2014a and 2014b), and Massoudi et al. (2012). This model considers plasma as a continuous Newtonian fluid whereas the RBCs are considered as a shear-thinning fluid whose viscosity rely upon the hematocrit according to experimental investigations of Brooks et al. (1970). For examine this two-phase system, a 3D CFD solver is employed based on the ANSYS FLUENT solver.

2.8 HEMODYNAMIC DESCRIPTORS BASED ON WALL SHEAR STRESS AND THE DEVELOPMENT OF ATHEROSCLEROSIS

In arteries, the endothelium has been recognized as a shear-conscious layer. It reacts differently to hemodynamic WSS by triggering various biological developments to accomplish the case of equilibrium for which it was intended. In the past, several shear stress measurement methods have been proposed to elucidate the influence of pulsatile shear stress on the morphological and biological reactions of the vascular system. Different investigators used different descriptors of shear stress in an effort to pronounce the association between steady or unsteady WSS and function of artery wall. Mainly, Zarins et al. (1987) in his studies used a magnitude of instantaneous WSS instead of stress vector (stress directions) to link monkey aorta to the intimal thickening. Kohler et al. (1991) recommended that the stiffening of intimal layer is more sensible to the absolute WSS instead of the amount of WSS. Work carried out by Nagel et al. (1999) observed that the gradients of spatial WSS (WSSG) is known to be an essential factor signifying the manifestation of local endothelium changes. The investigation by White et al. (2001) has revealed that the gradients of temporal WSS encourage EC proliferation.

The HDs of shear stress are widely used to explain the biological reactions of the arterial wall to the hemodynamic WSS. The HDs mainly include steady or instantaneous WSS, time-averaged WSS (TAWSS), WSS gradient (WSSG), oscillatory shear index (OSI), relative residence time (RRT) and endothelial cell activation potential (ECAP). These various types of HDs of WSS and their threshold values corresponding to the risk of CVDs from the literature are deliberated in the following section.

2.8.1 Steady or Instantaneous WSS

The study of blood flow in human arterial system is a crucial part to understand the complete reaction of hemodynamic WSS to arterial wall function. For the last few decades, the impact of hemodynamic WSS in several decades ago was alleged is considered as a key variable in controlling the behavior of human vascular system.

The initial experimental study by Fry (1976) delivered the initial understanding into impairment of endothelium as a result of instantaneous WSS persuaded by a high blood flow rate. Here, in order to understand the endothelium etiology, the dog's aorta was used and were exposed to a broader range of WSS levels. Outcomes revealed that the precarious steady WSS of the ECs was establish to be about 30-40 Pa and observed a substantial impairment of ECs as the cells were wide-open for one hour to this ranges of WSS. Under this ranges of WSS the ECs remained in a normal situation. Later, to detail understand the ECs response to various ranges of WSS more efforts were made based on various types of blood flow, containing WSS persuaded by oscillating flow, turbulent flow and pulsating flow. Therefore, now it is accepted that WSS is a key provocation that regulates the condition of arterial wall morphology, the endothelial genes expression, and the ECs inactivity (Pohl et al. 1986, Lansman 1988, Dekker et al. 2006). Several investigations revealed that under laminar steady blood flow situation, the ECs propagation was fully inhibited as distinguished to the pulsatile blood flow condition (Levesque et al. 1990, White et al. 2001). The researchers have found different responses of endothelium depending on the form and magnitude of WSS by articulating different molecules and genes that have various protagonists in the prevention and development of CVDs. In an investigation by Topper et al. (1996) on human umbilical vein ECs (HUVECs) with 1 Pa of WSS it was revealed that the NO atheroprotective genes was up-regulated approximately three times as many as associated to the static endothelium ailment.

2.8.2 Time-Averaged WSS (TAWSS)

Evaluation of the ECs biological reaction exposed to WSS persuaded by oscillating or pulsating flows is interesting in both *in vitro* or *in vivo* studies. Various methods have been anticipated by several investigators to associate the process of endothelium and the biological response to instable WSS *in vitro* or *in vivo*. TAWSS is another HD of shear stress used to evaluate the formation of atherosclerosis. TAWSS is the average of WSS experienced in the left coronary artery (LCA) walls for a period of one cardiac cycle as pronounced by Lee et al. (2009).

The latest *in vivo* study by Samady et al. (2011) on the human CA concentrating on impacts of TAWSS have specified that TAWSS lower than 0.1 Pa increases the coronary plaque growth rates in patients, while TAWSS higher than 2.5 Pa is alleged to be related with weakening of plaque. The study of Chatzizisis et al. (2011) on pig CAs, emphasizes that areas of low WSS is associated with the raise of plaque development owing to the accumulation of inflammation cells and the deformation of ECs. There after several study outcomes indicated that the mainstream of plaque about 72% was found at areas in lower TAWSS (0.64–0.70 Pa), as associated to areas with higher TAWSS (1.52–1.66 Pa). The assumption of lower TAWSS linked with CVDs is also substantiated by earlier *in vivo* results established on animal models comprising the carotid artery (Mondy et al. 1997, Cheng et al. 2006) and the iliac artery (Zarins et al. 1987), wherein it was proposed that areas showing to lower TAWSS associated with the atherosclerotic plaques development. These results and observations comparative to the effect of TAWSS are reliable by means of previous experimental works by Ku et al. (1985) on a human carotid artery patient-specific models, which indicated that the regions of low WSS are correlates with atherosclerotic plaque in the human arterial system, hence signifying that noticeable oscillatory shear stress may increase the atherosclerotic lesions growth.

2.8.3 WSS Gradient (WSSG)

A number of investigations have revealed that the WSSG or rate of alteration of WSS may produce superior evidence on certain atherogenetic inheritable factors in ECs exposed to oscillating or pulsating flow. The spatial WSSG (SWSSG) and temporal WSSG (TWSSG) are the two most generally used HDs dependent on the WSSG, in which the WSSG is evaluated with difference in the amount of change of the location (distance) with the time respectively. The morphological and biological reactions of ECs persuaded by both descriptors have been described by a number of researchers. Though, the relation of these two descriptors on atherogenesis is still questionable. Numerous experimental studies have used a steady laminar step flow method to create both a spatial and a temporal effect on ECs over the recirculation zone that is created among the reattachment and separation points.

The effect of SWSSG on HUVEC monolayers was investigated by Tardy et al. (1997) by comparing the ECs exposed to SWSSG varies among -0.3 and +0.5 Pa per mm, that relates to WSS levels from -1 Pa and +10 Pa in contradiction of those with a steady WSS of 1.4 Pa. Study outcome indicates that the EC layer open to a higher SWSSG (mainly at the regions wherever the WSS is very less and near to zero i.e. at the reattachment zone) shown a higher detachment rate, ECs proliferation and migration than that of laminar flow zones. This opinion is also promoted in earlier study by DePaola et al. (1992) who used a related approach on cultured bovine aortic ECs (BAECs) by means of an SWSSG that ranges among 0 and +0.6 Pa per mm, which agrees to a WSS varies among -1.5 and +2.5 Pa. Below a high SWSSG the ECs remained exposed to have higher division rate and more morphological changes than those cells under a laminar WSS conditions.

The several studies have shown the ECs response to the TWSSG that a high TWSSG can cause EC damage or injury (Ojha 1994) and excites the adhesion of molecules and positive pro-atherogenetic inheritable factor in the EC monolayer (Hsiai et al. 2003, Bao et al. 1999). Using the footstep flow method, White et al. (2001) investigated the difference between the influence of SWSSG and TWSSG on ECs. Results revealed that substantial ECs propagation was perceived at the flow detachment areas exposed to a TWSSG of around 300 Pa/s however, such flow behavior did not take place when the influence of TWSSG is far away and the ECs were only exposed to the SWSSG of (0-40 Pa/mm). ECs in these areas remained pronounced as behaving correspondingly to those exposed to steady flow.

2.8.4 Oscillatory Shear Index (OSI)

The area exposed to lower WSS with intense fluctuating flow is possibly the utmost predictable disorder for atherosclerotic sites. An initial investigational work by Ku et al. (1985) on human patient-specific carotid bifurcation geometry has revealed that the areas with prominent and low oscillatory WSS remained correlated intensely to the intimal plaque growth. This opinion is in close agreement with the earlier experimental study of Zarins et al. (1983) and Bharadvaj et al. (1982) who used flow visualization techniques to study arterial sites on functional replicas of human carotid

artery. So as to measure the repeated deviation of WSS vectors, Ku et al. (1985) presented the descriptor called OSI to interpret the variation in WSS directions that are applied on the arterial wall in the instable pulsating situation. Such descriptors can be employed to find flow setback that occurs in a CVS.

The theory created by Ku et al. (1985) on oscillatory and low WSS remained promoted by many investigators in both human and animal models. Bassiouny et al. (1992) obtained the intimal hyperplasia (IH) of prosthetic and venous implants inserted in animals to study the effects triggered by hemodynamic and mechanical aspects. The study outcomes demonstrated that IH, which intended on the vascular wall is correlated to oscillatory low WSS flow. The perception of oscillatory and low WSS is also reinforced in the study by Moore et al. (1994) who used magnetic resonance imaging (MRI) velocimetry method to investigate the blood flow in the human abdominal aorta. The results revealed that the areas associated with oscillatory flow and low mean WSS were correlated highly to sites with atherosclerotic lesions. The results also pointed out that under an exercise condition the WSS is stimulated to provide an encouraging hemodynamic atmosphere that can rise magnitude of mean low WSS and reduce the flow reversal and oscillatory effects.

As related to TAWSS, SWSSG, and TWSSG, OSI has been identified to control altered molecules and genes that have various effects on ECs. The study carried by Helmlinger (1995) has proved that calcium on structured BAECs inversely responded as the ECs were exposed to various types of WSS produced by pulsatile, oscillatory and steady flows. The study exhibited that pulsating flow with WSS varying between -2 and +2 Pa did not favor the production of (Ca²⁺) (a key constituent in the stimulation of NO enzyme) as related to pulsatile WSS varying between -2 and 6 Pa and among 2 and 6 Pa and steady WSS varies among 0.02 and 7 Pa. A related work carried by Ziegler et al. (1998) indicated that the areas with oscillatory low WSS varying among -0.3 and +0.3 Pa, reduced the endothelial nitric oxide synthase (eNOS) level though the areas with laminar WSS as less as 0.03 Pa persuaded as much as six-times of eNOS as associated to the static endothelium disorder.

Additional latest studies have proved that areas open to oscillatory and low WSS may promote proatherogenic fragments that advance the growth of aneurysms (Kojima et al. 2012) and instigation of atherosclerosis (Himburg et al. 2004, Takabe et al. 2011). A recent clinical study by Markl et al. (2013) used a 4D-MRI technique to quantify the OSI and WSS among 12 healthy volunteers and 70 patients, and stated that the most of the areas of intricate plaque are correlated with higher OSI. These areas have been exposed to have higher endothelium penetrability to macromolecules and disturbance of the ECs orientation (Himburg et al. 2004).

2.8.5 Relative Residence Time (RRT)

The RRT is a HD based WSS used in year 2004 in correlating the vascular lesions. This descriptor was proposed by Himburg et al. (2004) who examined the effects of hemodynamic WSS on the penetrability of ECs to macromolecules established on computational and experimental methods. Owing to the circumstances where the OSI descriptor is unresponsive to WSS and it is hard to associate it to the deviation of ECs permeability. Areas with high OSI may not inevitably have a low TAWSS, and vice versa. Bridging the gap among the descriptors of TAWSS and OSI Himburg et al. (2004) presented the concept of RRT based on non-adhesive element flow to point out the areas of higher OSI and low TAWSS ailment. Based on the high OSI and low TAWSS theory, more the RRT more possibility of having atherosclerotic sites.

The number of investigations have shown that the areas with extended RRT are susceptible and vulnerable to CVDs. Study carried by Hoi et al. (2011) correlated the dispersion of aortic plaques of rats with three types of HDs, namely TAWSS, OSI, and RRT. The authors revealed that plaque developing in the arteries is interrelated to the RRT and OSI but not with TAWSS. A few investigations also propose that OSI and TAWSS can be interchanged by the single descriptor RRT only (Lee et al. 2009). The study of Soulis et al. (2011) indicated that the aortic arch open to higher RRT is associated to high oscillatory, low shear flow, signifying that higher RRT can exist as a suitable pointer to relate the concentrations of atheroma. Work by Sugiyama et al. (2013) revealed that the atherosclerotic grazes produced in the walls of aneurysmal

walls of 30 patients linked by means of highest RRTs that were calculated using numerical techniques.

It must also be pointed out that currently none of the hypothesis completely elucidate or correlate accurately the development and initiation of CVDs due to presence of hemodynamic WSS. These HDs has been revealed to have certain restrictions. In the study of cell culture with mortal ECs by White et al. (2001) it was revealed that the TWSSG is the foremost cause in ECs propagation, while the propagation of ECs produced by the SWSSG is at par with that of uniform steady WSS. Rikhtegar et al. (2012) investigated the relationship between plaque locations and different HDs (such as OSI, TAWSS, TAWSSG and RRT) using 30 subject-specific LCA geometries extracted from 30 patients. Using the subject-specific reconstructed artery geometries with removed plaque from the geometries, computational consequences revealed that TAWSS has a substantial sophisticated sensitivity compared to other HDs. The current review study by Peiffer et al. (2013) concentrated on the effect of oscillatory and low WSS has also emphasize the limits of these HDs. In more recent study of Di Achille et al. (2014) a new HD called ECAP was proposed to highlight the areas wherever WSS is considered by a both pronounced and low concentration alterations in way during a pulsatile cycle. The ECAP demarcated the vulnerability of EC and associate the OSI with the TAWSS. The key purpose of ECAP is to pinpoint the local areas of the arterial wall that can be open to pro-thrombotic WSS incitements. The regions with high ECAP values will thus is link to conditions of low TAWSS and high OSI.

A whole detailed theory to expose the pathology and mechanism of CVD owing to blood flow is still under research. Even though the role of WSS on arterial biological reaction, particularly on ECs function, has been very established, supported and accepted in a huge body of literature. Nowadays, the combination of these WSS based HDs are used as encouraging HDs of the cardiovascular pathologies. In the current study, the multiphase approach is successfully employed in tortuous and stenotic CAs to investigate the various HDs and study the effect of stenosis severity and different morphological coronary tortuosity indices on these HDs in relation to hemodynamics.

2.9 SHEAR INDUCED MIGRATION

In arteries, at low Reynolds number the flowing concentrated suspensions exhibit many interesting phenomena like aggregation, shear induced migration (SIM), sedimentation etc. These phenomena which arise from fluid-particle and particle-particle interactions depends on numerous factors such as the viscosity of the suspending fluid, shear rate, and the density and concentration of the particles. In this work, we focus on SIM phenomenon which has attracted huge attention in most recent years due to its industrial, technological and biological applications.

The SIM is defined as a phenomenon in which well mixed neutrally buoyant, non-colloidal particles in a viscous Newtonian fluid when exposed to non-homogeneous shear flow, becomes non-uniform because of particles flux migrating from high shear rate regions to low shear rate regions and from high particle concentration regions to low particle concentration regions. This phenomenon results from the fluid-particle and particle-particle interactions (Gadala-Maria and Acrivos 1980, Leighton and Acrivos 1986).

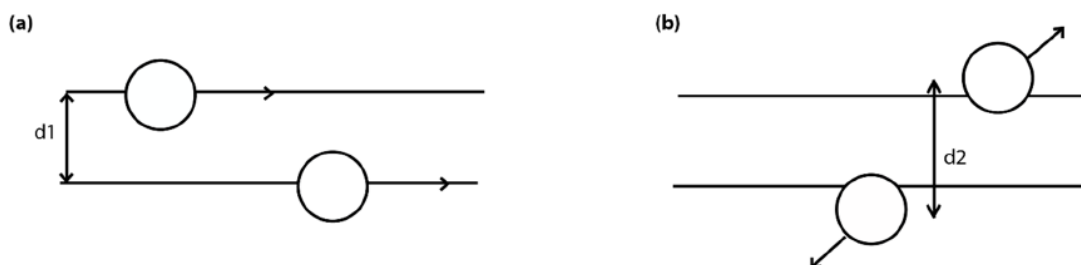


Figure 2.3 Two solid spheres interaction in a simple shear flow, before interaction (a) and after interaction (b) (Leighton and Acrivos 1987a)

For better understanding of this SIM, we have elucidated this by example in the Fig. 2.3 given below. Consider two spherical solid particles present in suspension. In laminar flow the layers of fluid move one over the other with different velocities, and the particles also move in those layers with different velocities. The particle flowing with higher velocity interacts with the particle flowing with lower velocity. If the interaction of particle is reversible, then the particle should return to their initial position at the end of collision. After particle return to their initial position the same

initial distance (d_1) has to retain between them. But the particles never return to their initial position after their interaction and are detached by distance (d_2) different from the initial distance. Hence, this shows an irreversible interaction taking place between the particles, and relocating the particles away from their initial streamlines. The key reason for this irreversible interaction happens because of multi body inter-particle interactions, Brownian motion of particles and particles surface roughness. If the distance separating the particles moved is measured in the order of radius of particle (say a), then between the particles the relative velocity is $\dot{\gamma}a$. Here a is the radius of particle and $\dot{\gamma}$ is the local shear rate. Thus, the shear induced (SI) particle diffusivity is proportional to $a^2\dot{\gamma}$. If there is a more shear rate gradient across the particle, then the particle experiences a more irreversible interaction. Likewise, if there is a lesser shear rate gradient across the particle, then the particle experiences less irreversible interactions. Therefore, more migration occurs from high shear rate regions compared to low shear rate regions. This increases the particles concentration at low shear rate regions which leads to particle concentration gradients.

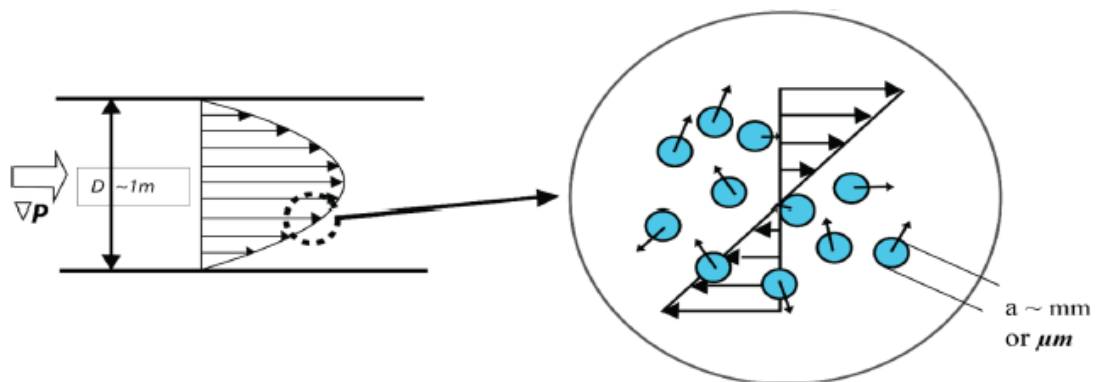


Figure 2.4 A Suspension microscopic flow behaviour depend on the dynamics at micro structure level (Krishnan 2010)

However, this particle concentration gradient results in particles migration from high concentration regions to low concentration regions. This whole phenomenon associated with the shear flow of suspensions is known as SIM and is described in detail by Leighton and Acrivos (1987a). The tube flow is the most practical application for this where the particles get concentrated in the tube center due to SIM.

As a result, the velocity parabolic profile becomes flattened or blunted as shown in Fig. 2.4.

2.10 SHEAR INDUCED MIGRATION OF RBCs

A large body of experimental evidence indicates that the flowing suspensions show particle migration (Abbott et al. 1991, Arp and Mason 1977, Chow et al. 1994, Gadala-Maria and Acrivos 1980, Hookham 1986, Karnis et al. 1966, Koh et al. 1994, Leighton and Acrivos 1987b) with a general tendency showing migration from higher shear rate regions to lower shear rate regions. In small and micro vessels (microns to millimeter size) the RBCs also displays this migration behavior to the center of the vessel and the subsequent separation of platelets near the artery wall has been subject of powerful research in the previous years, both experimentally (Aarts et al. 1988, Cokelet 1999, Pries et al. 1992) and numerically (Bagchi 2007, Mansour et al. 2010, Sharan and Popel 2001, Van Weert 1996). Distribution of RBCs affects viscosity of blood, and therefore the velocity profile, and also affects a sequence of biological activities such as distribution of oxygen in the lumen and scavenging of NO by hemoglobin present in the RBCs (Liu et al. 2012).

Local vessel wall hypoxia has been projected as a subsidizing factor to IH and atherosclerosis (Tarbell 2003) and changed NO transport in the artery has been hypothesized to induce atherogenesis (Liu et al. 2012). Based on deliberations on the Sherwood and Damkholer numbers, it is believed that (Tarbell 2003) the supply of oxygen to the vessel wall is more possible to be fluid-phase restricted, therefore emphasizing the significance of mass carrying from the lumen to the artery wall. It has been shown that, the concentration of hemoglobin and oxygen transport decreases in the artery wall due to migration of RBCs (Moore and Ethier, 1997). Therefore, given the more importance of RBC concentration in the above-mentioned sequence of biological activities and the assessment of RBC distribution as a result of SIM is of main importance. A modified version of Phillips model (Phillips et al. 1992) for SIM of particles in concentrated suspensions was used to model and study the effects of stenosis severity on SID of RBCs. The more detail about SIM is explained in chapter 5.

2.11 SUMMARY OF LITERATURE

The present study focuses on the hydrodynamic forces that influence the cell distribution in the flow disturbance and recirculation regions of a stenosed artery where WSS is low. Despite all the previous studies presented above, numerical simulation incorporating cellular interactions, multiphase characteristics of the blood and the distribution of cell has not been presented yet. The distribution of blood cell is not uniform in the network of arteries. Blood viscosity models and blood composition have been discussed and it has been found that the blood viscosity models have a major influence on WSS calculated from experimental work and CFD study. In large arteries, most of the rheological blood models calculating WSS and other hemodynamic parameters have assumed blood as a homogeneous fluid which is not the true in in-vitro. The models studied and discussed in the literature have treated blood as a single phase fluid.

The WSS plays a key role on the progression and development of atherosclerosis. Low WSS has been interrelated with thickening of atheromatous plaque. Under low WSS, cellular interactions could lead to the onset of atherogenesis, thrombosis and the inflammatory process. This suggests that particle parameters are important where the multiphase nature of blood could not be neglected. Also, the qualitative data on WSS and WSS based parameters with the progression of tortuosity and stenosis in arteries remains limited. With the current non-invasive imaging techniques the calculation of the WSS are difficult and pose substantial measurement error. More hemodynamic studies in this field by considering blood as a multiphase fluid are necessary to determine the WSS. For the same, computational models need to be validated against experimental models which are recognized as gold standard.

2.12 MOTIVATION

The study of blood flow dynamics that causes atherosclerosis and restenosis is very essential for clinicians, patients and biomedical engineers. The key motivation for the present research is the application of numerical and mathematical models in the detailed diagnosis of the CVDs when used with non-invasive techniques such as

intravascular ultrasound (IVUS), computerized tomography (CT) and MRI. In biomedical engineering and clinical practice, the planning of medical intervention for CVDs will become progressively important providing accurate test data. The different WSS and WSS based HDs such as TAWSS, OSI, TAWSSG, RRT and ECAP play a crucial role in the understanding the onset and development of atherosclerosis.

There are three key methods towards the study of stenotic and tortuous CA blood flow dynamics: *In Vitro*, *In Vivo*, and *In Silico*. *In Vitro* approach involves the experimental methods to study and understand the mechanics of the blood flow in the stenosed vessels (artificial models) (Ahmed and Giddens et al. 1983). *In Vivo* approach includes the inserting of stenosis, stents in humans or animals monitored by radiographic imaging (Wang et al. 2000b, Kastrati et al. 2001b), or certainly later martyr of the animal, i.e., histological studies (Wilson et al. 2007). Lastly, *In Silico* method involves the simulations of the blood flow by means of computers, notably through CFD.

In CFD, the 3D artery geometry specimen is generally acquired both through a non-invasive (medical) imaging (Myers et al. 2001, Wentzel et al. 2003) or ideal model (LaDisa et al. 2005b). It is then remodeled into a mesh consisting of several finite volumes or elements. The flow of fluid with blood properties is then computed by solving the Navier-Stokes equations for each of these finite volumes or elements (Steinman 2002). Normally the blood is assumed to be a Newtonian or non-Newtonian fluid based on the diameter of the arteries (Murphy and Boyle 2010, Steinman 2002). The different parameters (i.e., HDs) persuading the development of neo-IH can then be measured over the post-processing of the computation results.

2.13 OBJECTIVES OF THE PRESENT STUDY

Using multiphase approach, the objectives of this research are as follows:

1. To investigate the effect of stenosis severity (degree of stenosis) on the pulsatile coronary hemodynamics.
2. To investigate the impact of coronary tortuosity (tortuosity morphological indices) on the artery hemodynamics.

3. To investigate the effect of stenosis severity on shear induced diffusion of red blood cells in an stenosed left coronary artery.

CHAPTER 3

EFFECT OF STENOSIS SEVERITY ON WALL SHEAR STRESS BASED HEMODYNAMIC DESCRIPTORS USING MULTIPHASE MIXTURE THEORY

3.1 INTRODUCTION

Atherosclerosis is considered to be an endothelial disease which is generally found in medium and large sized arteries. This causes the narrowing of arteries which hinders the blood flow to the tissues (Vlachopoulos et al. 2011). In CAs, the hemodynamic changes due to the presence of plaque buildup are correlated with higher risk of adverse clinical outcome. One substantial implication revealed from recent studies (Malek et al. 1999, Chatzizisis et al. 2007) states that regional WSS plays a key and fundamental role in the localization of atherosclerosis and in particular, low and oscillatory WSS (± 0.5 Pa) has been correlated to region of localization of atherosclerosis and the magnitude of low WSS been associated with the severity of atherosclerosis.

Oscillatory shear index (OSI) which is another WSS based hemodynamic parameter is used as a predictor for the atherosclerosis plaque formation and susceptibility of plaque in CAs (Zhang et al. 2008, Ryou et al. 2012). High OSI value is strongly related to the development of atherosclerosis since it affects the ECs arrangement in adjacent tissues. Also, high OSI value regions are generally located in the low WSS regions (Ryou et al. 2012, Stadler et al. 1990, Ren et al. 2016).

Hitherto, most of the hemodynamics studies have used CFD techniques to better understand the various HDs by considering blood as a single-phase Newtonian (He and Ku, 1996, Berthier et al. 2002, Zeng et al. 2003, Hoi et al. 2004, Hasan and Das, 2008, Aayani et al. 2016, Mesri et al. 2017, Li et al. 2015, Tang et al. 2015, Carty et al. 2016) and non-Newtonian fluid (Carty et al. 2016, Gijsen et al. 1999,

Steinman 2002, Razavi et al. 2011, Li et al. 2015, Yan et al. 2017). However, the blood is intrinsically a suspension of RBCs, WBCs, platelets and other lipoproteins in blood plasma. Several experimental studies (Haynes 1960, Reinke et al. 1987, Stadler et al. 1990, Egorov et al. 1994) have observed the dense granular nature of blood and its heterogeneous distribution and concluded that simulation of blood requires a multiphase approach/model to explain clearly the interaction of blood particulates with the lumen surface and its complex behavior. In single-phase studies, the details of blood cells transport and their interactions with varying percentage of stenosis severities were missing. Therefore, a good multiphase approach considering the blood cell transport and their interactions is essential for better understanding the underlying pathology and pathological development of CAD.

A large number of research articles have been published typically wherein one of the two multi-component theories; the Mixture Theory (Rajagopal et al. 1992) and averaging methods (Ishii and Hibiki, 2010) have been used. The approach of both theories is based on an assumption that each phase may be represented mathematically as a continuum (Kizilova et al. 2012). Although the approaches of both the theories look similar, their formulations of constitutive models are completely different. Indeed, many studies have been reported that the interaction models used in averaging methods are not frame-indifferent, hence violating the fundamentals of physics as revealed by Massoudi (2002). Generally, the drag models used along with the averaging methods holds good only for fluid particles or solid spherical particles which are in low concentration and sufficiently small in size. Hence, in this chapter, we use the theory of interacting continua or mixture theory to model the blood consisting of two-phase mixture (i.e., plasma and RBCs).

The effects of the platelets, WBCs and other components in the blood are neglected owing to their negligible volume concentration. The effect of mass or biochemical inter conversions are not considered in this chapter. The RBC's volume fraction is treated as a scalar field variable. In addition, we assumed that the plasma acts as a Newtonian fluid and RBCs were considered as solid spherical particles with

its viscosity dependent on the hematocrit and local shear rate. Plasma-RBC interaction forces are considered by implementing the drag and lift forces.

To date, according to the best knowledge of the authors, only limited research has been done on studying clinically relevant WSS based hemodynamic indicators considering blood as multi-component fluid and there is no published data on the effect of stenosis severity in the CA considering blood as multiphase fluid. Hence, the present computational study was set up to assess the influence of different DOS severities such as 30%, 50%, 70% and 85% stenosis on WSS based hemodynamic parameters such as TAWSS, TAWSSG and OSI using multiphase approach. Finally, the relationships between the bulk flow hemodynamics and various WSS based HDs have been established. The current multiphase mixture model has been compared with single phase model and validated with experimental studies.

3.2 MATERIALS AND METHODS

3.2.1 Geometry Representation and Computational Mesh Generation

In the present multiphase blood flow modelling an ideal arterial geometry model for various DOS severity has been considered. Figure 3.1 shows the blood vessel model (with dimensions) including its stenosis as a 3D axisymmetric straight tube for the numerical blood flow analysis. The geometry of stenosis is defined by the cosine function (Rabby et al. 2014):

$$\frac{r(x)}{R} = 1 - \delta_c \left[1 + \cos\left(\frac{x\pi}{D}\right) \right], -D \leq x \leq D \quad (3.1)$$

Where, x and r are the axial and radial coordinates, respectively. R and D , respectively correspond to the radius and diameter of un-stenosed vessel. The δ_c is a constant and takes the value of 0.70, 0.50, 0.30 and 0.15 resulting in 30%, 50%, 70% and 85% of diameter reduction at the stenosis throat as shown in Fig. 3.2. The length of the stenosed zone, inlet zone and outlet zone is 8 mm (2D), 56 mm (14D) and 116 mm (29D), respectively and combining all lengths gives a total length of 180 mm. The

selected CA geometry had a 4 mm of lumen diameter which is typical of left main CA (Nosovitsky et al. 1997).

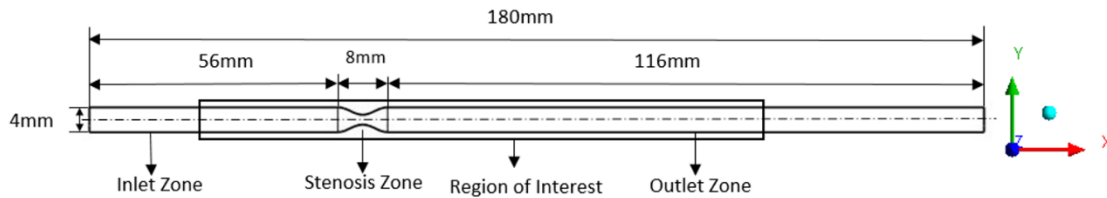


Figure 3.1 Ideal stenosed vessel geometry with dimensions showing the boundary conditions and region of interest where four different stenosis geometries are simulated to demonstrate hemodynamic variations



Figure 3.2 Idealized stenosis vessel geometries for different DOS severity, a). 30%, b). 50%, c). 70%, and d). 85% stenosis

The computer-aided design software GAMBIT 2.4.6 (FLUENT, ANSYS, Canonsburg, PA, USA) is used for the generation of 3D idealized geometries and the grid. For generation of unstructured tetrahedral mesh with variable mesh spacing a robust scheme was adapted to signify the rapidly and small varying features in the stenosis region. The final grid contains 389180 elements as shown in Fig. 3.3.

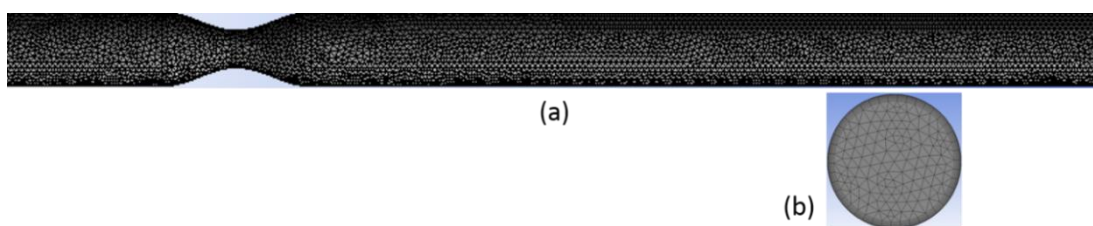


Figure 3.3 Computational grid. (a) 3-D computational grid for idealized CA with 50% diameter reduction stenosis, (b) Zoomed view of inlet grid presenting the prism layer to capture the flow near wall

3.2.2 Multiphase Blood Flow Model

Developments in the field of CFD have imparted the basis for garnering further insight into the multiphase flow dynamics. In the present study, the theory of interacting continua is used to study the hemodynamics in an idealized CA since it has better accuracy compared to the Euler-Euler method. The mixture theory model solves the conservation of mass, momentum and energy equation for the mixture. In addition, for the secondary phases it solves volume fraction (hematocrit) equations and for the relative velocities it solves the set of algebraic equations which are also presented in below.

3.2.2.1 Continuity Equation

Using the mixture theory model the continuity equation is given as:

$$\frac{\partial}{\partial t}(\rho_m) + \nabla \cdot (\rho_m \vec{v}_m) = 0 \quad (3.2)$$

$$\vec{v}_m = \frac{\sum_{k=1}^n \varepsilon_k \rho_k \vec{v}_k}{\rho_m} \quad (3.3)$$

$$\rho_m = \sum_{k=1}^n \varepsilon_k \rho_k \quad (3.4)$$

Where, \vec{v}_m , ρ_m and ε_k , correspond to the mass-averaged velocity, mixture density and the hematocrit of phase k respectively.

For different phases, the sum of all the hematocrits must be equal to 1:

$$\sum_{k=1}^n \rho_k \varepsilon_k = 1 \quad (3.5)$$

3.2.2.2 Momentum Equation

The summation of individual momentum equations for all the phases is used to obtain the momentum equation for the mixture (Eqn. 3.6).

$$\frac{\partial}{\partial t}(\rho_m \vec{v}_m) + \nabla \cdot (\rho_m \vec{v}_m \vec{v}_m) = -\nabla p + \nabla \cdot [\mu_m (\nabla \vec{v}_m + \nabla \vec{v}_m^T)] + \rho_m \vec{g} + \vec{F} - \nabla \cdot \left(\sum_{k=1}^n \varepsilon_k \rho_k \vec{v}_{dr,k} \vec{v}_{dr,k} \right) \quad (3.6)$$

Where, n , \vec{F} and μ_m correspond to the number of phases, body force and the mixture viscosity, respectively. μ_m is expressed as:

$$\mu_m = \sum_{k=1}^n \varepsilon_k \mu_k \quad (3.7)$$

And $\vec{v}_{dr,k}$ - secondary phase (k) drift velocity:

$$\vec{v}_{dr,k} = \vec{v}_k - \vec{v}_m \quad (3.8)$$

The drift velocity is active when any one of the two phases is present in particle form. Due to the minimal influence of buoyancy force and external force (rotational, shear lift, and virtual mass) on blood they are neglected in momentum equations.

3.2.2.3 Slip and Drift Velocity

The secondary phase (p) velocity relative to the primary phase velocity (q) is called as the slip velocity. It is expressed as:

$$\vec{v}_{pq} = \vec{v}_p - \vec{v}_q \quad (3.9)$$

Also, for any phase (k) the mass fraction (c_k) is expressed as:

$$c_k = \frac{\varepsilon_k \rho_k}{\rho_m} \quad (3.10)$$

\vec{v}_{pq} and $\vec{v}_{dr,p}$ are related by the following equation:

$$\vec{v}_{dr,p} = \vec{v}_{pq} - \sum_{k=1}^n c_k \vec{v}_{qk} \quad (3.11)$$

The relative velocity (\vec{v}_{pq}) is given by (Manninen et al. 1996),

$$\vec{v}_{pq} = \frac{\tau_p (\rho_p - \rho_m)}{f_d \rho_p} \vec{a} \quad (3.12)$$

Where τ_p represents the relaxation time of particle

$$\tau_p = \frac{\rho_p d_p^2}{18\mu_q} \quad (3.13)$$

Where, d_p and \vec{a} , respectively correspond to the diameter and acceleration of secondary phase particles and f_d is the drag force applied by the fluid on spherical particles. For the Two phases, an interphase drag term is added to consider the exerted force of drag by fluid on spherical rigid particles. For the force of drag, between RBCs and plasma, the Gidaspow model (Gidaspow 1994) was embraced to validate the densely distributed RBCs.

The drag force term is expressed as

$$f_{d(rbc,plasma)} = c_{rbc} (\mathbf{u}_{rbc} - \mathbf{u}_{plasma}) \quad (3.14)$$

Where u_{plasma} and u_{rbc} , respectively correspond to the plasma and RBCs phase velocity, c_{rbc} denotes the momentum exchange coefficient between phases, is given by:

$$c_{rbc} = \frac{3}{4} \frac{C_D}{d_{rbc}} \varepsilon_{rbc} \varepsilon_{plasma} \rho_{plasma} |u_{rbc} - u_{plasma}| \quad (3.15)$$

Where d_{rbc} is the diameter of RBC i.e. 8 μm . For both dilute and dense particles, the Gidaspow model (Gidaspow 1994) assumes two different systems of equations for drag coefficient.

For, $\varepsilon_{rbc} < 0.2$, C_D is defined as

$$C_D = \varepsilon_{rbc}^{-1.65} \max \left(\frac{24}{\text{Re}'_p} (1 + 0.15 \text{Re}'_p^{0.687}), 0.44 \right) \quad (3.16)$$

where, Re'_p represents the modified Reynolds number of particle and represented as:

$$\text{Re}'_p = \frac{\rho_{plasma} \varepsilon_{plasma} d_{rbc} |u_{rbc} - u_{plasma}|}{\mu_{plasma}} \quad (3.17)$$

For $\varepsilon_{rbc} > 0.2$, the momentum exchange coefficient between phases (c_{rbc}) is directly expressed as:

$$c_{rbc} = 150 \frac{(1 - \varepsilon_{rbc})^2 \mu_{plasma}}{\varepsilon_{rbc} d_{rbc}^2} + 1.35 \frac{(1 - \varepsilon_{rbc}) \rho_{plasma} |u_{rbc} - u_{plasma}|}{d_{rbc}} \quad (3.18)$$

3.2.2.4 Constitutive Model

The strain rate tensor $\dot{\underline{\underline{\gamma}}}$ and viscous stress tensor $\underline{\underline{\tau}}$ are considered to represent the constitutive model. It is expressed as:

$$\underline{\underline{\dot{\gamma}}} = \nabla \vec{v} + (\nabla \vec{v})^T \quad (3.19)$$

The significance of $\underline{\underline{\dot{\gamma}}}$ and $\underline{\underline{\tau}}$, are expressed by $\dot{\gamma}$ and τ , respectively and is expressed as:

$$\dot{\gamma} = \sqrt{\frac{1}{2} \underline{\underline{\dot{\gamma}}} : \underline{\underline{\dot{\gamma}}}} = \sqrt{\frac{1}{2} \underline{\underline{\dot{\gamma}}} : \underline{\underline{\dot{\gamma}}}} \quad (3.20)$$

$$\tau = \sqrt{\frac{1}{2} \underline{\underline{\tau}} : \underline{\underline{\tau}}} = \sqrt{\frac{1}{2} \underline{\underline{\tau}} : \underline{\underline{\tau}}} \quad (3.21)$$

Where, $\nabla \vec{v}$, \vec{v} and $\underline{\underline{\Pi}}$ is respectively denotes the velocity-gradient tensor, velocity vector and second invariant of a stress tensor, whereas, the superscript T represents its transpose. For the viscous fluid the constitutive behavior is expressed by

$$\underline{\underline{\tau}} = \mu \underline{\underline{\dot{\gamma}}} \quad (3.22)$$

Where, μ is the dynamic viscosity of blood.

In general, the rheological properties of blood are complex in small arteries because of its strong non-Newtonian behavior such as viscoelasticity, shear-thinning, and thixotropic (Oka 1981) and the time dependent viscosity of blood is determined by the aggregation and disaggregation of particles (RBCs). In the present study, the viscosity is considered as a function of shear rate and hematocrit (Quemada 1981). To account the blood non-Newtonian behavior, Quemada viscosity model (Quemada 1977, Quemada 1978) is used in this chapter. Compared to the different non-Newtonian models, the Quemada viscosity model is exclusively reliant on the RBC's hematocrit and local shear rate and holds good for broader range of shear rates during each cardiac cycle from end-diastole (low shear) to peak systole (high shear). The change in RBC volume fraction cannot be calculated directly using single phase models. This is one added advantage of the present model over traditional single

phase models. Also, the distribution and time evolution of RBC's is correlated to the blood flow field through dynamic shear viscosity and defined as

$$\mu = \mu(\varepsilon_{rbc}, \dot{\gamma}) = \mu_{plasma} \left[1 - \frac{1}{2} \left(k_{\infty} + \frac{k_0 - k_{\infty}}{1 + (\dot{\gamma} / \dot{\gamma}_c)^q} \right) \varepsilon_{rbc} \right]^{-2} \quad (3.23)$$

Where $\mu_{plasma} = 0.00132$ Pa s (Lowe et al. 1993, Caro 2012) is the plasma viscosity, q is an empirical parameter, ε_{rbc} is the RBC hematocrit and parameters k_0 , k_{∞} and $\dot{\gamma}_c$, respectively, correspond to the lower, higher and critical shear rates of non-dimensional intrinsic viscosities. Cokelet (1987) investigated various empirical correlations and expressed as a function of RBC hematocrit for each of these parameters, which is given by:

$$\dot{\gamma}_c(\varepsilon_{rbc}) = e^{(-6.1508 + 27.923\varepsilon_{rbc} - 25.6\varepsilon_{rbc}^2 + 3.697\varepsilon_{rbc}^3)} \quad (3.24)$$

$$k_0(\varepsilon_{rbc}) = e^{(3.874 - 10.41\varepsilon_{rbc} + 13.8\varepsilon_{rbc}^2 - 6.738\varepsilon_{rbc}^3)} \quad (3.25)$$

$$k_{\infty}(\varepsilon_{rbc}) = e^{(1.3435 - 2.803\varepsilon_{rbc} + 2.711\varepsilon_{rbc}^2 - 0.6479\varepsilon_{rbc}^3)} \quad (3.26)$$

3.2.3 Boundary Conditions

A transient simulation was carried out using fluid and rheological properties of blood. The volume inflow velocity profile was used as velocity inlet boundary conditions obtained from Berne and Levy (1967) and shown in Fig. 3.4. At inlet, a fully developed time-dependent velocity profile is considered and used in ANSYS Fluent as a C language user-defined function (UDF) code and coupled to the CFD code. Maximum Reynolds numbers of 410 is attained at the inlet based on the diameter of the artery during maximum flow at beginning of diastole. The stenosis and blood-vessels were assumed to be rigid and the flow of blood was assumed to be laminar.

The outflow and no-slip conditions were applied to outlet and wall boundary conditions respectively.

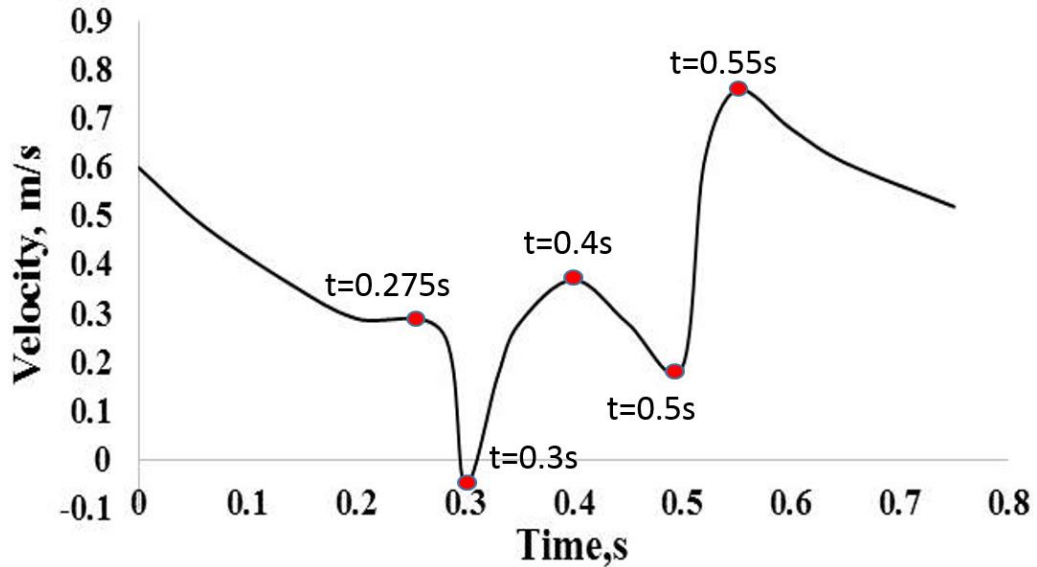


Figure 3.4 Inlet pulsatile coronary velocity profile for blood (plasma and RBC) along the time of the cardiac cycle (Berne and Levy, 1967). End of diastole (0.275s), reversed flow in early systole (0.30s), local maximum systole (0.4s), local minimum systole (0.5s), and maximum flow at beginning of diastole (0.55s)

3.2.4 Numerical Scheme

With appropriate inlet and outlet boundary conditions, an ANSYS FLUENT 14.5 commercial code (ANSYS Inc. 2012) with multiphase mixture model was employed to solve the coupled nonlinear PDE (partial differential equation) of blood flow. For pressure-velocity coupling the coupled scheme was employed. A coupled solver with first-order and second-order upwind schemes is used for spatial discretization of volume fraction and momentum terms respectively. Figure 3.4 shows the pulsatile phasic inflow velocity waveform used at inlet boundary conditions for plasma and RBCs. In this chapter, 1025 kg/m^3 and 1100 kg/m^3 were chosen as the density of plasma and RBCs respectively (Caro 2012, Bronzino 1999). Uniform velocity profiles were maintained at the inlet cross section. At the artery wall the boundary condition of zero slip velocity was applied for both plasma and RBC's. The volume fraction of RBC is maintained steady and uniform with 45% at the inlet. The particles of RBCs

were assumed to be spherical with $8\mu\text{m}$ as average diameter and a shape factor of $\phi = 1$.

The simulations were carried out with a maximum residual corresponding to the convergence flow of 10^{-3} . Also, constant time step of 0.001s was chosen with 200 iterations for each time-step. To ensure the periodicity, the simulations were carried out for four pulsatile cycles and the analysis was carried out for the third cycle. Reynolds number and Womersley parameter, respectively found to be 737 and 3.2. The Reynolds number and Womersley parameter were calculated, respectively using the equation $R_e = \rho_{mix} U_0 D / \mu_{mix}$ and $W_o = D / 2\sqrt{2\pi / T(\rho_{mix} / \mu_{mix})}$, where, U_0 is the inlet velocity (ms^{-1}) and T is the cardiac cycle time period.

3.2.5 WSS Based Hemodynamic Descriptors

The various WSS based HDs are calculated by using the stated equations below. The WSS is a biomechanical parameter, producing a tangential force on the vascular EC surface and near the wall it is a function of the velocity gradient and regulates the arterial wall remodeling. The WSS is given by

$$\tau = \mu \left(\frac{\partial u}{\partial y} \right)_w \quad (3.27)$$

3.2.5.1 Time-Averaged Wall Shear Stress (TAWSS)

It is the averaged WSS over one pulsatile cycle, used to determine the shear stress magnitude applied on the vascular wall surface during one cardiac cycle. The absolute WSS is integrated over a one pulsatile cycle to calculate the TAWSS and dividing it by the time period of one cycle. It is given as

$$TAWSS = \frac{1}{T} \int_0^T |WSS| dt \quad (3.28)$$

Since the TAWSS depend on the magnitude of absolute WSS, it does not identify any information regarding the direction of WSS. The values of TAWSS lower than 0.4 Pa endorses an atherogenic endothelial phenotype whereas the values

with high TAWSS (15-45 Pa) are linked to thrombogenic sites (Malek et al. 1999). The high values of TAWSS can lead to damage of ECs (Suess et al. 2016).

3.2.5.2 Time-Averaged Wall Shear Stress Gradient (TAWSSG)

It is a transient fluid flow property, correlated to the wall of the artery throughout a pulsatile cycle. Speedy changes of WSS over small spaces are measured by TAWSSG and is defined as

$$TAWSSG = \frac{1}{T} \int_0^T \sqrt{\left(\frac{\partial \tau_x}{\partial x}\right)^2 + \left(\frac{\partial \tau_y}{\partial y}\right)^2 + \left(\frac{\partial \tau_z}{\partial z}\right)^2} dt \quad (3.29)$$

3.2.5.3 Oscillatory Shear Index (OSI)

Generally, in the arterial system the reversed blood flow is found through the diastolic phase of the pulsatile cycle. OSI is a HD used to measure the WSS directional change during one pulsatile cycle in the arterial system. The OSI value falls between the ranges of 0 and 0.5, corresponding to least and severe temporal shear rate conditions respectively. It is given by

$$OSI = 0.5 \times \left(1 - \frac{\left| \int_0^T WSS dt \right|}{\int_0^T |WSS| dt} \right) \quad (3.30)$$

OSI is generally used to describe the flow field disorder (pure oscillatory flow) near the wall and high OSI (near 0.5) highlights the possible atherosclerosis prone regions (He and Ku, 1996).

3.2.6 Model Validation

3.2.6.1 Blood Flow and Velocity Distribution Study

To demonstrate the accuracy of the multiphase mixture model, an initial blood flow simulation was performed in a rectangular microchannel (Patrick et al. 2011) as shown in Fig. 3.5 with 45% of RBCs hematocrit. The inlet velocity was given as 350

$\mu\text{m/s}$ and the inlet RBC volume fraction was 0.45. Numerical results using single phase and multiphase mixture model were obtained for RBC velocity distribution under fully developed steady flow conditions and presented in Fig. 3.6 along with experimental data.

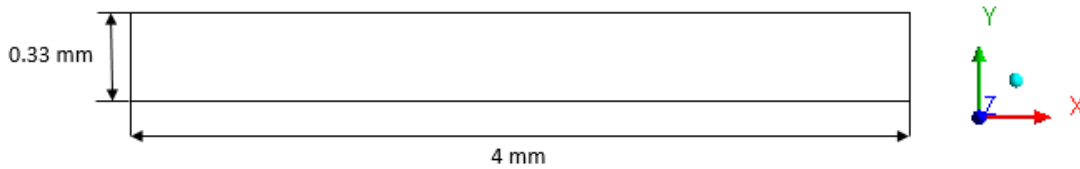


Figure 3.5 Micro-channel rectangular flow system, with $100\ \mu\text{m}$ depth in z-direction (Patrick et al. 2011)

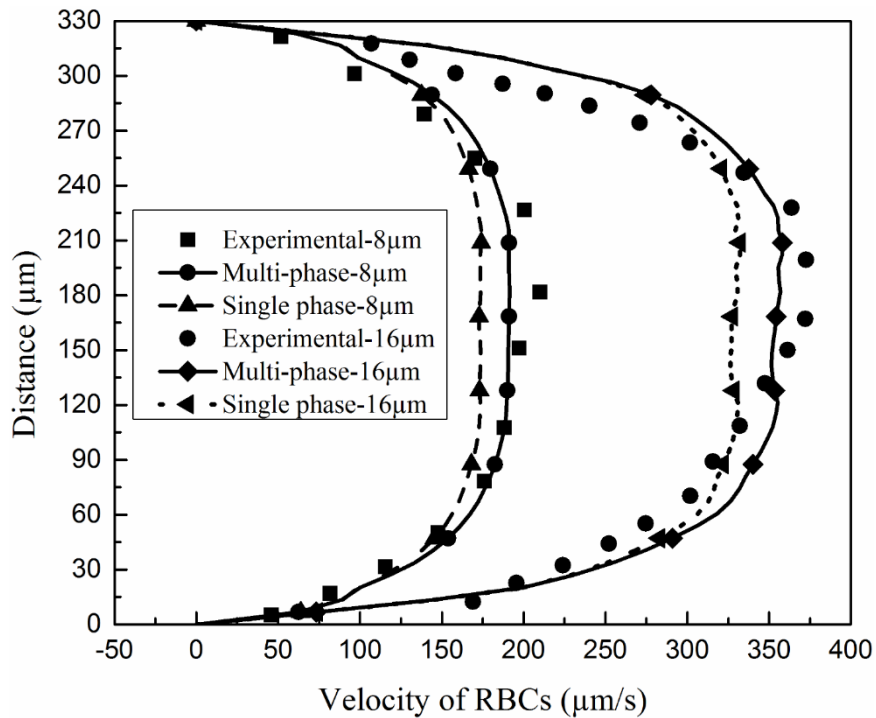


Figure 3.6 Comparison of present numerical (Single phase and Multiphase) and experimental results (Patrick et al. 2011) of RBC velocity distribution along stream-wise direction (x) as a function of the wall distance (y) at the depths $z = 8\ \mu\text{m}$ and $z = 16\ \mu\text{m}$

From Fig. 3.6 it is evident that the multiphase mixture model predicted the velocity profiles at different downstream locations in the microchannel better than

single phase model. Whereas, there is a slight discrepancy in results between the numerical simulation and experimental data, this is mainly due to the flexibility of RBCs, wall porosity and the flexibility of blood vessels which has been ignored in the present study. The percentage error between predicted peak velocities and the experimental values is quantified in Table 3.1. It is observed that the percentage error in calculated maximum peak velocity reduced significantly for the multiphase model when compared to the error corresponding to the use of single phase model. Hence, in the present study multiphase mixture theory model is employed for blood flow simulations in idealized stenosed CAs with different DOS severities.

Table 3.1 Maximum peak velocity and percentage error between single phase and multiphase model compared to experimental data at the depths $z = 8 \mu\text{m}$ and $z = 16 \mu\text{m}$

Validation study	At depth Z=8 μm		At depth Z=16 μm	
	Maximum Peak	%	Maximum Peak	%
	Velocity in $\mu\text{m/s}$	Error	Velocity in $\mu\text{m/s}$	Error
Experimental (Patrick et al. 2011)	209.92	-	373.03	-
Single-Phase Model	147.16	17.03	332.18	10.95
Multi-phase Model	191.36	8.84	358.10	4

3.2.7 Model Verification

Apart from the validation, model verification process is used to confirm the numerical results. It includes the mesh sensitivity analysis of the input parameters applied to the numerical model.

3.2.7.1 Grid Independence Study

The grid independence study has been carried out with four tetrahedral meshes for the fluid domain geometry of the idealized CA model with mesh elements 230659, 286142, 389180 and 445680. The mesh independence study was performed with

steady state boundary conditions using the laminar blood flow model by monitoring the axial velocity profile of the model at different axial locations before the stenosis (i.e., 1D and 2D) as seen in Fig. 3.7.

It can be perceived from the axial velocity profiles plot that meshes with 286142 and 389180 elements are following the same velocity profile trend of finest mesh elements 445680. Hence, the model with 389180 mesh elements was considered for further numerical analysis which reduces the calculation time without negotiating accuracy of the results. Also, the same number of mesh elements is adopted for all stenosed artery models.

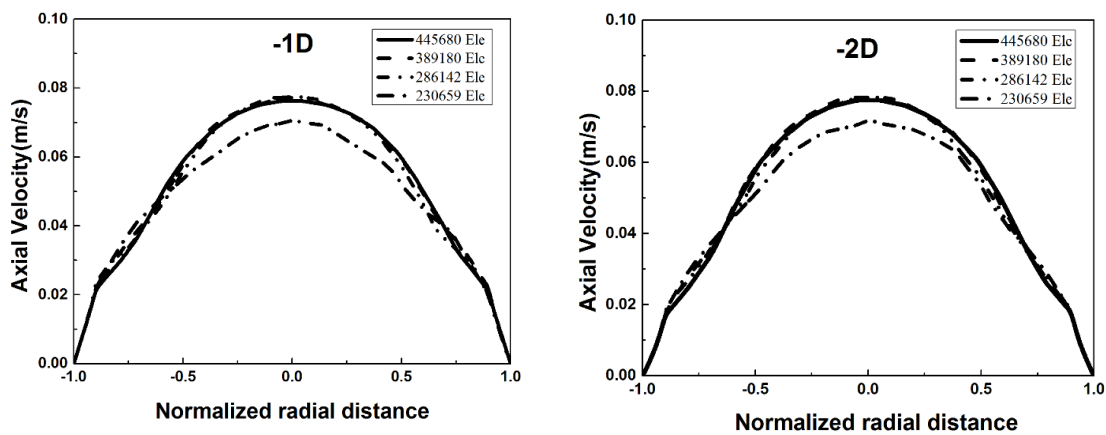


Figure 3.7 Axial velocity profiles measured at distances 1D and 2D, before the stenosis region for different grid elements

3.3 RESULTS

The demonstration of numerical results emphasizes on multiphase blood flow through idealized straight CAs with different DOS severities. All results were obtained for peak flow at the onset of diastole when the blood velocity reaches maximum at inlet for one cardiac cycle. A detailed numerical analysis of WSS based HDs distribution such as TAWSS, TAWSSG and OSI over the artery wall has been calculated for different DOS severities.

3.3.1 Distribution of WSS and WSS Based HDs

In various blood flow studies, it has been revealed that distribution of high OSI and low WSS are strongly correlated with the crucial spots of atheroma (He and Ku, 1996). Furthermore, the wall permeability is enhanced and atherosclerotic locations spread to sites where the WSSGs are large (DePaola et al. 1992) and amalgamation of high WSS and high exposure times for blood particles can lead to platelets activation (Ramstack et al. 1979, Hellums 1994, Hosseinzadegan and Tafti, 2017). Hence, in this multiphase non-Newtonian blood flow study, the spatial distributions of WSS based hemodynamic parameters including WSS, TAWSS, TAWSSG (Ryou et al. 2012, Buchanan et al. 2003, Ellwein et al. 2011) and OSI (He and Ku, 1996) were calculated according to (Eq. 3.27-3.30) respectively, and compared the same for different DOS severities in idealized human CA.

3.3.1.1 WSS Distributions in Stenosed Arteries

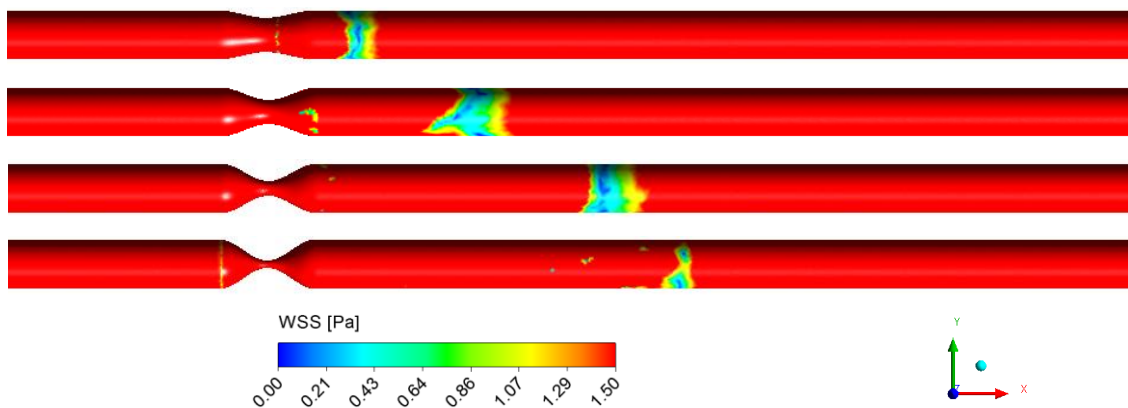


Figure 3.8 WSS distributions in idealized CA for different DOS severity models for one cardiac cycle at 0.55s

Figure 3.8 illustrates the effect of DOS severity on the WSS distributions. Though the peak WSS changes from 0 to several hundreds of Pascal for all the DOS cases it is believed that the neointimal growth risk is higher when the luminal surface subjected to lower WSS than the physiological levels of WSS (<1.5 Pa) (Malek et al. 1999, LaDisa et al. 2005a). Hence, in Fig. 3.8 WSS is plotted for a range of 0-1.5 Pa in order to study the change in clinically relevant sites for various DOS. Comparing the WSS contour plots between different DOS models in Fig. 3.8 the stenosis formation

had a noticeable influence on the WSS distributions. Especially large areas of the low WSS endothelial surface are visible in the distal section of the stenosis which is mainly due to low velocity in that region. Also, it is seen that the low WSS (<1.5 Pa) sites in post stenosis region increases for 30% stenosis to 70% stenosis, whereas it decreases for 85% stenosis models.

3.3.1.2 TAWSS Distributions in Stenosed Arteries

For analyzing the hemodynamics in the artery, TAWSS is averaged over one pulsatile cycle. Figure 3.9 illustrates the effect of DOS severities on the TAWSS distributions. The TAWSS sites where the values are ≥ 10 Pa are shown in red colour. These sites are of clinical relevance as high values of TAWSS (≥ 10 Pa) can lead to the damage of ECs (Suess et al. 2016). Hence, in Fig. 3.9 TAWSS is plotted for a range of 0-10 Pa in order to study the change in clinically relevant sites for various DOS. The low TAWSS is associated with low velocity and subsequently suggest the more likely occurrence of particle immobility. The TAWSS is high (≥ 10 Pa) in the stenosis region for 30% and 50% stenosis models whereas for 70% and 85% stenosis models the TAWSS high (≥ 10 Pa) regions are observed both in stenosis and distal region. Further, as the DOS severity increases TAWSS consistently increases both in stenosis throat and downstream regions.

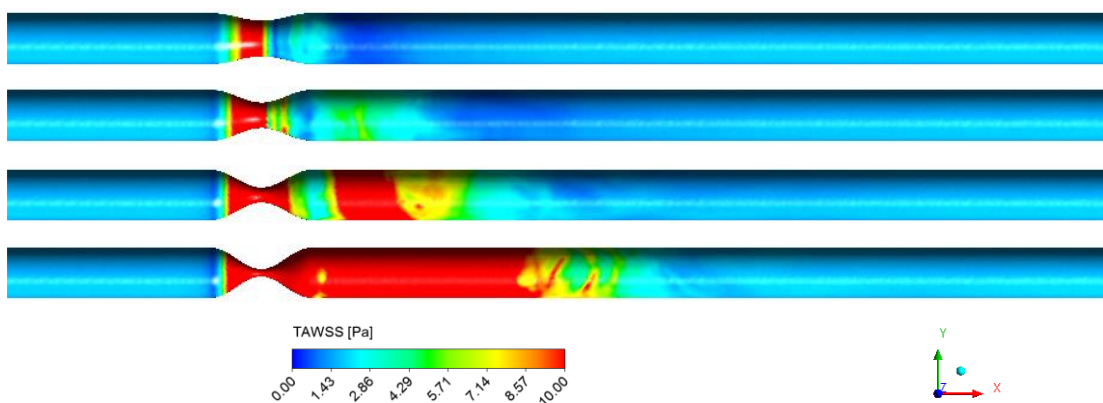


Figure 3.9 TAWSS distributions in idealized CA for different DOS severity models averaged over one pulsatile cycle

3.3.1.3 TAWSSG Distributions in Stenosed Arteries

The TAWSSG is a transient blood flow property correlated to the wall of the artery. Speedy WSS changes over short distances are measured by the TAWSSG. Figure 3.10 illustrates the effect of DOS severities on the TAWSSG distributions. The magnitudes of TAWSSG for all stenosis models were ranging from 0 to 200 Pa m⁻¹. The endothelial surface area higher than the physiological levels of TAWSSG (≥ 200 Pa m⁻¹) have been associated to atherosclerotic lesions formation, intimal hyperplasia, and accelerate platelet activation and thrombus formation (DePaola et al. 1992, Hosseinzadegan and Tafti, 2017). Hence, in Fig. 3.10 TAWSSG is plotted for a range of 0-200 Pa m⁻¹ in order to study the change in clinically relevant sites for various DOS. The large values of TAWSSG (≥ 200 Pa m⁻¹) were observed in the stenosis throat region for 70 and 85% DOS severity models, whereas for the 30 and 50% stenosis models low TAWSSG values ranging from 0 to 57.14 Pa m⁻¹ only was seen.

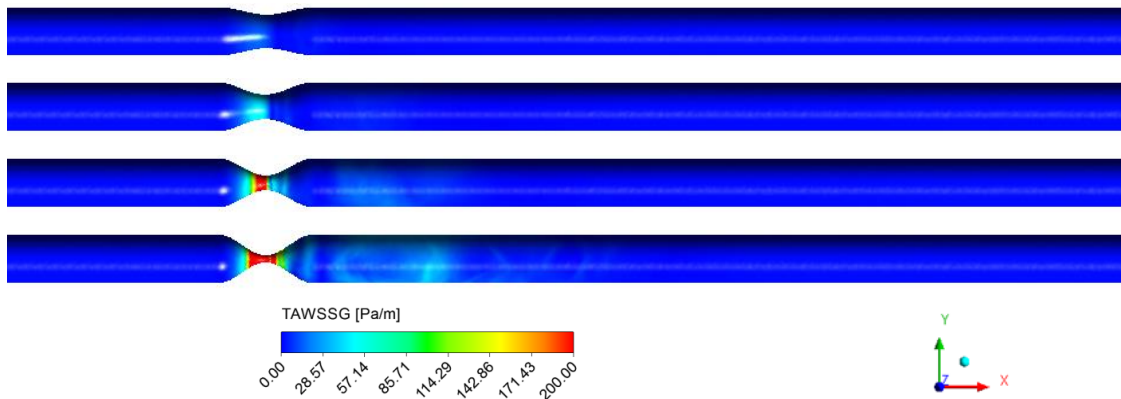


Figure 3.10 TAWSSG distributions in idealized CA for different DOS severity models over one cardiac cycle.

3.3.1.4 OSI Distributions in Stenosed Arteries

The OSI is a WSS based dimensionless hemodynamic parameter that provides a measure of the oscillating nature of WSS. Figure 3.11 depicts the distribution of OSI contours predicted on the artery luminal surface for different DOS severity models over one pulsatile period. It is believed that the neointimal growth risk is higher when the luminal surface is exposed to higher OSI than the physiological levels of OSI

(>0.3) and hence susceptible to atherogenesis and ED (Ku et al. 1985, Davies 1995, Thury et al. 2002). In Fig. 3.11, OSI contours were plotted for a range of 0-0.3 Pa in order to study the change in clinically relevant sites for various DOS. The higher OSI values were predicted in the distal region of the stenosis and in downstream region of the stenosis for all DOS severity models.

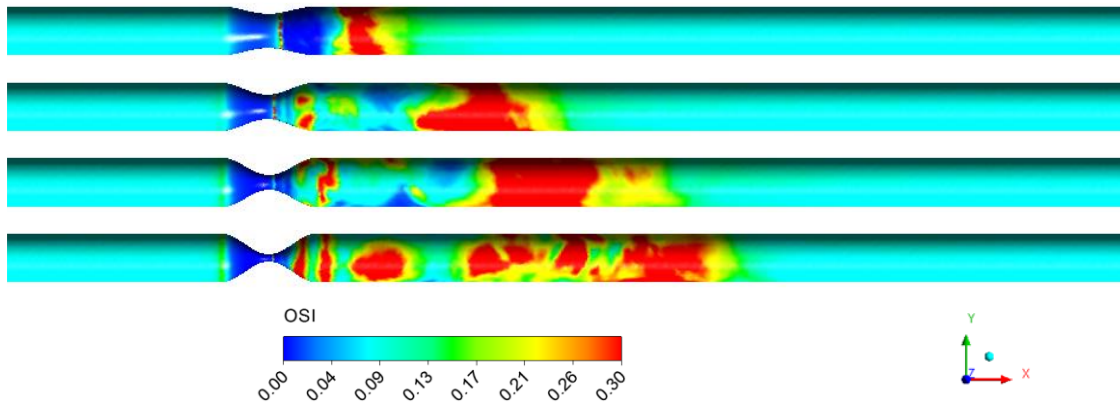


Figure 3.11 OSI distributions in idealized CA for different DOS severity models and averaged over one pulsatile cycle

The maximum and average values of WSS and WSS based HDs and their percentage increase from the baseline value of 30% DOS were tabulated in Table 3.2 and 3.3 respectively. A relatively high positive correlation was observed in maximum and average values of WSS, TAWSS and TAWSSG with DOS and the indicators value increases as the DOS severity increase. However, the OSI indicator is relatively less affected by the DOS.

3.4 DISCUSSIONS

The present multiphase blood flow study demonstrated that the presence of different DOS severities in CAs produces a synergistic effect on the subsequent WSS and WSS based HDs distribution. The variation in the lumen surface area of potential atherosclerotic lesion sites based on WSS, TAWSS, TAWSSG and OSI indicators were studied using their corresponding clinically proven threshold values above or below which endothelial pathological response is induced. The changes in WSS based hemodynamic indicators with respect to DOS were quantified. This is clinically

significant as these hemodynamic changes will contribute to further atherosclerotic progress in the CA leading to potential damage to the arterial wall.

Healthy WSS levels for arteries was reported to vary between 2 to 16 Pa (Cheng et al. 2007). The WSS as low as 1.5 Pa (Malek et al. 1999) triggers a biological inflammatory process which leads to the development of atheromatous plaque. From Fig. 3.8, it is observed that WSS regions having less than 1.5 Pa increases with DOS up to 70% and reduces drastically for 85% DOS. This may be due to the fact that blood flow through 85% stenosis behaves like a strong jet with high velocity after the stenosis and hence high WSS.

For DOS 30% and 50% endothelial surface sites where TAWSS ≥ 10 Pa were found to occur only in the proximal region of stenosis as a result of protuberance of the plaque which leads to the effective flow area reduction (c.f. Fig. 3.9). The endothelium surface experiencing TAWSS ≥ 10 Pa spreads to distal regions of the stenosis for DOS greater than 50%. Hence, damage to ECs in the distal regions likely to occur only when DOS severity increases beyond 50%. Also, higher levels of TAWSS is naturally expected when the fluid flow is maximum i.e., at the cycle systole, where maximum amount of fluid flows through the artery.

In the stenosed artery region as the cross sectional area reduces the peak fluid velocity increases. TAWSSG is a strong function of peak velocity at the center of the artery cross section hence, pathological levels of TAWSSG (>200 Pa m^{-1}) were observed only around the stenosis throat region (Fig. 3.10). It is interesting to note that adverse clinical outcomes such as intimal hyperplasia and accelerated platelet activation linked with TAWSSG > 200 Pa m^{-1} indicator value is likely to occur for DOS $\geq 50\%$ and more likely to occur at the throat than anywhere else in the stenosis.

Table 3.2 Maximum WSS and WSS based HDs and their % increase for different DOS severities

DOS in %	WSS in Pa		TAWSS in Pa		TAWSSG in Pam ⁻¹		OSI	
	Maximum	% Increase	Maximum	% Increase	Maximum	% Increase	Maximum	% Increase
30	118.38	-	36.65	-	36.23	-	0.495	-
50	144.06	21.69	47.80	30.42	47.19	30.52	0.496	0.23
70	881.22	644.39	283.56	673.69	281.95	678.22	0.497	0.47
85	7030.2	5838.67	2608.01	7015.98	2597.67	7069.94	0.495	-0.016

Table 3.3 Average WSS and WSS based HDs and their % increase for different DOS severities

DOS in %	WSS in Pa		TAWSS in Pa		TAWSSG in Pam ⁻¹		OSI	
	Average	% Increase	Average	% Increase	Average	% Increase	Average	% Increase
30	4.11	-	1.69	-	1.43	-	0.08758	-
50	4.82	17.27	1.98	17.15	1.69	18.18	0.09571	9.28
70	8.33	102.67	3.25	92.30	2.78	94.40	0.10349	18.16
85	35.33	759.61	14.16	737.86	12.94	804.89	0.10398	18.72

The OSI is used to measure the oscillating nature and the cyclic departure of WSS magnitudes from its main flow direction. The regions with high OSI value experiences severe stretching and compression of endothelial wall which quickens the rupture of plaque and cause sufficient ECs damage. Comparing the OSI contours (Fig. 3.11) it is clear that the regions of the arterial wall surface subjected to higher physiological value ($OSI > 0.3$) steadily increases with increase in DOS. Also, the length of the artery distal section affected by OSI above 0.3 consistently increases with DOS severity.

The percentage change in maximum and average values of WSS, TAWSS, TAWSSG and OSI with respect to DOS is quantified in Table 3.2 and 3.3. It is observed that the values increase almost linearly up to DOS 50% and exponentially with DOS beyond 50% DOS. Though potential atherosclerotic sites increase steadily with DOS in general, the increase is exponential with respect to DOS beyond 50%. It is also observed that the maximum value of OSI does not vary with DOS whereas the average value of OSI changes linearly up to 70% DOS and remains unaffected above 70% DOS. This is due to the fact that OSI is strongly dependent on flow pulsatility and turbulence generated. In the present study flow pulsatility is kept constant for all the DOS severities.

3.4.1 Limitations of the Study

In present study, the idealized CA model with DOS severities were analyzed quantitatively in terms of WSS based HDs. This model approaches with an assumption that the blood behaves as a mixture of blood borne particulates and that mixture is considered to be continuum. The present study considers laminar blood flow through a non-compliant artery instead of turbulent flow, as a recent study by Mahalingam et al. (2016) showed that in stenosed CAs the blood flow becomes turbulent in nature for 70% stenosis and above whereas, the transition to turbulent flow is begins from 50% stenosis.

3.5 SUMMARY

In this chapter, to the best of our knowledge, we have addressed for the first time a multiphase blood flow study using mixture-theory to investigate the WSS and WSS based HDs in idealized CA for different DOS severities. A hemodynamic model based on mixture theory is utilized to study the transport and interactions of RBCs in the blood plasma. Further, the model was validated with the earlier reported experiments and demonstrated to be more accurate than single phase models. If the stenosis severity is more than 50%, the WSS is very high in stenosis throat and the formation of recirculation zone is higher in post-stenosis region. The risk of plaque rupture increases for the degree of stenosis above 70% due to very high WSS (> 800 Pa).

It can be concluded that WSS and WSS based hemodynamic indicators were significantly affected by the presence of stenosis and increases with DOS. The values of indicators increase exponentially with DOS above 50% suggesting that the plaque progression rate could be substantially accelerated in the region distal to stenosis for DOS beyond 50%.

This detailed multiphase hemodynamic analysis gives information for deeper understanding of the atherosclerosis formation and plaque progression. Based on the obtained results with the problems studied, we believe that the current multiphase mixture model can be a useful numerical tool for analyzing the blood flow and its transport within the stenosed artery models. Finally, for clinical usage, the average value of OSI must be used in order to represent the risk instead of maximum values of OSI.

CHAPTER 4

IMPACT OF CORONARY TORTUOSITY ON THE ARTERY HEMODYNAMICS

4.1 INTRODUCTION

Normally CAs are not tortuous, sometimes the branches of the left and right CAs show tortuosity that have a major impact on the supply of blood to the heart during exercise and at rest. Generally, the tortuosity is observed in the left anterior descending (LAD) branch of CA and the degree of tortuosity varies from mild to severe depending on the curves of the blood vessel (Li et al. 2011, Himabindu 2018). For efficient transport of blood, the arteries are normally straight and they show tortuosity due to abnormal arterial remodeling (Himabindu 2018, Han 2012). Tortuosity in CAs leads to a variation of blood flow causing a reduction in blood pressure distal to the tortuous segment of CA leading to ischemia. It is also linked with prolonged stable angina reversible myocardial perfusion defects (Yang et al. 2012), arterial hypertension, age, diabetes mellitus and atherosclerosis (Li et al. 2011, Han 2012). The person with tortuosity in CAs often suffers from chest pain during exercise that disappears typically at rest (Yang et al. 2012, Gaibazzi et al. 2011). The presence of sharp bends in tortuous CAs results in separation and disruption of laminar blood flow. This result in loss of energy and increase in artery WSS that may weaken the artery and lead to spontaneous coronary artery dissection (SCAD), a leading source of the acute coronary syndrome affecting young individuals (Zegers et al. 2007).

Recently, only few computational studies have used CFD technique to investigate the impact of tortuosity in arteries by considering blood as a single-phase fluid. The computational study by Qiao et al. (2004) proposed that tortuosity in CAs leads to blood flow alteration. The shear stress on arterial lumen is also altered owing

to the presence of tortuosity (Liu et al. 2008). In microvessels the tortuosity was believed to trigger thrombus formation by platelet activation (Chesnutt and Han 2011). Xie et al. (2013a) performed a patient-specific numerical study to examine the influence of the coronary tortuosity on coronary hemodynamics. CFD analysis was performed on two 3D LAD patient-specific CA models by considering blood as Newtonian incompressible fluid. The study revealed that due to the presence of tortuosity in CAs the blood flow rate has decreased by 8% than mean blood flow rate under the resting condition, whereas it decreased by 14.9% under exercise conditions. Hence, it was concluded that tortuosity in CAs has more influence on coronary hemodynamics during exercise than at rest conditions. The numerical study of Xie et al. (2013b) showed the formation of low and oscillating WSS at coronary tortuosity bends at the inner side of the wall and in downstream of the bend section. This study also revealed that tortuosity in CAs has a lesser influence on blood flow at rest condition; however, tortuosity may represent larger resistance to blood flow up to 92% during exercise conditions that may lead to failure of coronary autoregulation.

Li et al. (2012) executed several numerical simulations using finite volume (FV) method to evaluate the coronary tortuosity impact on the distribution of coronary pressure inside the coronary blood flow. They used 21 idealized artery models with varying coronary tortuosity number (0, 1, 2, 3, 4, and 5) and angle (30, 60, 90, and 120 degrees) with Newtonian 2D incompressible flow assumption. Their study revealed that more the severity of coronary tortuosity angle and number, more was the pressure drop between the start and end of the tortuosity segment which may lead to myocardial ischemia. Xie et al. (2014) performed a parametric morphological study on 3D left tortuous CA and computed the blood flow. The study revealed that the length between bends and center line radius had more effect on the WSS derived descriptors whereas bend angle had less effect on the blood flows in tortuous arteries. Vorobtsova et al. (2016) carried a computational study on patient-specific and idealized CAs to investigate the tortuosity influence on hemodynamics. The result shows that with increasing tortuosity there is a decrease in perfusion pressure. The results of patient specific model showed higher physiological WSS for more tortuous arteries.

Until recently there was little attention paid on underlying HDs in tortuous CAs by considering blood as a non-Newtonian multiphase fluid. Several experimental studies (Haynes 1960, Stadler and Zilow 1990, Egorov et al. 1994) have observed blood's multicomponent nature and concluded that modelling of blood requires a multiphase approach. Buradi and Mahalingam (2018) compared the single phase model and multi-phase model for the simulation of blood flow through stenosed arteries. They concluded that multiphase approach reduced the simulation error by 50%. In the present study, to the best of knowledge of the authors, for the first time, computational modelling with multiphase mixture theory model is employed to analyze the influence of coronary tortuosity on blood flow and HDs in idealized CA with varying different tortuosity morphological indices. The tortuosity morphological indices namely, the angle of bend (AoB), distance between bends (DBB) and a curvature radius (CR) are important morphological indices characterizing the tortuosity in CAs. Finally, the HDs, namely TAWSS, OSI, RRT, TAWSSG, and ECAP were calculated to identify the artery wall regions prone to atherogenesis and endothelial dysfunction in tortuous CAs.

4.2 MATERIALS AND METHODS

4.2.1 Geometric Model of the Idealized Tortuous Coronary Artery

For the computational multiphase blood flow analysis, a 3D idealized tortuous CA models were created by choosing the three different morphological indices namely, the CR, the DBB, and the AoB that fully characterize the tortuous geodesic patterns of CA. The Fig. 4.1 shows the idealized tortuous CA geometry with a set of boundary conditions, different morphological indices and the region of interest. To examine the impact of these three different tortuous morphological indices on the distribution of various HDs the idealized artery models were created with the CR of 3, 4.5 and 6 mm, the DBB of 0, 3, and 6 mm, and the AoB of 90° , 120° , 150° and 180° . All the idealized tortuous artery models were created as circular conduits with a constant diameter of $d=4$ mm. Geometry consists of two bend sections viz. bend section 1 (BS1) and bend section 2 (BS2). Both outlet and inlet of bend sections were

protracted by 50 mm to reduce the boundary conditions influence while ensuring the smooth flow entry.

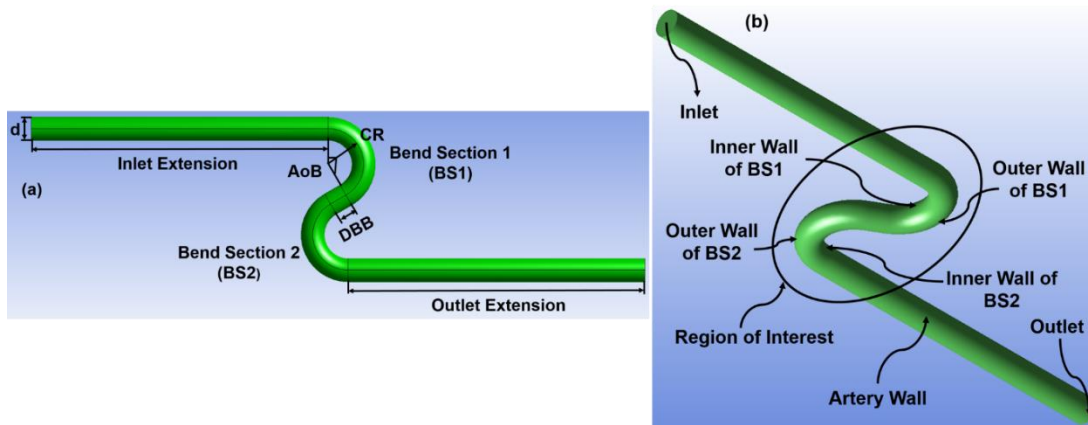


Figure 4.1 Geometry of the tortuous CA. (a) Idealized tortuous artery model with three different morphological indices: the CR, the AoB, and the DBB. (b) Artery model with 150° AoB, 6mm CR and 3 mm DBB showing the different boundary conditions and region of interest

4.2.2 Governing Equations

In this chapter the multiphase mixture approach is applied to investigate the characteristics of HDs in idealized tortuous CA with varying different morphological indices. Under multiphase mixture approach, the blood is modelled as a multiphase fluid considering the suspension of red blood cells in viscous plasma. The blood is presumed to be non-Newtonian, incompressible, and homogeneous fluid. To solve the set of governing equations the multiphase mixture theory model is employed. The detailed explanation regarding the multiphase mixture approach and the model equations were given in detail in chapter 3.

4.2.3 Computational Modelling

4.2.3.1 Computational Mesh Generation and Mesh Independence Study

The Fig. 4.2 shows the computational mesh used for the computational hemodynamic analysis. Prism layers at the inlet were applied to capture the flow effects near the

wall. The computational mesh is created using ANSYS ICEM CFD (ANSYS Inc. 2012) software. In detail a mesh independence study was carried out by discretizing the whole computational domain using an unstructured tetrahedral mesh on representative model geometry having AoB150⁰, CR6, DBB3.

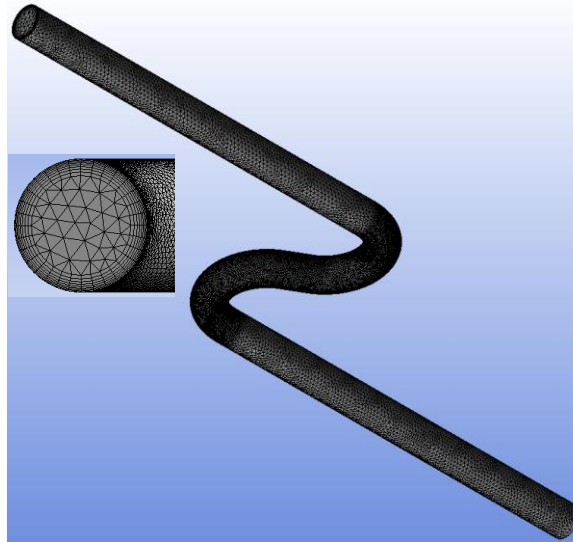


Figure 4.2 Computational mesh model with prism layers to capture flow effects near the wall

Table 4.1 Number of mesh elements and grid independence study results

Number of Elements	Peak velocity [m/s]	Percentage Difference [%]	Max. WSS [Pa]	Percentage Difference [%]	Avg. WSS [Pa]	Percentage Difference [%]
1,57,023 (coarse)	0.969	1.048%	42.104	6.96%	10.032	2.09%
2,35,534 (medium)	0.980	0.982%	45.144	1.20%	10.245	1.38%
3,53,301 (fine)	0.989	-	45.692	-	10.104	-

Three different meshes were created namely coarse, medium and fine mesh by increasing the number of mesh elements by a factor of 1.5 between each consecutive mesh: 1,57,023, 2,35,534, 3,53,301 elements. The different meshes were compared by calculating the peak WSS on the wall and maximum velocity in the fluid domain. The results are listed in Table 4.1. The percentage change among the medium and fine mesh was lesser than 1% for the peak velocity and 1.5% for the maximum and average WSS as compared to coarse mesh. Hence the medium mesh with 2,35,534 elements was selected for further calculations and a similar number of mesh elements were used for other geometries.

4.2.3.2 Boundary Conditions

In this chapter, the fluid and rheological properties of blood are used to perform a transient simulation in idealized tortuous CAs with varying morphological tortuous indices. The volume inflow time-dependent velocity profile obtained from Berne and levy (1967) shown in Fig. 4.3 was used as inlet velocity boundary condition for both primary (plasma) and secondary (RBC) phases. At inlet the density of RBC and plasma were chosen as 1096 kg/m^3 and 1003 kg/m^3 respectively (Huang et al. 2009). The RBCs were assumed to be spherical particles with $8 \text{ }\mu\text{m}$ as average diameter and RBC volume fraction is maintained steady and uniform with 45% at the inlet. The no-slip and outflow conditions were applied as wall and outlet boundary conditions respectively for both plasma and RBCs.

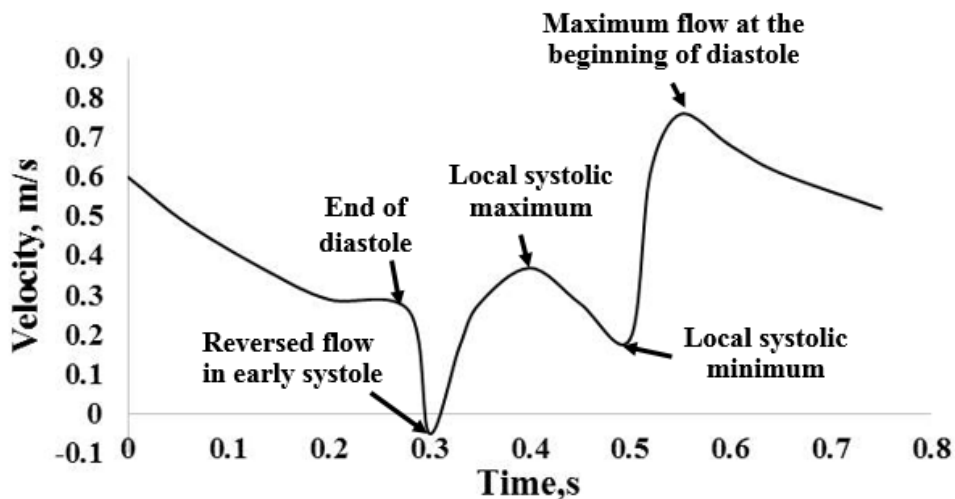


Figure 4.3 In-flow velocity profile for blood (plasma and RBC) during one pulsatile cycle (Berne and Levy 1967)

4.2.3.3 Computational Fluid Dynamics Simulation Settings

To carry out the multiphase hemodynamic analysis, the ANSYS Fluent V.14.5 (ANSYS Inc. 2012) was used which is based on the FV method. The coupled scheme with pressure based solver was used for the pressure-velocity coupling. Whereas, for transient formulation the second order implicit scheme was adopted. For the spatial discretization of pressure and momentum the PRESTO (PREssure Staggering Option) scheme and second order upwind schemes were chosen respectively. The Courant number for the flow was set to 200. For the pressure and momentum, the explicit relaxation factors were set to 0.75. The under-relaxation factors for the density and slip velocity were set to 1 and 0.1 respectively. For velocity and continuity residuals the convergence criterion was set to 10^{-4} and 10^{-5} respectively. For each cardiac cycle a time step of 0.001s with 500 time steps was used. Three cardiac cycles were simulated to ensure a repeatable solution and the results are obtained for the second cycles to analyze the distribution and variation of different HDs for different tortuous artery models.

4.2.4 WSS Based Hemodynamic Descriptors

Over the last few decades there has been a substantial attention on describing the different HDs that stimulate EC gene manifestation and leads to both pro-thrombogenic and pro-atherosclerotic phenotypes. To identify arterial EC regions, open to both oscillatory and low shear flows that stimulate a pro-atherosclerotic phenotype (Chiu and Chien, 2011, Wolberg et al. 2012) five different HDs were evaluated in terms of TAWSS, TAWSSG, OSI, RRT and ECAP near the wall. These different descriptors were also used to quantify its local magnitude, spatial and temporal variations and the WSS gradient accomplished by the arterial endothelial surface. TAWSS, TAWSSG, and OSI are defined by equations (3.28), (3.29) and (3.30) respectively.

The ratio of both high OSI and low TAWSS were used to identify the regions of the wall which has more thrombogenic susceptibility by using the parameter called ECAP (Di Achille et al. 2014). A value of higher ECAP corresponds to situations of low TAWSS and high OSI, which represents endothelial susceptibility. The ECAP is defined as:

$$ECAP = \frac{OSI}{TAWSS} \quad (4.1)$$

RRT is an HD used to pinpoint the regions of oscillatory and low WSS (Himburg et al. 2004) and to locate the regions in which high particle residence time befalls. High OSI and low TAWSS values are identified to promote a pro-atherogenic endothelial phenotype (He and Ku, 1996, Malek et al. 1999). The RRT is expressed as:

$$RRT = [(1 - (2 \times OSI)) \times TAWSS]^{-1} \quad (4.2)$$

4.2.5 Multiphase Eulerian and Mixture Theory Models

To compare the performance of present multiphase mixture model with Euler-Euler multiphase model, a blood flow simulation was performed in a rectangular microchannel (Patrick et al. 2011) as presented in Fig. 4.4. At inlet the velocity and volume fraction of RBC was given as 350 $\mu\text{m/s}$ and 0.45 respectively. Figure. 4.5 shows the numerical results of RBC velocity distribution obtained for multiphase Eulerian and mixture theory model and compared with the experimental data of Patrick et al. (2011).



Figure 4.4 Rectangular micro-channel flow system, with depth 100 μm in z-direction (Patrick et al. 2011)

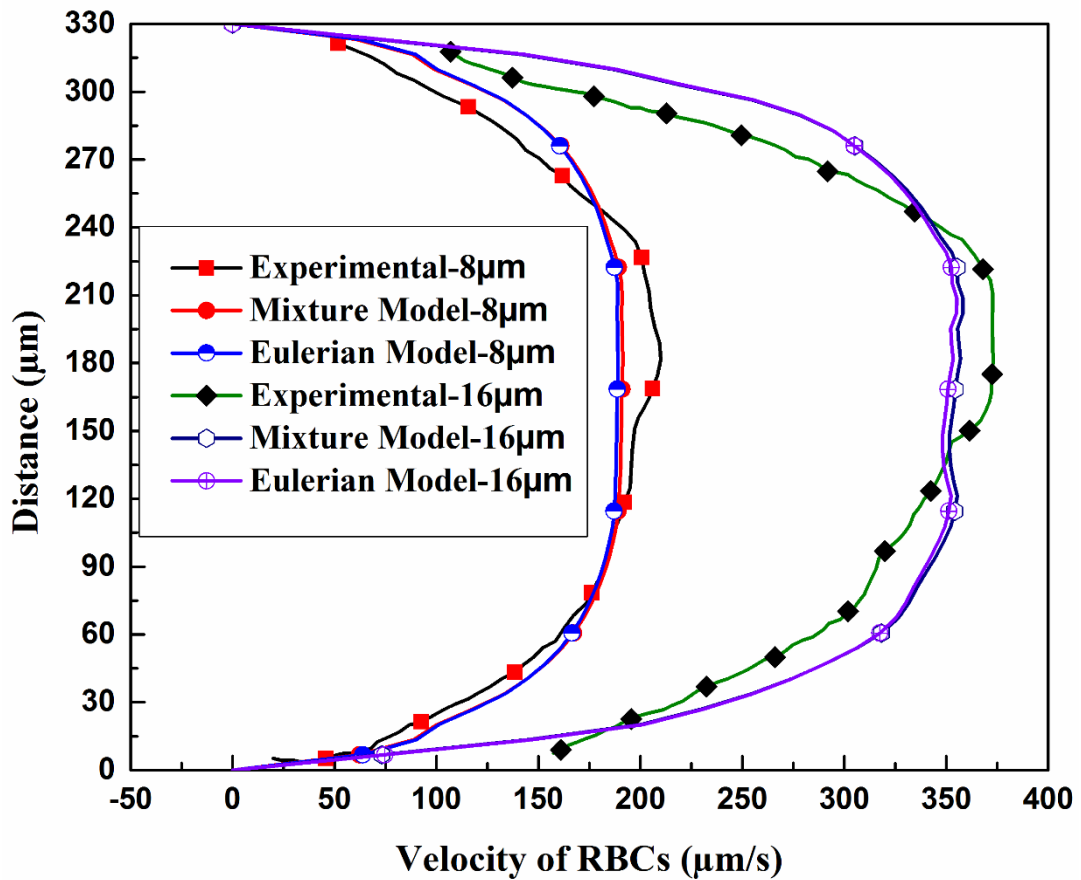


Figure 4.5 RBC velocity distribution comparison between present multiphase Eulerian, multiphase mixture model and experimental (Patrick et al. 2011) results along x-direction as a function of the wall distance (y) at $Z=8\ \mu\text{m}$ and $16\ \mu\text{m}$ depth

From Fig. 4.5 it is evident that the present multiphase mixture model predicted the RBC velocity profiles better than multiphase Eulerian model at different locations in the microchannel. However, there is a minor inconsistency in results among the experimental data and numerical simulation. This is mainly due to the wall porosity, flexibility of RBCs and the deformation of blood vessels which has been neglected in the present study. The percentage error between the experimental data and predicted peak velocity values are quantified in Table 4.2. It is observed from Table 4.2 that the percentage error in predicted peak velocities is reduced reasonably for the multiphase mixture model when compared with the Eulerian multiphase model. Therefore, in the present computational analysis the multiphase mixture theory model is employed for

simulation of hemodynamics in idealized tortuous CAs with varying morphological tortuosity indices.

Table 4.2 Comparison of peak velocity and percentage error between present multiphase Eulerian, mixture models and experimental (Patrick et al. 2011) data along at Z=8 μm and 16 μm depth

Validation Results	At Z=8 μm depth		At Z=16 μm depth	
	Peak velocity in $\mu\text{m/s}$	Error in %	Peak velocity in $\mu\text{m/s}$	Error in %
Experimental (Patrick et al. 2011)	209.92	-	373.03	-
Eulerian multiphase model	189.04	9.94	355.17	4.78
Mixture multiphase model	191.36	8.84	358.10	4

4.3 RESULTS

The numerical analysis using multiphase mixture theory model has been carried out to evaluate the distribution of five HDs viz., TAWSS, TAWSSG, OSI, RRT, and ECAP on the arterial luminal surface along the length of the artery. As mentioned earlier, the objective of the present study is to quantify the effect of various morphological indices such as CR, DBB and AoB on the HDs.

4.3.1 Effect of CR on HDs

The contours of the velocity field are presented at maximum blood flow and at the beginning of diastole ($t=0.55\text{s}$) for all tortuous artery models with varying morphological tortuosity indices. The velocity contours for different CRs and AoBs are shown in Fig. 4.6. At the inner walls of the BS1 and BS2 and outer wall of BS2 low velocity regions are observed due to the flow recirculation in those regions. As

observed from the Fig. 4.6, the high velocity regions reduce in magnitude as the CR and AoB increases.

Table 4.3 The maximum WSS based HDs for different CRs and AoBs (DBB= 0 mm)

Models Studied	CR, mm	Max. TAWSS, Pa	Max. TAWSSG, Pa/m	Max. OSI	Max. RRT, Pa⁻¹	Max. ECAP
AoB90 ⁰	3	30.136	29.781	0.440	16.891	1.075
	4.5	23.502	23.336	0.444	21.652	1.138
	6	16.649	16.395	0.481	63.186	1.145
AoB120 ⁰	3	28.498	28.292	0.450	14.971	1.029
	4.5	20.964	20.715	0.477	33.512	1.108
	6	20.667	20.410	0.480	43.588	1.136
AoB150 ⁰	3	35.313	35.010	0.452	22.940	0.991
	4.5	25.497	25.258	0.466	29.495	1.099
	6	17.296	16.987	0.471	31.461	1.185
AoB180 ⁰	3	35.254	34.929	0.465	28.812	1.083
	4.5	19.487	19.235	0.472	38.987	1.174
	6	15.629	15.412	0.481	43.646	1.219

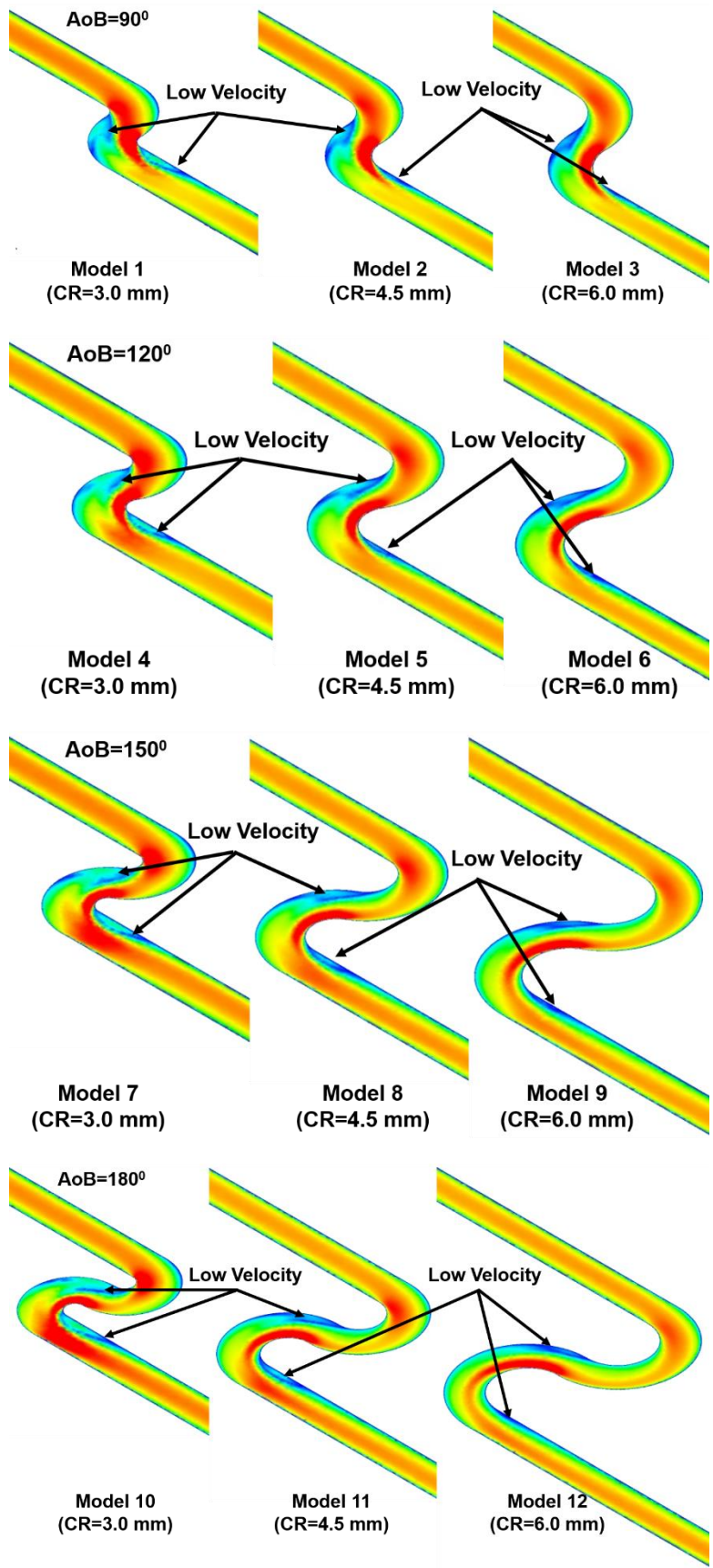
The influence of CR on TAWSS, TAWSSG, OSI, RRT and ECAP distribution were shown in Figs. 4.7-4.11 respectively and demonstrated for three different CRs (3, 4.5 and 6 mm), for four AoBs (90⁰, 120⁰, 150⁰, and 180⁰) and for DBB= 0 mm. High TAWSS and TAWSSG were observed in the sides of both the bend sections. Low TAWSS and TAWSSG were observed at the outer walls of BS1 and BS2 and at downstream portion of the BS2's inner wall curvature. Through observation it is found that the area of regions with low TAWSS and TAWSSG increases whereas, high TAWSS and TAWSSG area decreases with the increase of CR and increases with AoB. From Figs. 4.9 and 4.10, it is observed that the regions of high OSI increases with CR and AoB whereas the regions of high RRT increases only with CR and remains fairly unchanged with AoB. These trends are captured

quantitatively in Table 4.3 and 4.4 where the peak and average variations of different HDs for different CRs and AoBs are reported.

Table 4.4 Average variation of WSS based HDs for different CRs and AoBs (DBB= 0 mm)

Models Studied	CR, mm	Avg. TAWSS, Pa	Avg. TAWSSG, Pa/m	Avg. OSI	Avg. RRT, Pa⁻¹	Avg. ECAP
AoB90 ⁰	3	4.450	4.211	0.0364	0.345	0.0162
	4.5	4.314	4.063	0.0372	0.360	0.0177
	6	4.282	4.036	0.0377	0.369	0.0184
AoB120 ⁰	3	4.587	4.356	0.0352	0.351	0.0170
	4.5	4.530	4.297	0.0354	0.357	0.0178
	6	4.448	4.216	0.0362	0.378	0.0195
AoB150 ⁰	3	4.766	4.527	0.0357	0.327	0.0155
	4.5	4.614	4.384	0.0345	0.355	0.0169
	6	4.475	4.237	0.0370	0.368	0.0198
AoB180 ⁰	3	4.908	4.686	0.0329	0.357	0.0175
	4.5	4.722	4.502	0.0339	0.360	0.0181
	6	4.507	4.269	0.0360	0.367	0.0185

Regions of high OSI, high RRT and high ECAP coincides with the areas of low TAWSS and TAWSSG as observed from Figs. 4.9-4.11. From Table 4.3 and 4.4, it can be inferred that the maximum OSI, RRT and ECAP were observed for the model having the largest CR of 6 mm. Overall OSI, RRT and ECAP were found to increase with CR.



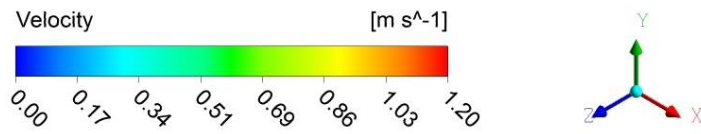
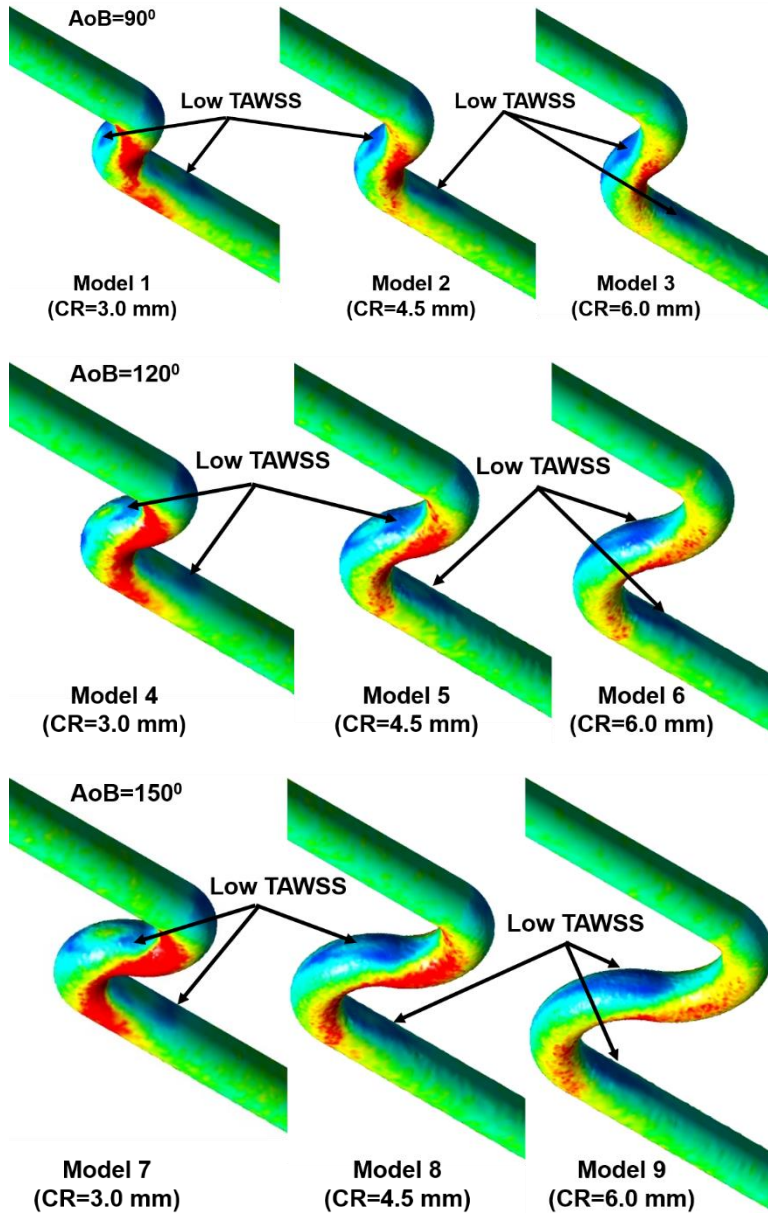


Figure 4.6 Spatial distributions of the velocity contours obtained at maximum flow rate ($t=0.55s$) for different CRs and AoBs with constant DBB= 0 mm



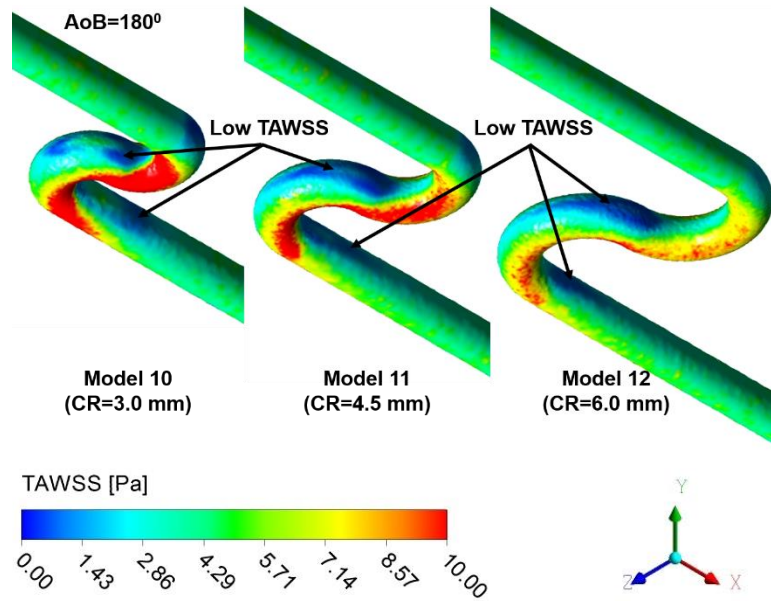
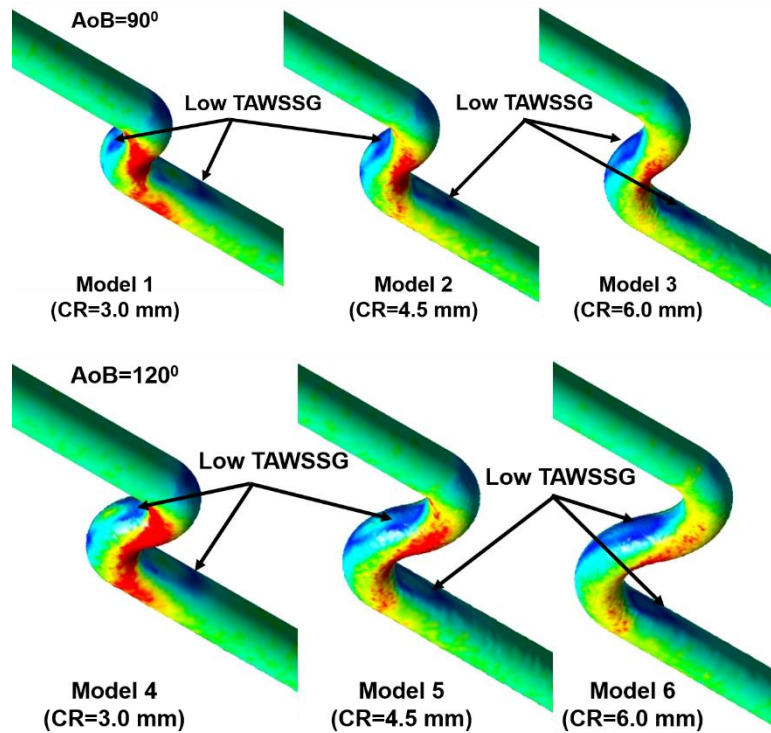


Figure 4.7 Spatial distributions of the TAWSS contours for different CRs and AoBs with constant DBB= 0 mm



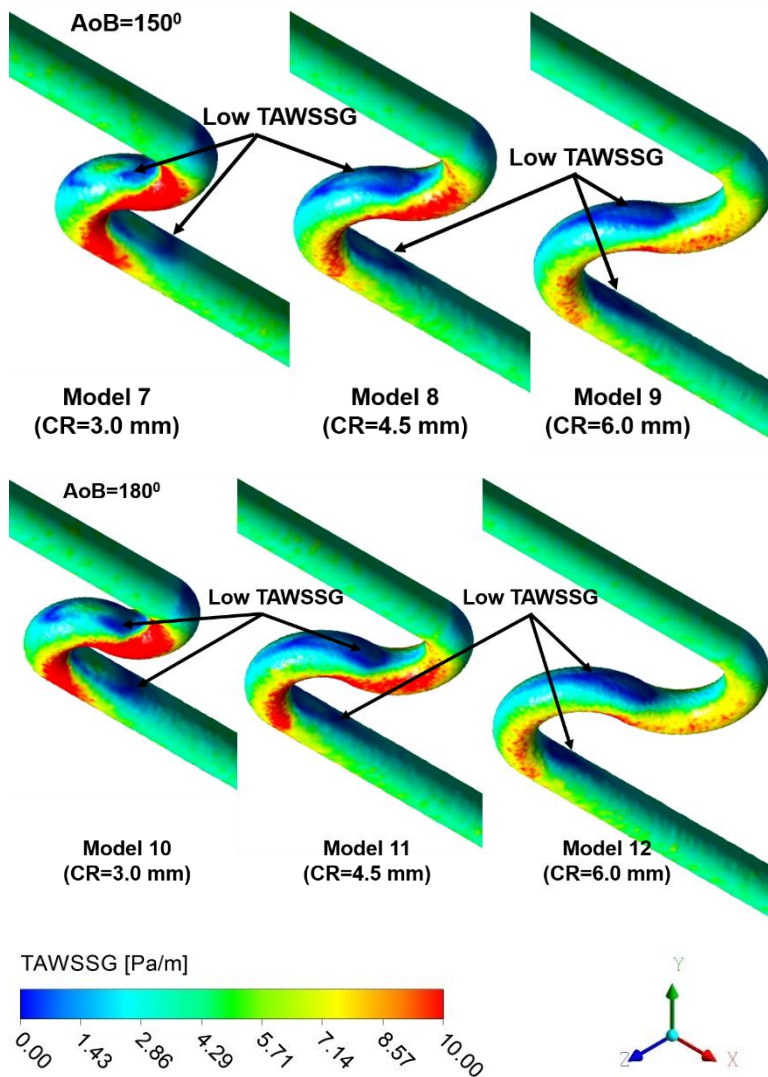
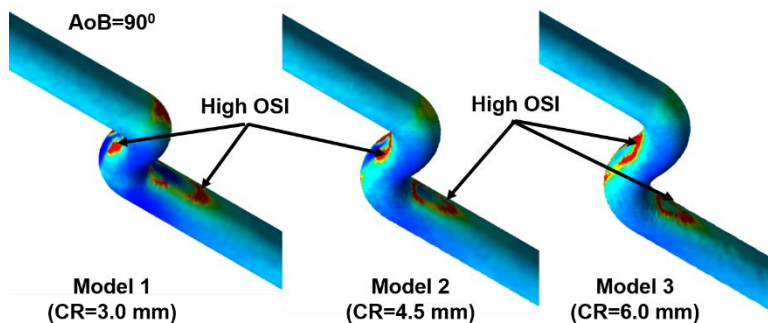


Figure 4.8 Spatial distributions of the TAWSSG contours for different CRs and AoBs with constant DBB= 0 mm



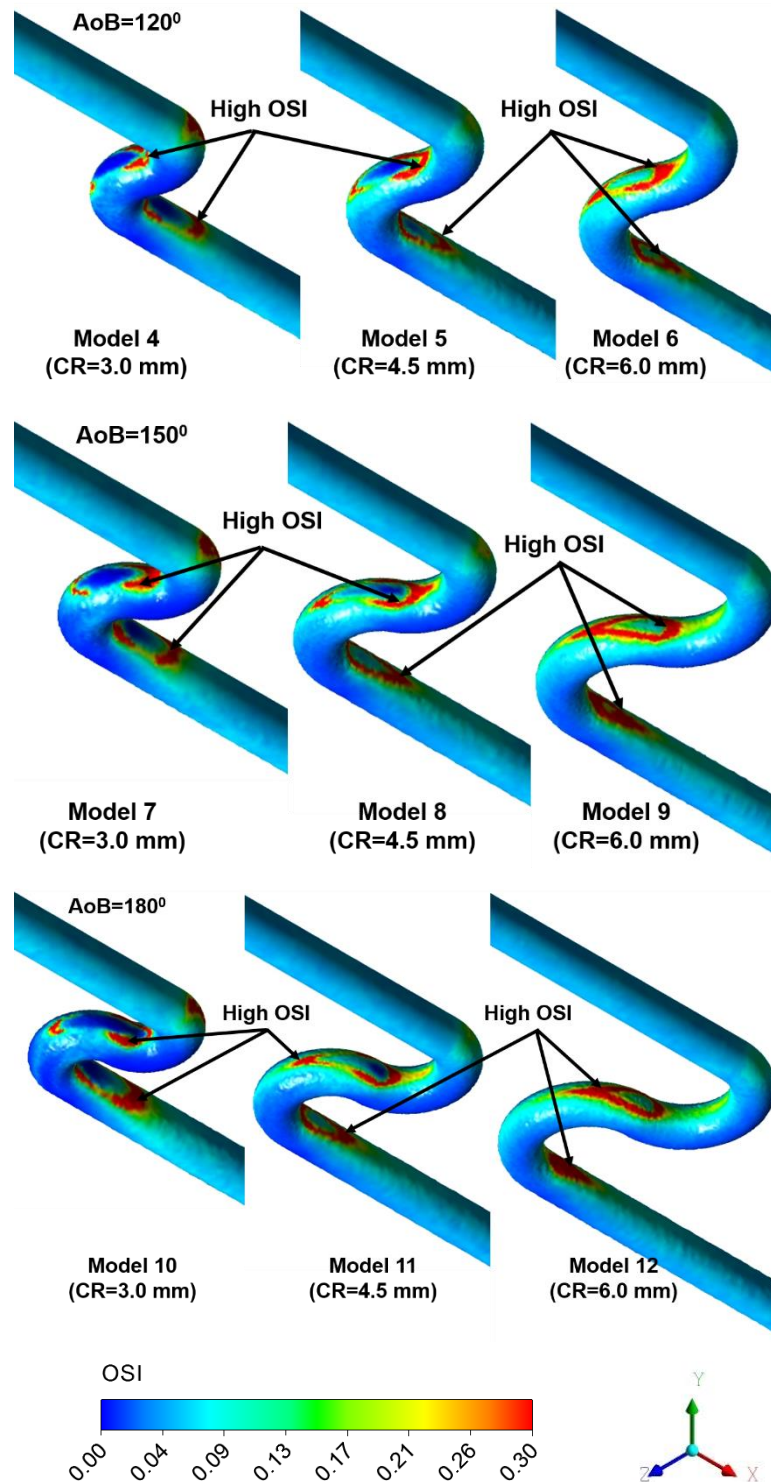
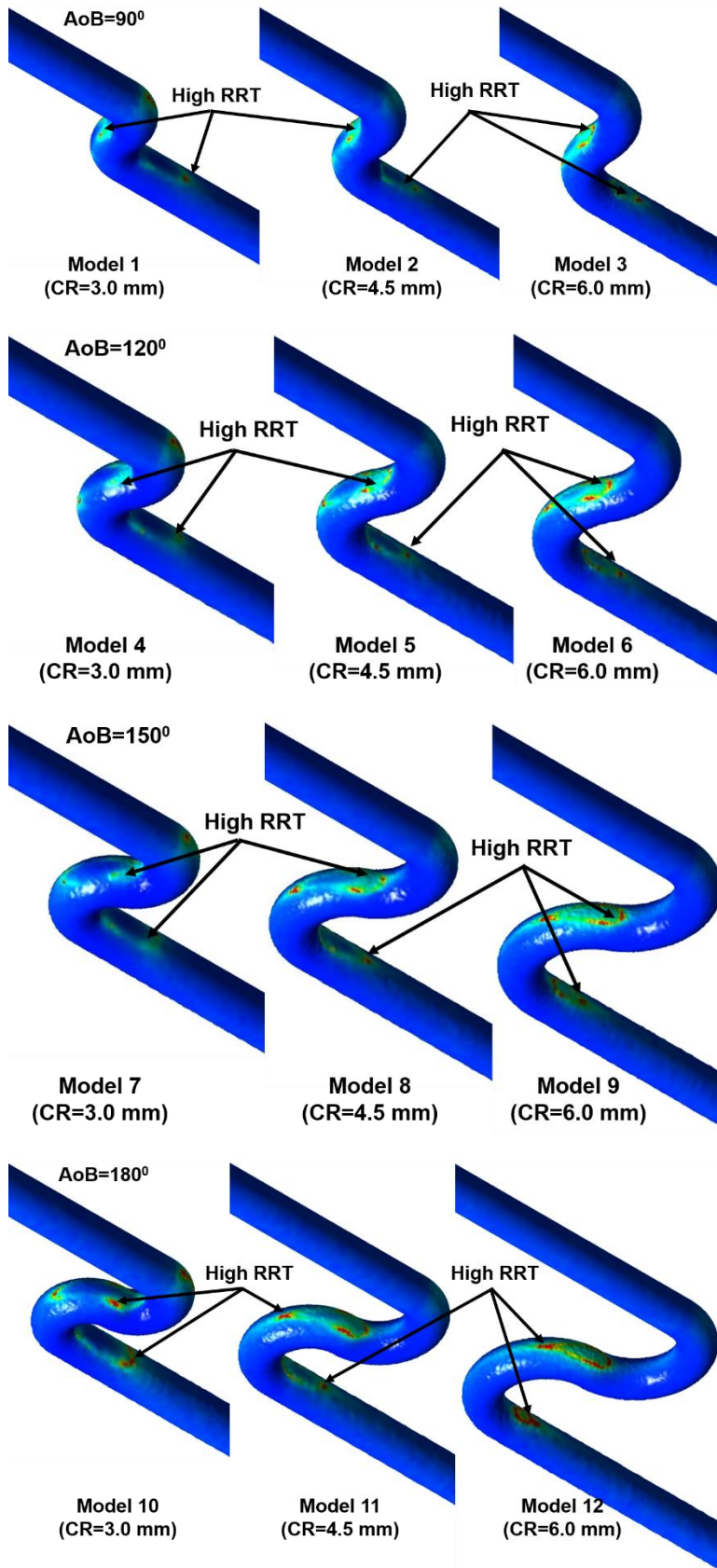


Figure 4.9 Spatial distributions of the OSI contours for different CRs and AoBs with constant DBB= 0 mm



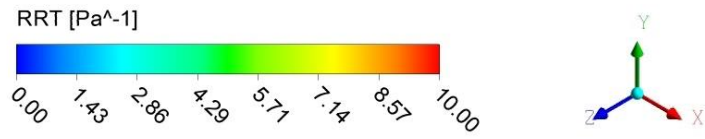
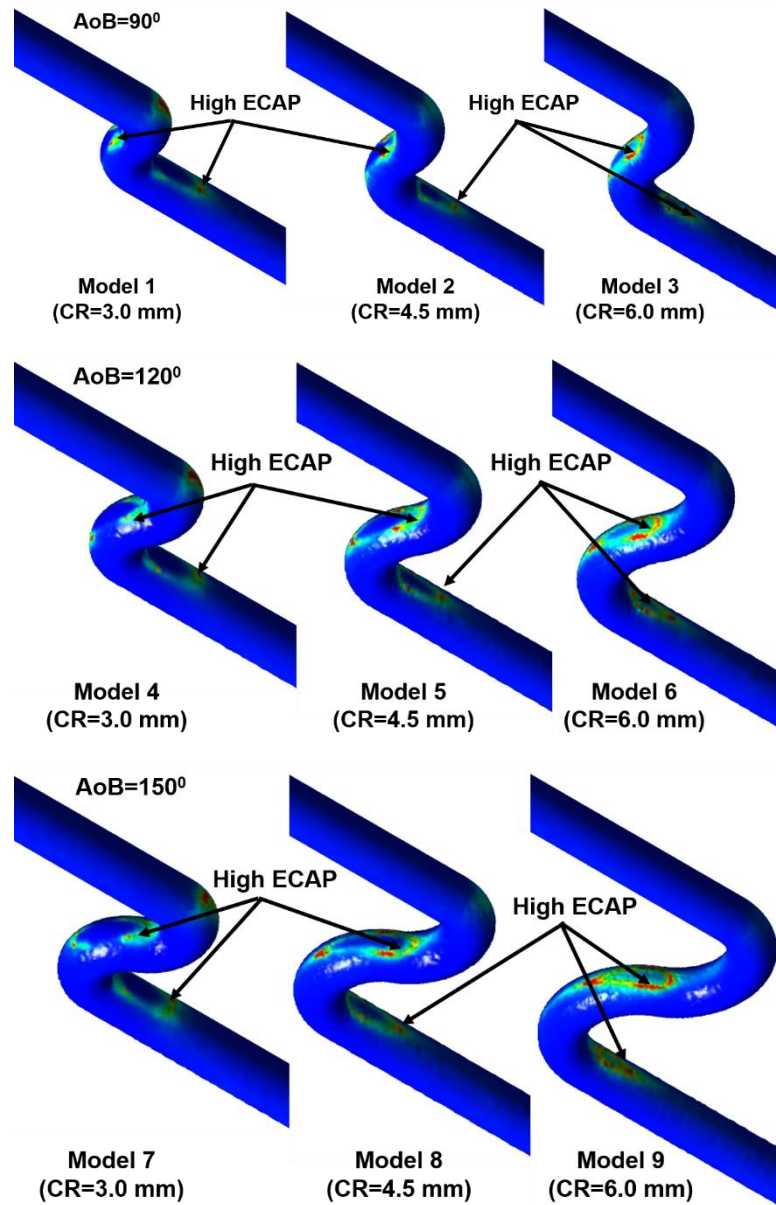


Figure 4.10 Spatial distributions of the RRT contours for different CRs and AoBs with constant DBB= 0 mm



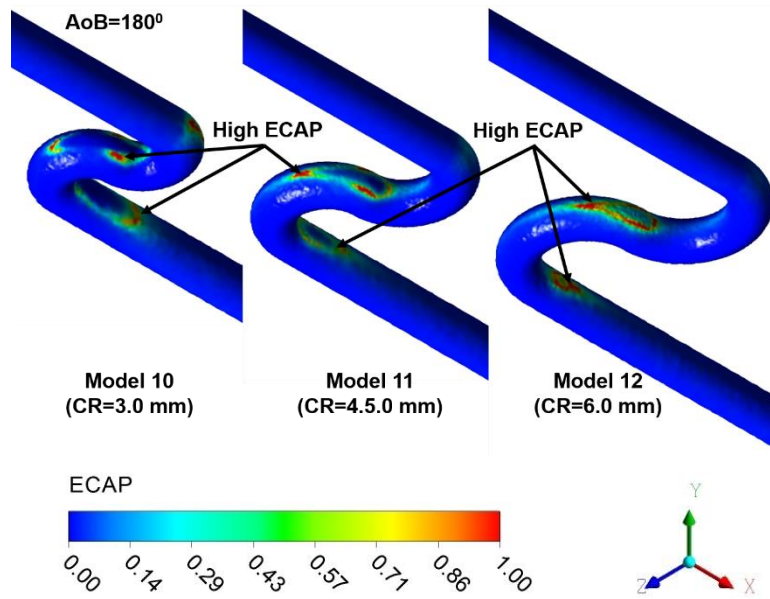


Figure 4.11 Spatial distributions of the ECAP contours for different CRs and AoBs with constant DBB= 0 mm

4.3.2 Effect of DBB on HDs

The contours of the velocity field are presented at maximum blood flow and at the beginning of diastole ($t=0.55s$) for all tortuous artery models with varying morphological tortuosity indices. The velocity contours for different DBBs and AoBs are shown in Fig. 4.12. At the downstream of inner wall of the BS1 and BS2 and outer wall of BS2 low velocity regions are observed due to the flow recirculation in those regions. On the other hand, high velocity regions were observed near the inner walls of the BS1 and BS2. The influence of DBB on velocity and different HDs are demonstrated for three different DBBs (0, 3 and 6 mm) for three AoBs (90^0 , 120^0 , 150^0 , and 180^0) and for a CR= 6 mm. The TAWSS, TAWSSG, OSI, RRT and ECAP distribution were shown in Figs. 4.13-4.17 respectively. High TAWSS and TAWSSG were observed in the sides of both the bend sections. Low TAWSS and TAWSSG were observed in outer walls of BS1 and at downstream portion of the BS2's inner wall. Through observation it is found that the regions of low and high TAWSS and TAWSSG remains fairly unchanged with DBB and AoB.

Table 4.5 The maximum HDs for different DBBs and AoBs (CR= 6 mm)

Models Studied	DBB in mm	Max. TAWSS, Pa	Max. TAWSSG, Pa/m	Max. OSI	Max. RRT, Pa⁻¹	Max. ECAP
AoB90 ⁰	0	16.649	16.395	0.481	63.186	1.144
	3	14.227	13.954	0.484	108.534	1.089
	6	12.609	12.306	0.495	183.338	1.054
AoB120 ⁰	0	20.667	20.410	0.480	43.58	1.136
	3	15.575	15.294	0.491	87.52	1.126
	6	12.509	12.213	0.490	106.64	1.057
AoB150 ⁰	0	17.296	16.987	0.471	31.461	1.185
	3	13.353	13.104	0.484	48.200	1.155
	6	8.694	8.466	0.487	77.157	1.135
AoB180 ⁰	0	15.629	15.412	0.4813	43.6459	0.958
	3	13.866	13.605	0.4867	74.6841	1.204
	6	10.941	10.615	0.4922	116.935	1.219

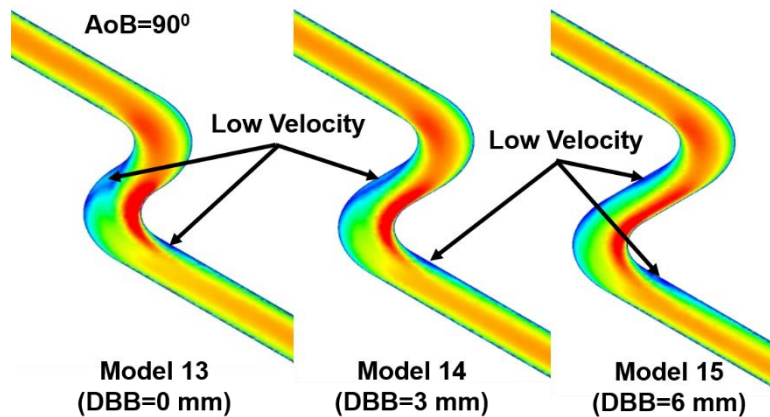
Table 4.6 Average HDs for different DBBs and AoBs (CR= 6 mm)

Models Studied	DBB in mm	Avg. TAWSS, Pa	Avg. TAWSSG, Pa/m	Avg. OSI	Avg. RRT, Pa⁻¹	Avg. ECAP
AoB90 ⁰	0	4.282	4.036	0.0377	0.369	0.0184
	3	4.213	4.012	0.0385	0.390	0.0208
	6	4.155	4.008	0.0405	0.457	0.0241
AoB120 ⁰	0	4.448	4.216	0.0362	0.378	0.0195
	3	4.423	4.187	0.0389	0.427	0.0230
	6	4.414	4.171	0.0401	0.455	0.0236
AoB150 ⁰	0	4.488	4.249	0.0351	0.368	0.0195
	3	4.475	4.237	0.0370	0.426	0.0232
	6	3.183	3.023	0.0389	0.578	0.0259

	0	4.516	4.279	0.0360	0.3669	0.0181
AoB180 ⁰	3	4.507	4.269	0.0363	0.3987	0.0186
	6	4.484	4.249	0.0371	0.4065	0.0208

From Figs. 4.15 and 4.16, it is observed that the regions of high OSI increases with DBB and AoB whereas the regions of high RRT increases only with DBB and remains fairly unchanged with AoB. The regions of high ECAP also increases with DBB and remains fairly unchanged for various AoBs. These trends are captured quantitatively in Table 4.5 and 4.6 where the peak and average values of different HDs for different DBBs and AoBs are reported.

Regions of high OSI, high RRT and high ECAP coincides with the areas of low TAWSS and TAWSSG as observed from Figs. 4.15-4.17. From Table 4.5 it can be inferred that the maximum OSI and RRT was observed for the model having the DBB of 6 mm whereas maximum ECAP was observed for the model having the DBB of 0 mm. Overall OSI, RRT and ECAP were found to decrease with decrease in DBB.



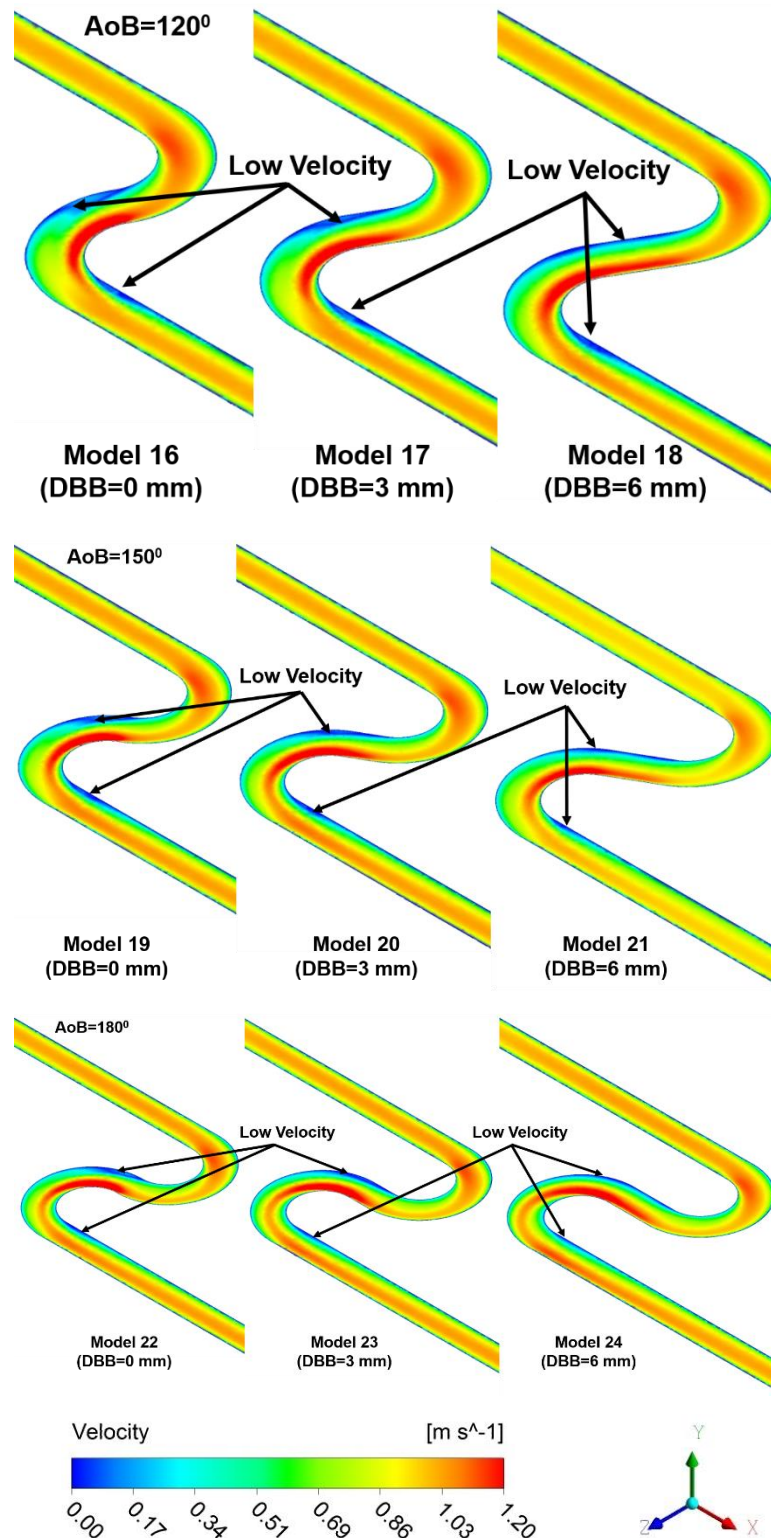
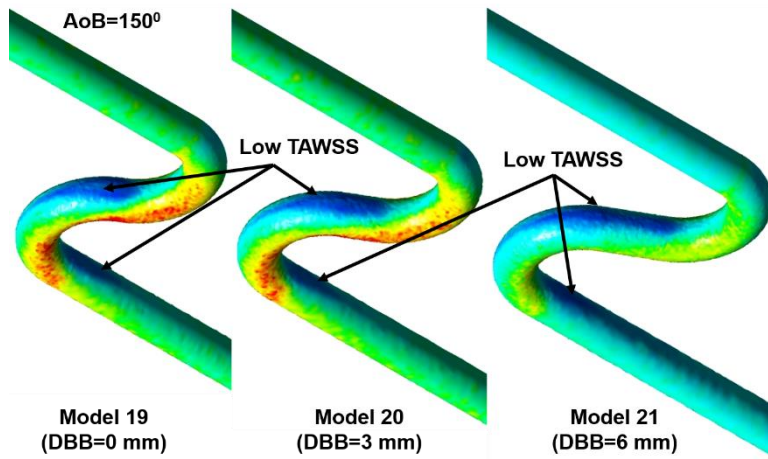
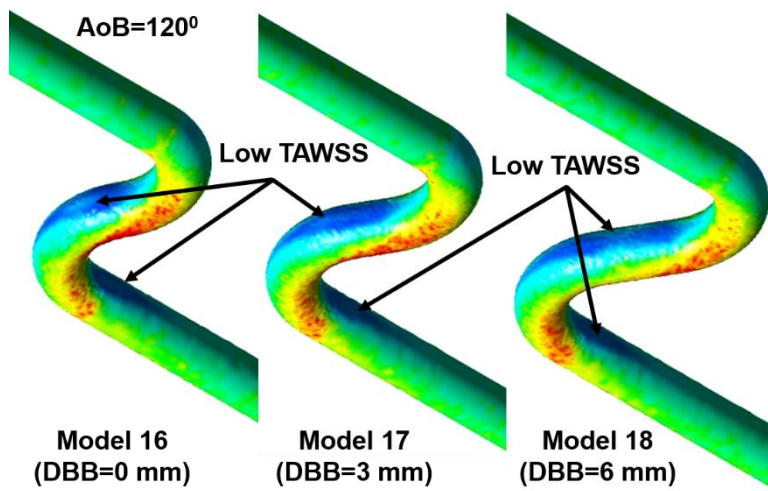
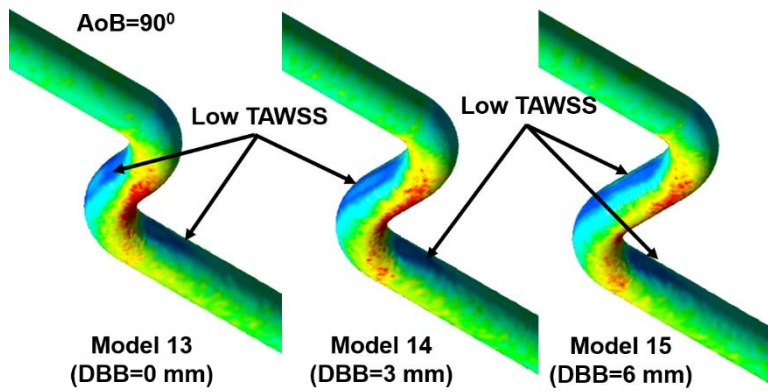


Figure 4.12 Spatial distributions of the velocity contours obtained at maximum flow rate ($t=0.55s$) for different DBBs and AoBs with constant CR=6 mm



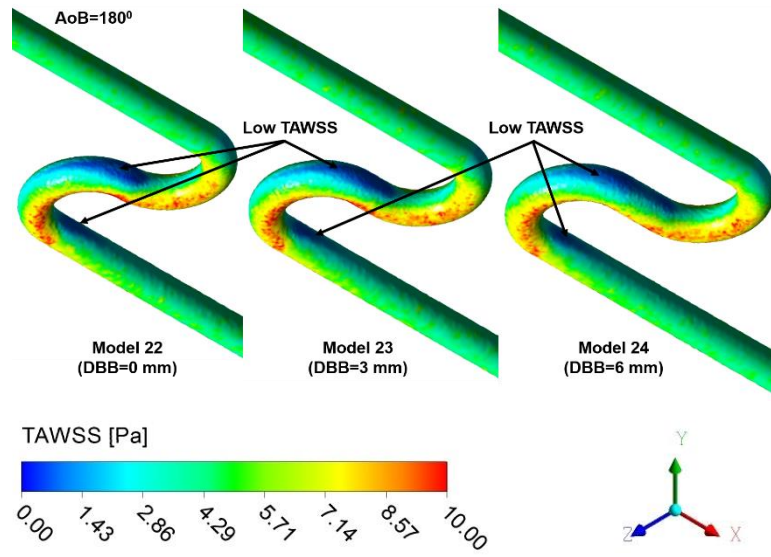
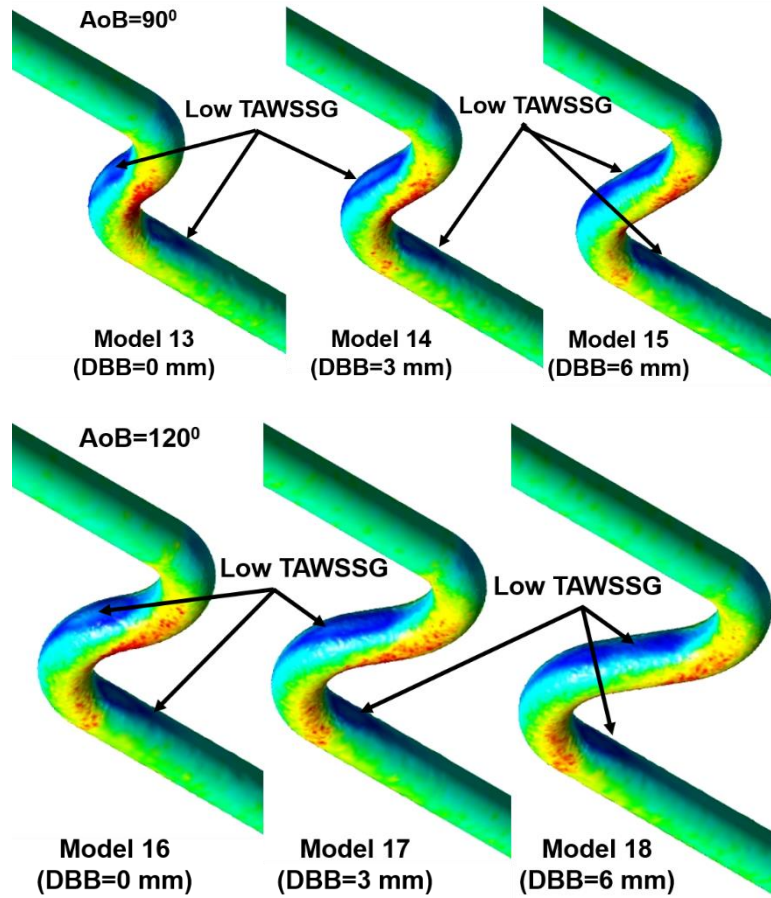


Figure 4.13 Spatial distributions of the TAWSS contours for different DBBs and AoBs with constant CR= 6 mm



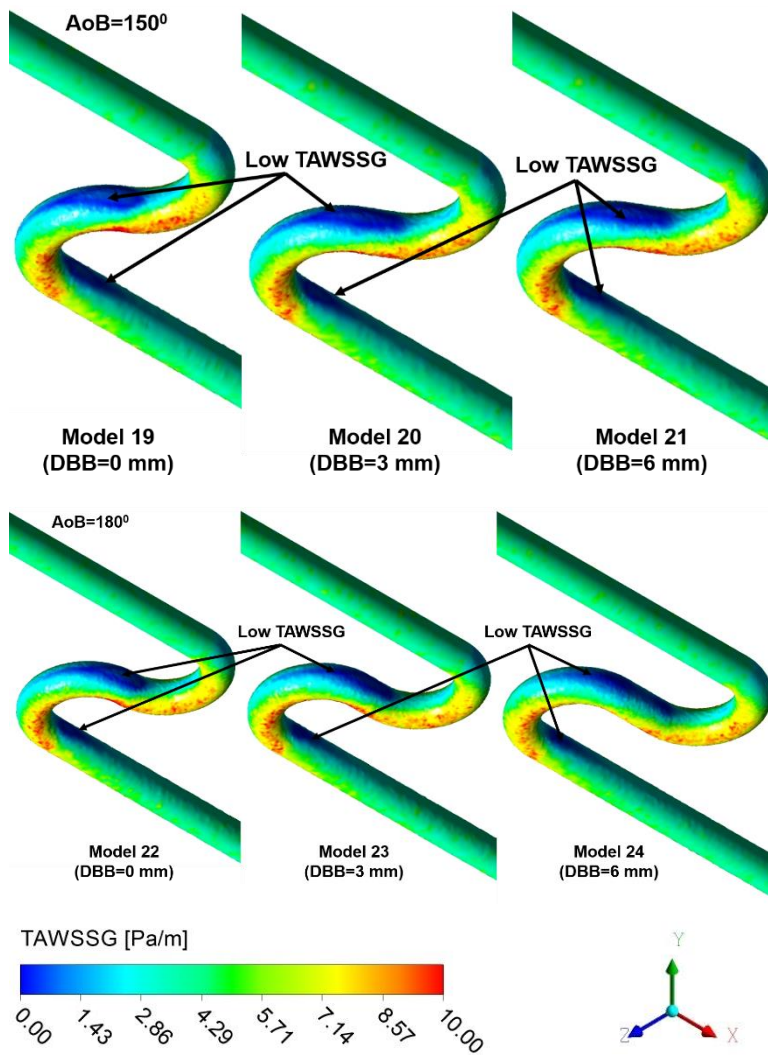
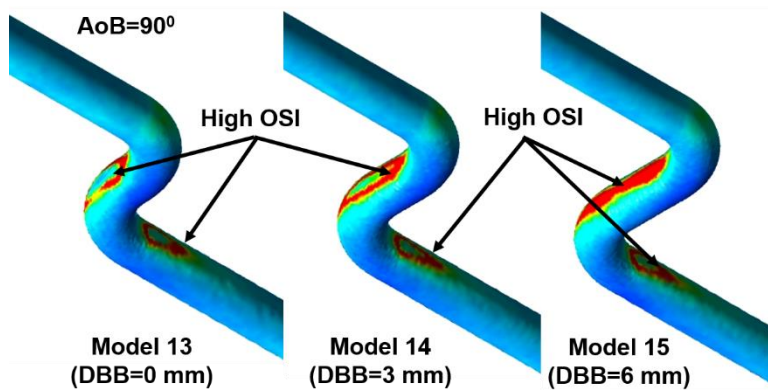


Figure 4.14 Spatial distributions of the TAWSSG contours for different DBBs and AoBs with constant CR= 6 mm



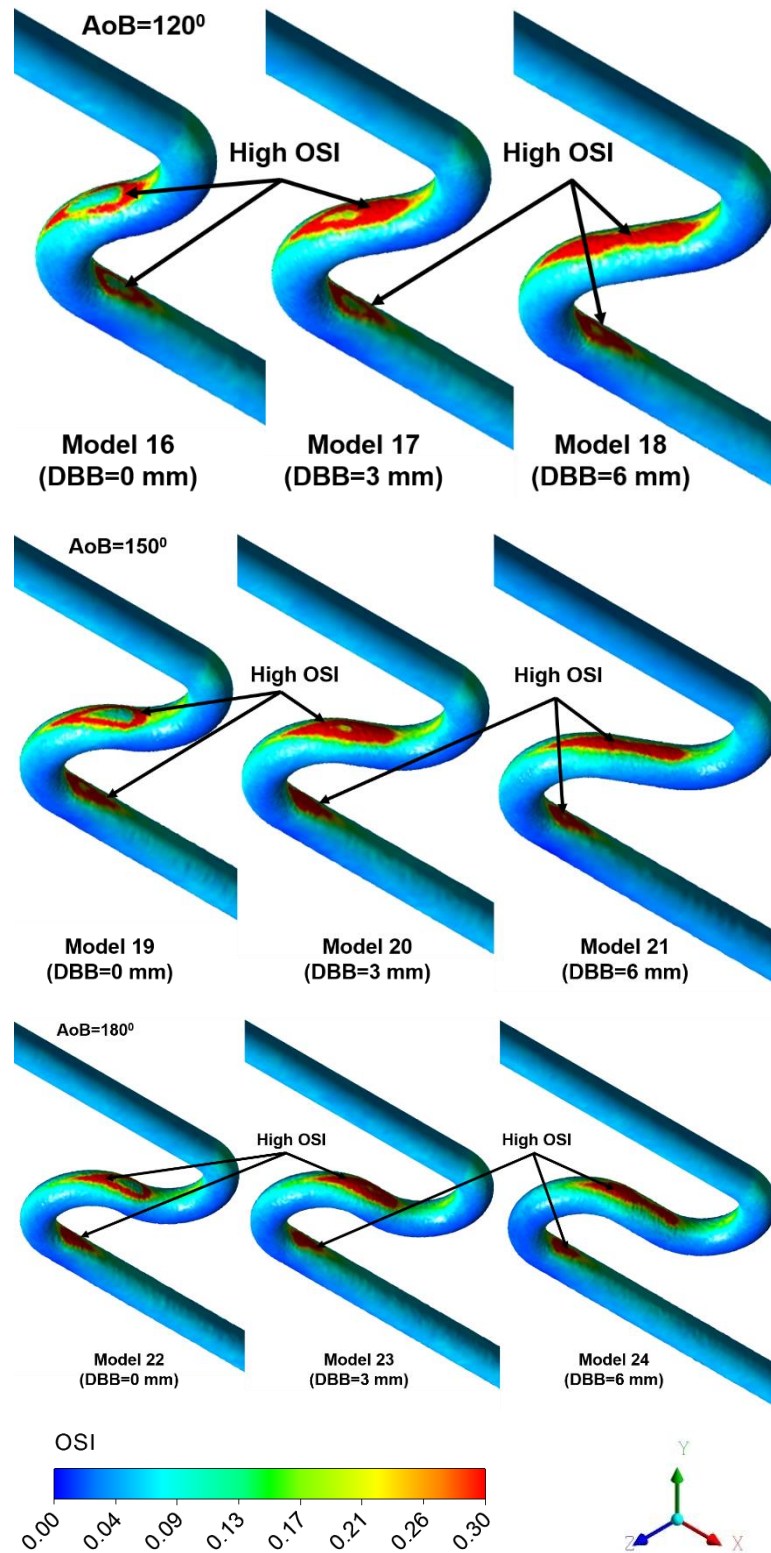
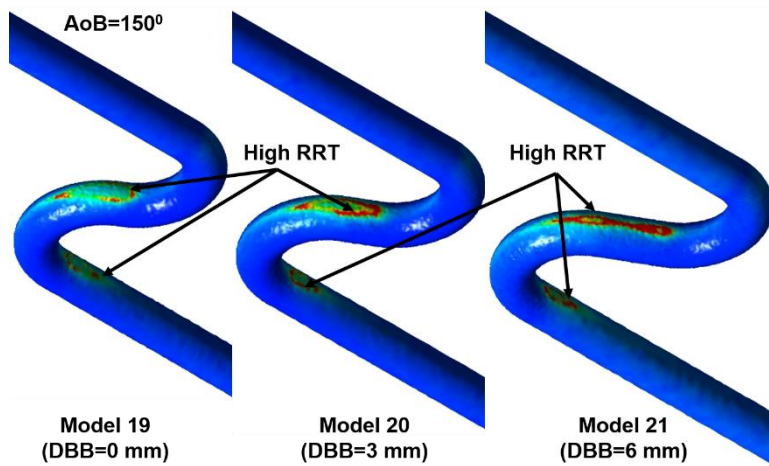
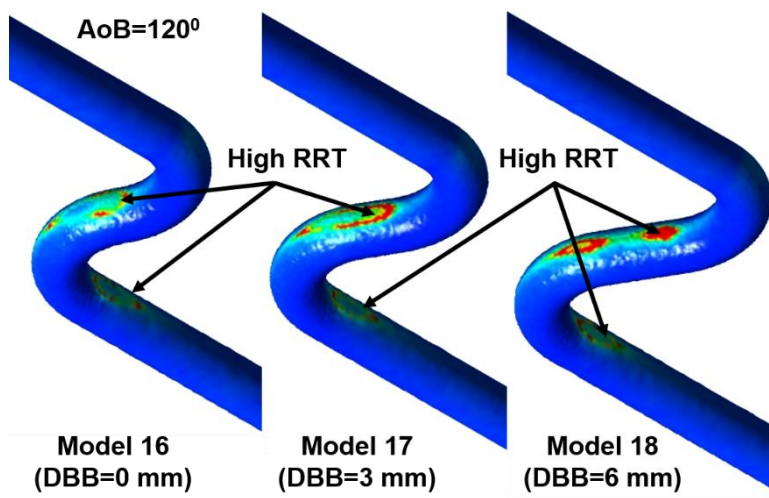
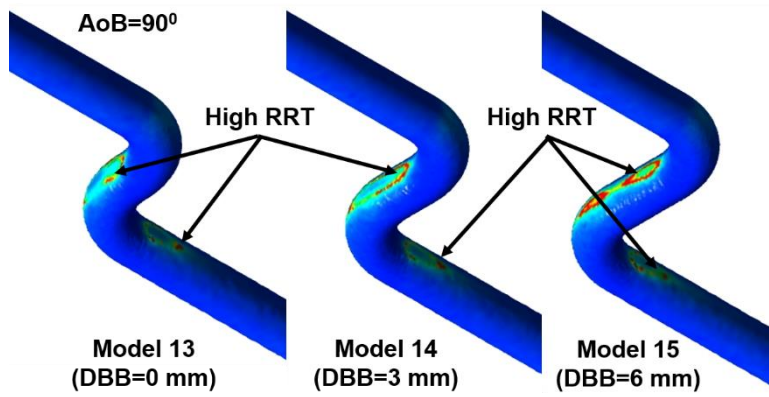


Figure 4.15 Spatial distributions of the OSI contours for different DBBs and AoBs with constant CR= 6 mm



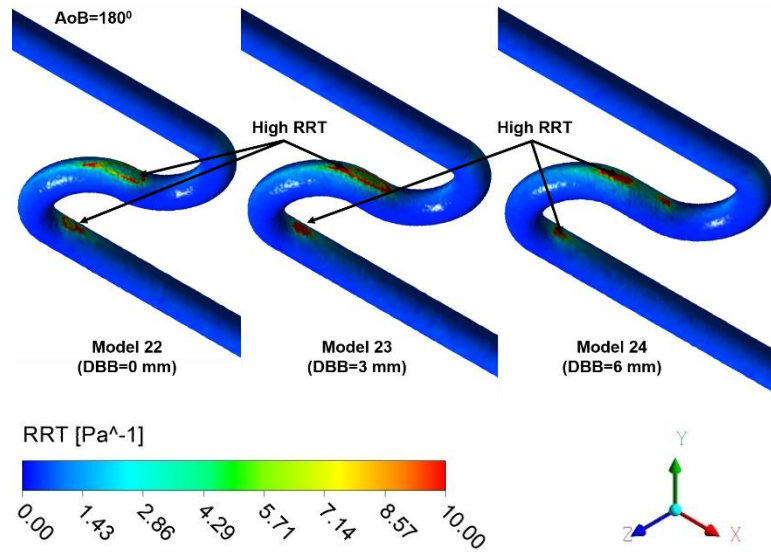
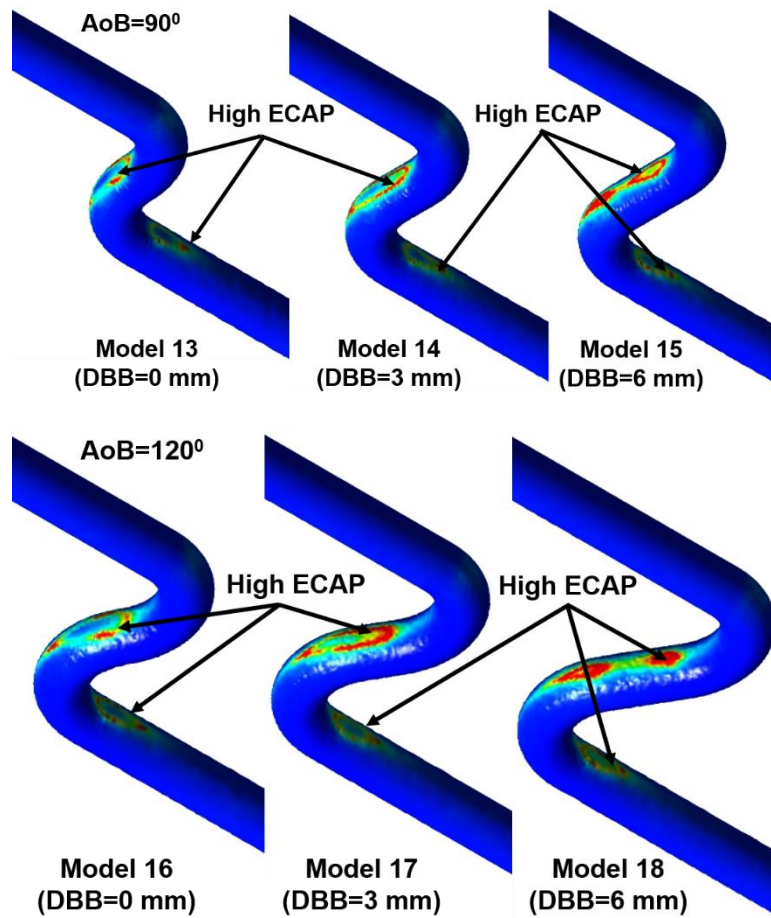


Figure 4.16 Spatial distributions of the RRT contours for different DBBs and AoBs with constant CR= 6 mm



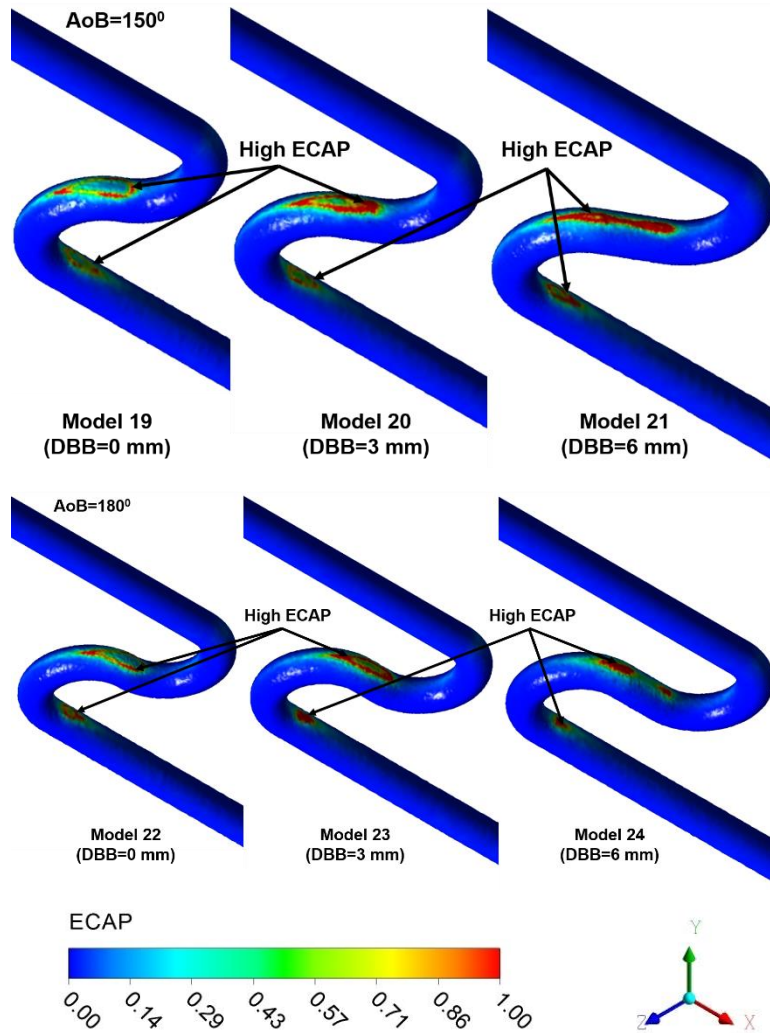


Figure 4.17 Spatial distributions of the ECAP contours for different DBBs and AoBs with constant CR= 6 mm

4.3.3 Effect of AoB on HDs

The influence of AoB on different HDs is demonstrated in this section for various AoBs (90° , 120° and 150°) by keeping the DBBs and the CRs as constant (DBB= 6 mm and CR= 6 mm). The maximum variations of different HDs for different AoBs are reported in Table 4.7.

As reported in Table 4.7, as the AoB increases from 90° to 150° , the maximum TAWSS reduced from 12.609 Pa to 8.69 Pa, maximum TAWSSG decreased from 12.306 Pa/m to 8.46 Pa/m, maximum OSI decreased from 0.495 to 0.487, and maximum RRT decreased from 183.33 Pa^{-1} to 77.15 Pa^{-1} . Whereas, maximum ECAP

increased from 1.054 to 0.135 as the AoB is increased. Also, in all tortuous artery models studied with different AoBs, similar trends were found with different CR models. Hence, from the above results the AoBs have much less influence on the distributions of the TAWSS, TAWSSG, RRT, OSI and ECAP upto AoB of 120⁰ but reduced by almost 50% for AoB 150⁰.

Table 4.7 The maximum HDs for different AoBs (DBB= 6 mm and CR= 6 mm)

Models Studied	Max. TAWSS, Pa	Max. TAWSSG, Pa/m	Max. OSI	Max. RRT, Pa⁻¹	Max. ECAP
AoB90 ⁰	12.609	12.306	0.495	183.338	1.054
AoB120 ⁰	12.509	12.213	0.490	106.64	1.057
AoB150 ⁰	8.690	8.46	0.487	77.15	1.135

4.4 DISCUSSION

In this chapter, we have investigated the influence of tortuosity morphological indices (CR, AoB, and DBB) on coronary hemodynamics and on HDs by conducting a detailed computational analysis using multiphase mixture theory model on several idealized tortuous CA models. Present study mainly focuses on three morphological geometric indices (viz., CR, AoB, and DBB) that fully characterize the geodesic patterns of tortuosity in CAs (Xie et al. 2014). The detailed study on these parametric idealized tortuous artery models indicates that all the tortuosity indices affect HDs substantially.

The WSS is a local HD which directly acts on the ECs and there is an increasing evidence that the low WSS plays a very significant role in the development of atherosclerotic lesions (Caro 2009) and plaque stability through modulation of EC function and gene expression, while high WSS is associated with the protection from atherosclerosis (Chatzizisis et al. 2007). In arteries the blood flow disturbance exerts uncharacteristic WSS that modifies physiology of blood cells (Cunningham and

Gotlieb, 2005). TAWSS is the time averaged WSS for one cardiac cycle. Under current practices only AoB is considered as the prominent tortuosity indices in clinical diagnosis owing to its easy access. The oscillating and low WSSs with continuous spatial gradient are influential parameters for development and progress of a premature atherosclerotic plaque and atherogenesis (Kleinstreuer et al. 2001). The presence of tortuosity in all artery models altered the distribution of TAWSS. Regions of low TAWSS, high OSI, high RRT and high ECAP were observed at downstream of inner wall of BS1 and upstream section of the outer wall of BS2. Also, the results confirmed that smaller CR might lead to the genesis of uncharacteristic regions of WSS.

In tortuous CAs the DBB is a morphological index which is consistently neglected in the hemodynamic analysis. However, the present computational results quantified that the DBB had a pronounced influence on the various HDs. For DBB = 0, the upstream segment of the BS2 is joined directly with the downstream segment of the BS1. Hence, the inner wall downstream of the BS1 is merged with outer wall upstream of the BS2. Similarly, the inner wall upstream of the BS2 is merged with the outer wall downstream of the BS1. The HDs between the two BSs i.e., BS1 and BS2 would alter largely and observed its anomalous values although the CR for the two bends was more. As seen in Fig. 4.6 and Fig. 4.12, the velocity at the BS cross sections is skewed due to the centrifugal effect. As defined by the Dean's number, this velocity skewness depends on the curvature of the artery, as well as the viscous and inertial forces. At the BSs the centrifugal force is larger for the smaller CR and DBB. Consequently, the blood flow at the downstream of the BS1 and BS2 turn into being more skewed and disturbed due to the flow recirculation (secondary flow) that results in low TAWSS. The recirculation of blood flow at the downstream of BS1 and BS2 increases the residence time of blood constituents such as low density lipoprotein (LDL) which might accelerate the plaque development.

4.4.1 Limitations of the Study

The authors believe that our computational hemodynamic analysis using multiphase mixture theory results are convincing. However, it is to be mentioned that there are

some modeling limitations still exist in our analysis. In this chapter the curvature of the heart which is much smaller than the curvature of tortuous CA has been neglected. For CAs, the previous study by Torii et al. (2009) exhibited the effect of wall circumferential deformation showed that it had a minor influence on the HDs mainly OSI and TAWSS. Hence, the wall compliance and elasticity of the artery wall was neglected. In reality, the CAs during each cardiac cycle is subjected to repetitive flexion and relaxation motion. In previous studies it has been mentioned that the CA dynamic motion has an influence on the WSS profiles however, it has negligible influence on the OSI and TAWSS (Xie et al. 2013a, Hasan et al. 2013). Thus in this chapter, the heart dynamic motion during each cardiac cycle was ignored. Also, the present numerical study deals only with idealized tortuous artery models, therefore the use of more realistic patient-specific artery models with coronary tortuosity would be desirable for better understanding of the pathophysiology of coronary atherosclerosis.

4.5 SUMMARY

In this chapter, we used multiphase mixture theory approach to investigate the influence of tortuosity morphological indices on the coronary hemodynamics and on the WSS based HDs in order to identify sites vulnerability to atherosclerosis. Our computational analysis is mainly concentrated on three different tortuous geometric indices namely, the CR, AoB, and DBB, which completely illustrate the tortuosity geodesic patterns in CAs. The five HDs, the TAWSS, TAWSSG, OSI, RRT and the ECAP were analyzed to find vulnerable locations for the genesis and onset of early atherosclerosis. The results clearly showed all the tortuosity morphological indices have significant influence on the HDs distributions. The artery walls regions with the high OSI (>0.2), low TAWSS (<0.4 Pa), high RRT (>8 Pa⁻¹), high TAWSSG (TAWSSG >8 Pa/m) and high ECAP (>1.0) were widely accepted as sites for more vulnerable atherogenesis and plaque progression. These sites were witnessed at the inner artery wall downstream regions of the BS1 and BS2 in all the tortuous artery models studied and found to increase as the CR and DBB were reduced however, found to increase as the AoB is increased.

CHAPTER 5

EFFECT OF STENOSIS SEVERITY ON SHEAR INDUCED DIFFUSION OF RED BLOOD CELLS IN CORONARY ARTERIES

5.1 INTRODUCTION

Blood is a two-phase complex liquid consisting of plasma and several constituents of blood such as RBCs, platelets, WBCs etc. which display significant non-Newtonian effects. These effects are mainly triggered by RBC-RBC interactions, aggregation and disaggregation of RBCs and their deformation (Chien et al. 1966). As the RBC volume fraction (VF) varies between 40% and 50%, the hydrodynamic and physicochemical interactions between blood cells become crucial in the structuring of the suspension and its rheological properties.

Shear-induced diffusion (SID) of RBCs in small arteries (micrometers to one millimeter size) of the cardiovascular system is a well-known phenomenon. There are two important processes that influence the rheological properties of blood. First, the RBCs aggregation at low shear rates to form aggregate structures of varying shapes and sizes. The second is the inward migration of RBCs resulting from the shear rate gradient effects on individual and groups of RBCs. In micrometer to millimeter sized blood vessels, RBCs shows migrational behaviour from high shear rate region to low shear rate region i.e. towards the centre of the vessel and consequently results in margination of platelets near the vessel walls. Margination of platelets results in the development of a thrombosis and hemostatic plug, and hence significant research has been carried out in the past three decades experimentally (Aarts et al. 1988, Pries et al. 1992) and numerically (Van Weert 1996, Sharan and Popel, 2001, Xie et al. 2015). Thus, the distribution of RBC influences the viscosity and velocity profile of blood and a series of biological activities (Liu et al. 2012).

A number of researchers have utilized several approaches numerically to understand the shear-induced diffusion effects. Sharan and Popel (2001) described a

biphasic model for blood flow in narrow tubes of diameter $20 \leq D \leq 300 \mu\text{m}$. Their approach contained suspended RBCs as a central core and a cell-free layer surrounding the core. However, the use of this method to complex geometries is very difficult. Bagchi (2007) presented a two-dimensional (2D) blood flow model in vessels ranging from 20-300 μm , and the behavior of blood particles and their deformation were considered. Based on the immersed boundary method, the results showed the formation of free cell layer and perpendicular migration of RBCs to the artery wall. Mansour et al. (2010) performed a numerical simulation to investigate the plasma-RBC interactions and RBC migration effects occurring in micro vessels of the diameter of 40 μm , 60 μm , 80 μm and 100 μm by using Phillips diffusive flux model (DFM).

Finite volume method (FVM) approach was used by some researchers to numerically simulate the dense suspension flow through 3D bifurcation channel (Y-shaped) with a particle diameter of 90 μm (Yadav et al. 2015) through an asymmetric 3D T-junction bifurcation channel with a particle diameter of 94 μm (Ahmed and Singh, 2011) by using Phillips diffusive flux model. Hofer and Perktold (1997) performed a simulation to investigate the fluid-particle interaction and migration effects in the flow of dense fluid-particle suspensions in axisymmetric geometries. The transport and flow equations were solved by applying a pressure-velocity projection scheme and the Galerkin finite element method. De Siqueira and da Carvalho (2018) used shear induced DFM to investigate the creeping flow of spherical, non-Brownian rigid particles suspension in a viscous fluid through an abrupt expansion channel by treating suspension as a single-phase liquid in the flow domain. The study revealed that particle Peclet number, bulk concentration of suspension and ratio of diffusivity coefficients has a significant effect on particle concentration field in the particle suspension flows. Biasseti et al. (2014) used Phillips shear-induced DFM to study the synergy between secondary flows and shear-induced migration on RBCs transport in different patient-specific luminal geometries by considering oxygen transport. At the inner curvature of the carotid wall, the oxygen partial pressure decreases due to the presence of secondary flows in carotid sinus (Biasseti et al. 2014).

To the best knowledge of authors, the effect of stenosis on SID of RBCs and its effect on the blood flow in large blood vessels (CAs and carotid artery) where the diameter ranges from few millimeters to a centimeter has not been reported elaborately. In the present numerical study, the Phillips model (Phillips et al. 1992) has been chosen to represent the behavior of RBC transport in blood flows. The particle fluxes in the Phillips model can be attributed to two effects, namely the spatial variation of interaction frequency and viscosity resulting from the interaction of two particles (Van Weert 1996). Also, Quemada model (Quemada 1977, Quemada 1978) that describes the viscosity behavior of blood is used to calculate viscosity in the Phillips model (Phillips et al. 1992). It is of great importance to gain an insight in to the role of SID in human circulation and the applicability of the transport equation to suspensions of RBCs.

Motivated by the above observations, the locations where hydrodynamic diffusion of RBCs occurs and the effect of stenosis severity on SID of RBCs, RBC concentration distribution and WSS are investigated. The multiphase mixture theory model is employed to solve the constitutive governing equations. The present CFD methodology is validated and found in good agreement with the analytical results of Phillips et al. (1992) and Lyon and Leal experiment results (Lyon and Leal, 1998).

5.2 MATERIALS AND METHODS

The present study deals with the numerical analysis of the dense suspension flow of rigid neutrally buoyant particles through idealized axisymmetric geometries. The effects of spatially varying viscosity and inter-particle interaction frequency are modelled to capture the migration of RBCs in inhomogeneous shear flows.

5.2.1 Governing Equations

In this chapter, RBCs are assumed to be a dense mono-mode suspension in plasma liquid. The flow is assumed to be laminar, axisymmetric and incompressible. The density difference between RBC and plasma is neglected. Both the RBC suspension and plasma fluid are modelled as a single continuum suspension fluid. The multiphase mixture theory model is used to solve the constitutive equations based on continuity,

momentum and transport equations and to achieve better correspondences with experimental results in literature (Beg et al., 2014). The detailed explanation regarding the multiphase mixture theory model is given in detail in chapter 3.

5.2.1.1 Convection – Diffusion Equation for RBCs

In the model, the RBC VF is governed by a typical convection-diffusion equation is as follows:

$$\frac{\partial \phi}{\partial t} + V \cdot \nabla(\phi) = \nabla \cdot N \quad (5.1)$$

The first, second and third terms in the (Eq. 5.1) represents accumulation of particles, convected particles and total diffusive flux of particles N, respectively.

The particle diffusivity flux is expressed as:

$$N = N_c + N_\mu \quad (5.2)$$

Where N_c and N_μ respectively correspond to the particle flux contribution due to the decreasing of hydrodynamic particle interaction frequency and due to a spatially varying viscosity that causes an opposition to the motion after the collision of two-particles. These particle fluxes are proposed based on the Leighton and Acrivos improved arguments (Leighton and Acrivos, 1987a) by Phillips et al. (1992).

$$N_\mu = -K_\mu \dot{\gamma} \phi^2 \left(\frac{a^2}{\mu} \right) \nabla \mu \quad (5.3)$$

$$N_c = -K_c a^2 (\phi^2 \nabla \dot{\gamma} + \phi \dot{\gamma} \nabla \phi) \quad (5.4)$$

Where ‘ $\dot{\gamma}$ ’ and ‘ a ’ denotes as local shear rate and radius of particle respectively. The K_μ and K_c are the empirical constants chosen experimentally by Phillips et al. (1992) and used in the present study namely, $K_\mu = 0.62$ and $K_c = 0.41$.

Combining Eqs. (5.1) - (5.4) results in a diffusion equation in a Eulerian reference frame:

$$\frac{\partial \phi}{\partial t} + V \cdot \nabla \phi - \nabla \cdot (\Gamma \nabla \phi) - S_\phi = 0 \quad (5.5)$$

Here, S_ϕ and Γ respectively correspond to the source term and the particle diffusion coefficient. It is expressed as:

$$S_\phi = \nabla \cdot (a^2 K_c \phi^2 \nabla \dot{\gamma}) \quad (5.6)$$

$$\Gamma = a^2 K_c \phi \dot{\gamma} + a^2 K_\mu \dot{\gamma} \phi^2 \frac{1}{\mu} \frac{\partial \mu}{\partial \phi} \quad (5.7)$$

The formation of a thin layer called the plasma skimming layer of around 3 μm thickness in-line to the wall without RBCs (Ethier and Simmons, 2007) is neglected in the present study.

5.2.2 Numerical Methodology

To solve the governing equations, Fluent 14.5 commercial code (ANSYS Inc. 2012) was used which utilizes FVM. The FVM have been used earlier for solving the suspension balance model and DFM (Fanz and Phan-Thien, 1995, Miller and Morris, 2006, Miller et al. 2009). To solve the scalar transport equation (Eq. 5.5) a UDF code was included in the source term to model the particle diffusion coefficient.

As already been noted in the literature, the areas where shear rate is zero, the DFM diverges. The equation (Eq. 5.7) indicates that the SID coefficient (Γ) is associated linearly to the shear rate ($\dot{\gamma}$). In pipe flow at the pipe centre the shear rate ($\dot{\gamma}$) is zero which makes the SID coefficient (Γ) as zero in our simulation. We used the Miller and Moris (2006) approach to overcome the setback by considering a non-local shear rate ($\dot{\gamma}_{nl}$) based on the particle size and shear rate.

$$\dot{\gamma}_{nl} = a_s (\varepsilon) \dot{\gamma}_s \text{ and } \dot{\gamma}_s = U_{\max} / R \quad (5.8)$$

Here, U_{\max} represents the maximum centre line velocity in the pipe of diameter $2R$. The factor $a_s(\varepsilon) = (a/R)^2$ was considered which limits the non-local effect to a thin area near the channel center (Reddy and Singh, 2014).

The second-order accurate discretization schemes and the Green-Gauss cell-based method for gradients were used for all the equations while the coupled scheme was used for pressure-velocity coupling. The simulations through the CA with different DOS were carried out with a maximum residual corresponding to the convergence flow of 10^{-4} . Also, a constant time-step of 0.001s was chosen with 50 iterations for every time-step. To ensure the periodicity, four pulsatile cycles were simulated and the analysis was performed for the third cycle.

5.2.3 Model Validation

Prior to simulating the blood flow through the idealized stenosed CA with varying DOS, the numerical methodology used in the present study was validated by carrying out a 2D ‘steady-state’ simulation in a straight rectangular conduit and the simulated results were compared with the experimental and analytical data reported in the literature (Phillips et al. 1992, Lyon and Leal, 1998).

To calculate the length required for the suspension flow to reach its steady state the following equations were used (Nott and Brady, 1994).

$$\left[\frac{L}{B} \right] = \frac{1}{12d(\phi)} \left[\frac{B}{a} \right]^2 \quad (5.9)$$

Where, ‘a’ and ‘B’ respectively correspond to the radius of particle and channel half-width and function $d(\phi)$ relates to the particle concentration effect on the SID coefficient and is given by:

$$d(\phi) = \frac{1}{3} \phi^2 \left(1 + \frac{1}{2} e^{8.8\phi} \right) \quad (5.10)$$

The following boundary conditions are used for suspension flow simulations:

- The particle VF and average velocity are specified at the inlet,
- A ‘outflow’ fully developed condition is employed at the outlet,
- The zero particle flux and no-slip (zero velocity) boundary condition are defined at the wall.

The particle size (B/a) of 18 was adopted for the simulations that were used in the experimental studies carried out by Lyon and Leal (1998) for the channel. The computational grid consists of 70,000 cells. Here, a suspension viscosity followed the relationship proposed by Krieger (1972) was used to describe the effective suspension viscosity:

$$\mu = \mu_f \left(1 - \frac{\phi}{\phi_{\max}} \right)^{-1.82} \quad (5.11)$$

Where μ_f is the pure suspending fluid viscosity and ϕ_{\max} is the maximum packing VF of particles and the value is chosen for this study is 0.68. The similar flow rate as used in the experiments of Lyon and Leal (1998) is used to perform the simulations. The parameters and their values used for validation of the DFM are summarized in Table 5.1.

Table 5.1 Simulation parameters considered for validation

Parameters	Symbol (Unit)	Experiment (Lyon and Leal, 1998)
Viscosity of suspending fluid	μ_f (kg/m-s)	0.48
Suspended fluid density	ρ (kg/m ³)	1190
Inlet velocity of suspension	U (m/s)	3.7×10^{-3}
VF of particle	ϕ (%)	0.3 and 0.4
Radius of particle	a (m)	4.7×10^{-5}
Channel half width	B (m)	8.5×10^{-4}
Length of channel	L (m)	0.8

Figure 5.1 shows the comparison of multiphase mixture model with SID (present study) with the analytical solution and experimental for bulk concentrations $\phi = 0.3$ and $\phi = 0.4$ in a planar Poiseuille flow. With an increase in the bulk volume concentration, the particles (uniform size) tend to accumulate near the centre of the channel. This results in the increase of suspension viscosity leading to flattened velocity profiles (c.f. Figs 5.1 (a) and (b)).

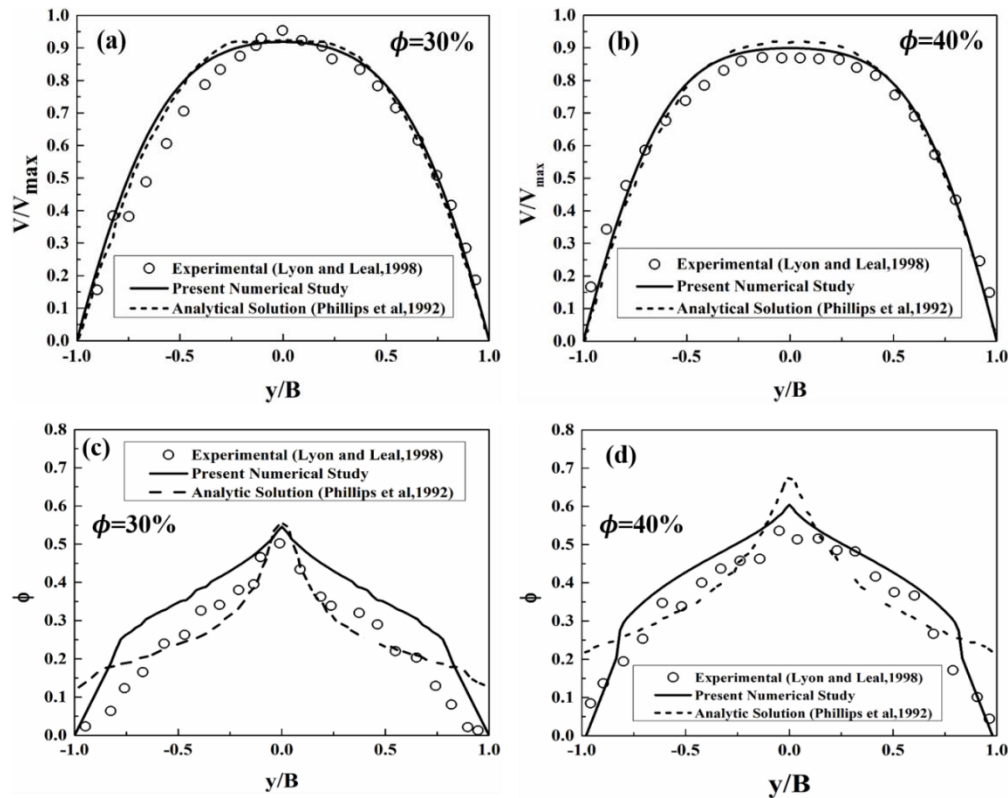


Figure 5.1 Velocity profiles for (a) 30% average particle VF, (b) 40% average particle VF, (c) corresponding particle concentration profile for 30% average particle VF and (d) 40% average particle VF

Figure 5.1(c) and (d) shows that the concentration profiles sharply peak at the centerline which is attributed to the model not considering particle collisions in the absence of velocity gradient while calculating the particle flux. The shear rate $\dot{\gamma} = 0$

and particle diffusive flux hinder the particles migration towards the channel centre. The present model when compared to the analytical model predicts the centerline concentration value closer to the experiment which is due to the inclusion of ‘non-local’ shear rate term in the current model. The multiphase mixture model used in the present study considering SID is found to be in good agreement with the experimental and analytical results.

5.3 SIMULATION OF SID OF RBCS IN AXISYMMETRIC STENOSED CORONARY ARTERIES

5.3.1 Problem Description and Computational Mesh

The 3D axisymmetric stenosed CA geometry with boundary conditions is shown in Fig. 5.2. The cosine function (Rabby et al. 2014) is used to define the geometry of stenosis and is given by:

$$\frac{r(x)}{R} = 1 - \delta_c \left[1 + \cos\left(\frac{x\pi}{D}\right) \right], -D \leq x \leq D \quad (5.12)$$

Where x and r corresponds to the axial and radial coordinates respectively. The R and D correspond to the radius and diameter of the un-stenosed vessel respectively. The δ_c is a constant and takes the value of 0.70, 0.50, 0.30 and 0.15 resulting in 30%, 50%, 70% and 85% of diameter reduction at the throat section. The length of the inlet zone, stenosis zone, and outlet zone are 56 mm, 8 mm and 116 mm respectively and combining all lengths gives a total length of 180 mm. The selected geometry of the CA had a 4 mm lumen diameter which is typical of a left main CA (Nosovitsky et al. 1997).

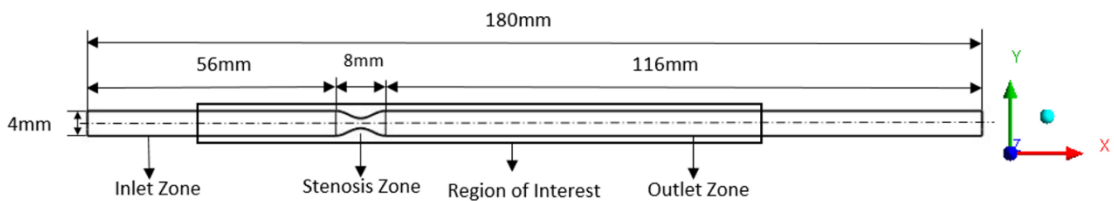


Figure 5.2 The geometry of ideal stenosed artery with dimensions showing the boundary conditions and region of interest

The computer-aided design software ANSYS design modelling is used for the generation of 3D idealized geometries and the grid. The CA geometry for different DOS severities is shown in the Fig. 5.3. For a generation of unstructured tetrahedral mesh with variable mesh spacing a robust scheme was adapted to signify rapidly and small varying features in the stenosis region. The final grid consisted of 389180 elements as shown in Fig. 5.4.

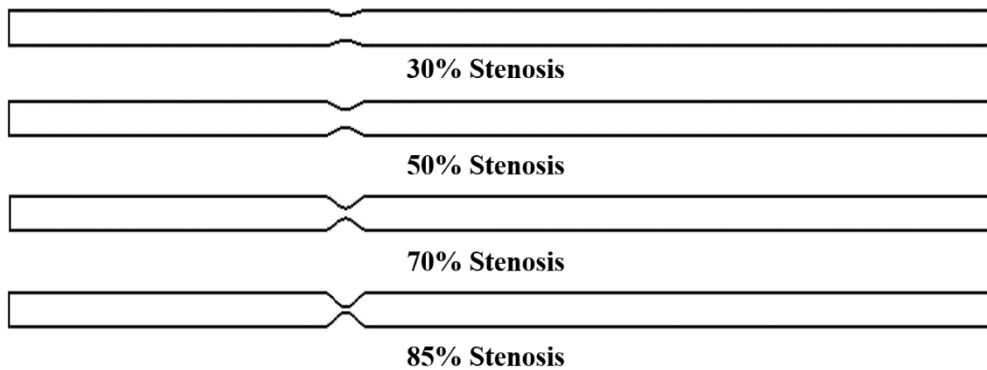


Figure 5.3 Idealized stenosis CA models having different DOS severities

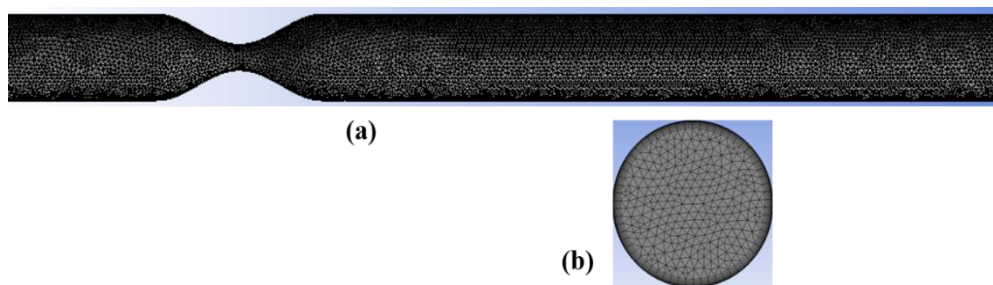


Figure 5.4 Computational grid: (a) 3-D computational grid for an idealized artery with 50% diameter reduction stenosis. (b) Cross section grid presenting the prism layers to acquire the flow near the wall

5.3.2 Boundary Conditions

A transient blood flow simulation was performed using rheological properties of blood. At the inlet, the pulsatile velocity waveform taken from Berne and Levy (1967)

as shown in Fig. 5.5 was imposed using an inlet UDF code and at the outlet, the ‘outflow’ boundary condition was applied. At the wall, ‘no-flux’ and ‘no-slip’ were applied as wall boundary condition. For all the DOS models, a uniform RBC haematocrit of 0.45 was used as an inlet boundary condition. The RBCs were assumed to be spherical rigid particles with average diameter of $8\mu\text{m}$. In this chapter, we used 1025 kg/m^3 as plasma density and 1100 kg/m^3 as RBC density (Caro 2012). A maximum Reynolds number of 410 is achieved at the inlet based on the artery diameter during maximum flow at beginning of diastole ($t=0.55\text{s}$). In this chapter, we assumed that the stenosis and artery wall is rigid and the blood flows as laminar.

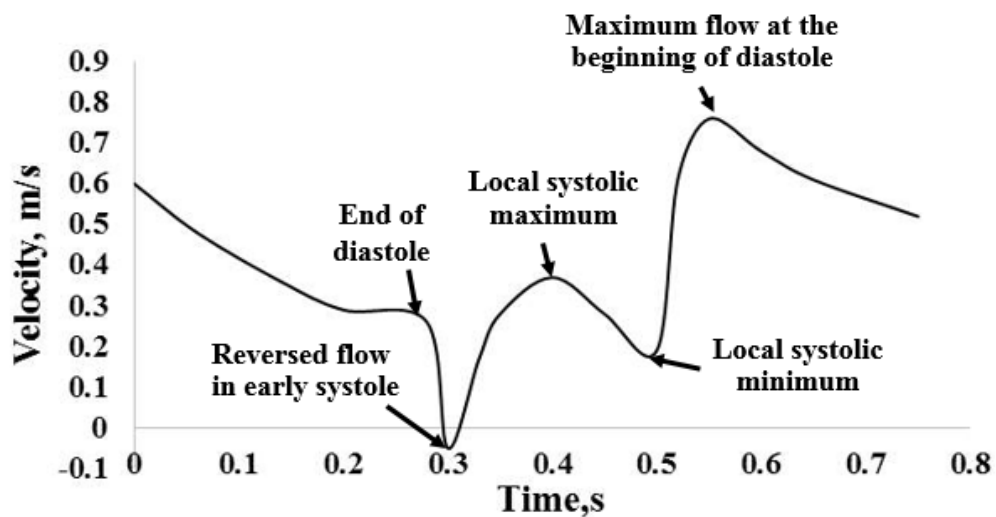


Figure 5.5 Inlet pulsatile coronary velocity profile for blood (plasma and RBC) during a single cardiac cycle (Berne and Levy 1967)

5.4 RESULTS AND DISCUSSIONS

5.4.1 Velocity Distribution

To understand the SID impact on velocity fields, simulation of non-Newtonian blood flow with and without SID models has been performed for 70% DOS. The comparison of velocity profiles at different axial positions (a) $Z/L = -1D$, (b) $Z/L = 0D$, (c) $Z/L = 1D$, and (d) $Z/L = 2D$ in the lateral direction of the artery for 70% DOS with and without consideration of SID are shown in Fig. 5.6. The velocity profiles are obtained at maximum blood flow which occurs at the beginning of diastole.

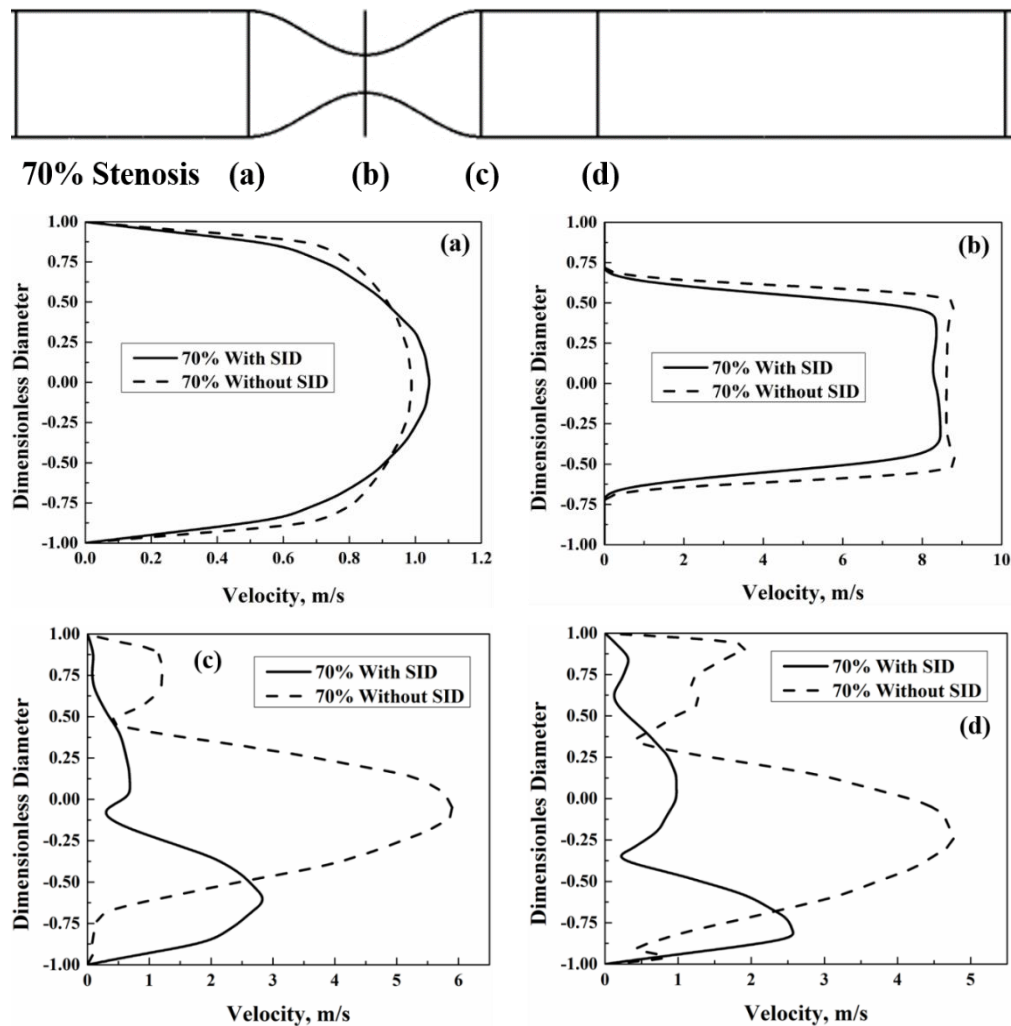


Figure 5.6 Comparison of lateral velocity profiles at different axial positions with and without consideration of SID of RBCs for 70% DOS (a) $Z/L=-1D$, (b) $Z/L=0D$, (c) $Z/L=1D$, and (d) $Z/L=2D$

It can be observed that both the non-Newtonian blood with and without RBCs suspensions shows axisymmetric velocity profile at the proximal region and disturbed profile in the distal region of stenosis. Also, for the non-Newtonian blood flow without the SID model, the velocity profile in the proximal region of the stenosis is flatter compared to velocity profile obtained without considering SID. In the proximal region of the stenosis, there is a decrease in RBC concentration towards the artery centre which decreases the viscosity at the centre and hence increases the velocity at the centre. At the stenosis throat, the velocity is reduced for model considering SID. This is due to the increase in haematocrit value at the throat.

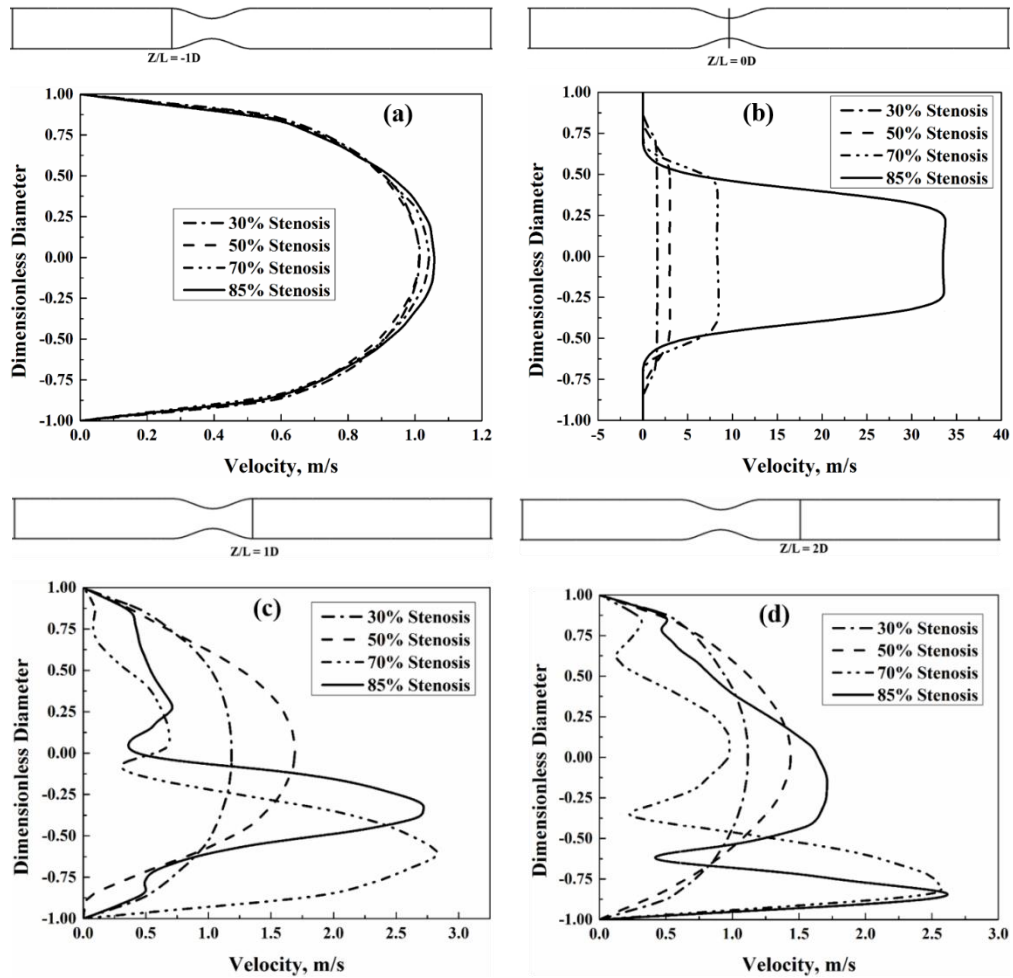


Figure 5.7 Effect of DOS severity on velocity profiles at different axial positions (a) $Z/L=-1D$, (b) $Z/L=0D$, (c) $Z/L=1D$, and (d) $Z/L=2D$ in the lateral direction

The effect of stenosis severity on blood velocity profiles obtained at maximum blood flow at different axial sites in the artery in lateral directions for different DOS severities is depicted in Fig. 5.7. Figure 5.7 (a) shows the velocity profile of blood is fully developed at the beginning of the stenosis and is not significantly affected by the DOS. The velocity gradient is high at the wall and decreases until it reaches zero at the centre. Whereas, in Fig. 5.7 (b), it can be clearly noticed that at the stenosis throat region ($Z/L=0D$) for all DOS severities the velocity profile has a blunted shape (plug-like profile) rather than a parabolic shape which may be attributed to the migration of the RBCs to the vessel core (centre) region. The degree of velocity profile bluntness was found to increase with the increase in DOS severity which is due to the increase in average flow velocity as the throat diameter reduces.

Figure 5.7 (c) and (d) shows the corresponding velocity profiles at locations 4 mm ($Z/L=1D$) and 8 mm ($Z/L= 2D$) in the downstream region of stenosis. The velocity profiles in the downstream region are fully disturbed and fluctuating due to the presence of large secondary recirculating flows for the DOS 70% and 85% models. As suggested by Zhao and Shaqfeh (2011), RBC migration away from the wall drives the platelets in to the cell-free layer towards the artery wall where these large fluctuations in velocity are negligible.

5.4.2 Particle Concentration Distribution

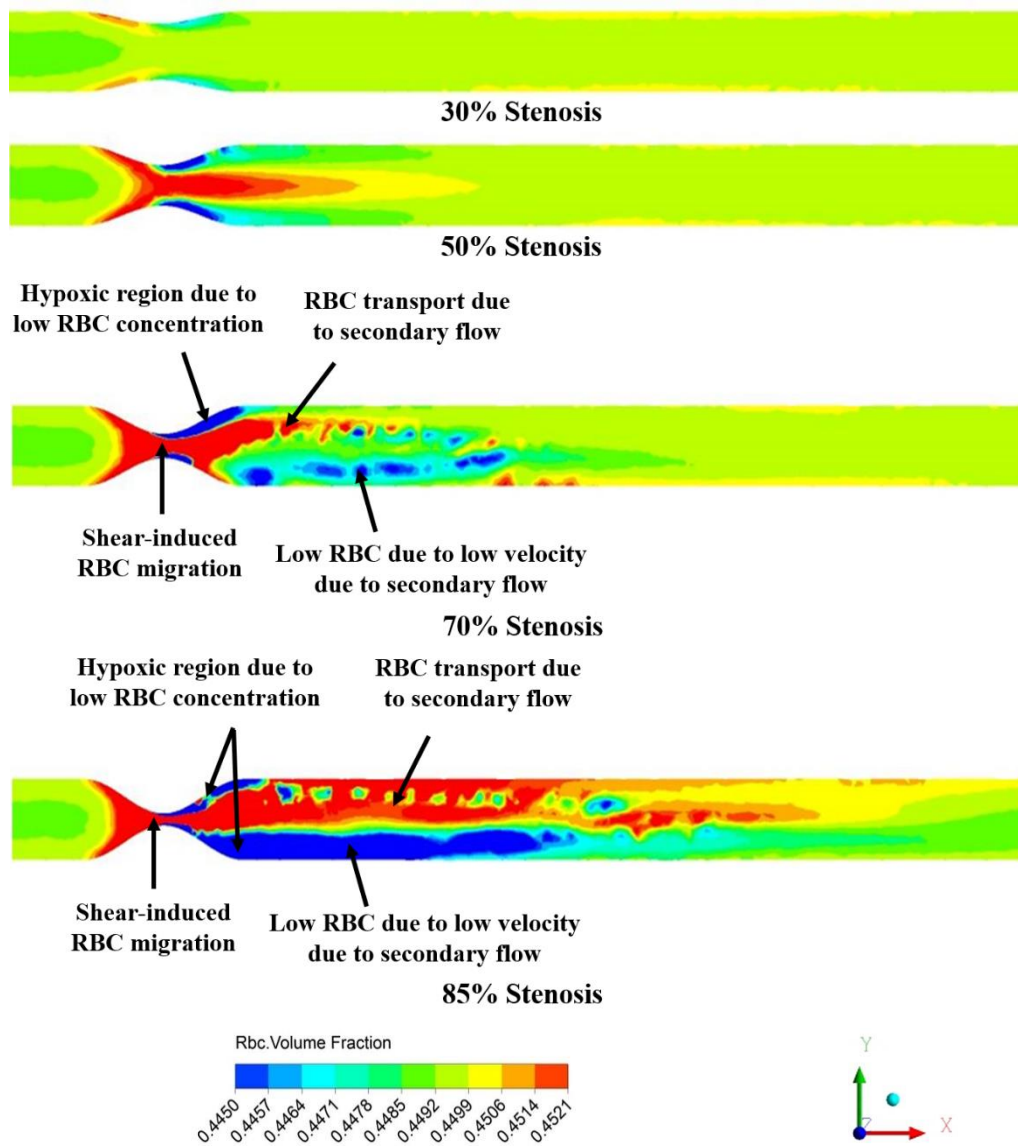


Figure 5.8 RBC VF contour maps at the midplane for different DOS severities
obtained at maximum blood flow

Figure 5.8 depicts the distribution of RBC VF on the symmetry cut plane for different DOS severities obtained when the blood flow was at maximum i.e. at the beginning of diastole ($t=0.55s$). For clarity, results are shown only in the region of interest around the stenosis. As the flow enters the stenosed region the SID causes the RBCs to move toward the centre of the tube. The migration of RBCs in the stenosis region increases gradually as the DOS severity increases. In the artery models with 50, 70 and 85% DOS the RBC VF is higher at the stenosis throat and RBCs have fully migrated towards the centre of stenosis region from the wall of the artery. In the downstream flow region of stenosis for models with DOS 50% and above, the SID of RBCs leads to a highly random distribution of RBC VF due to the presence of flow recirculation and secondary flow fields (Fig. 5.8).

In all the artery models the stenosis presents low RBC VF values in the distal section (expanding section) of stenosis throat caused by low shear rates that results in a noticeable RBC migration. This may lead to a reduction in the accessibility of oxygen at the arterial endothelial surface through a reduced RBC VF and hence contribute to local hypoxia (Biasetti et al. 2014). In Fig. 5.8 for all the models, it is observed that the pattern of low wall RBC VF coincides with the areas of low WSS (c.f. Fig. 5.10). Formation of atherosclerotic plaque is reported at low WSS sites (Zarins et al. 1983, Ku et al. 1985) i.e. behind the stenosis and in regions where the flow is recirculating. For the stenosis models with 70% and 85% DOS the inhomogeneties in wall RBC VF observed in the distal section of stenosis increases which is the result of the flow disturbances present in the stenosis distal section (c.f. Fig. 5.8). The length of the inhomogeneous zone increases with stenosis severity.

In order to comprehend the quantitative nature of variation in RBC wall concentration with respect to DOS severity, the RBC VF profiles in the lateral direction at different axial locations in an artery for different DOS severities are shown in Fig. 5.9. The RBC VF profile at location $Z/L = -1D$ becomes fully developed for all DOS models and it remains unaffected by the DOS severity (c.f.

Fig. 5.9 (a). Prior to stenosis region the migration of RBC is weaker (c.f. Fig. 5.9 (a)) and in fact the RBC concentration decreases slightly at the entrance, whereas the local RBC VF increases significantly at the stenosis throat due to enhanced SID of RBCs from maximum shear rate (near the wall) to the minimum shear rate (near center) regions as seen in Fig. 5.9 (b). At the stenosis throat, the RBC concentration increases at the centre with an increase in DOS and RBC concentration at the wall decreases as the DOS increases. The maximum variation of RBC wall concentration at the lumen surface is 0.0224%, 0.056%, 0.262% and 1.568% of the inlet haematocrit value for 30%, 50%, 70% and 85% DOS respectively. SID increases with flow velocity due to the increase in wall shear rate.

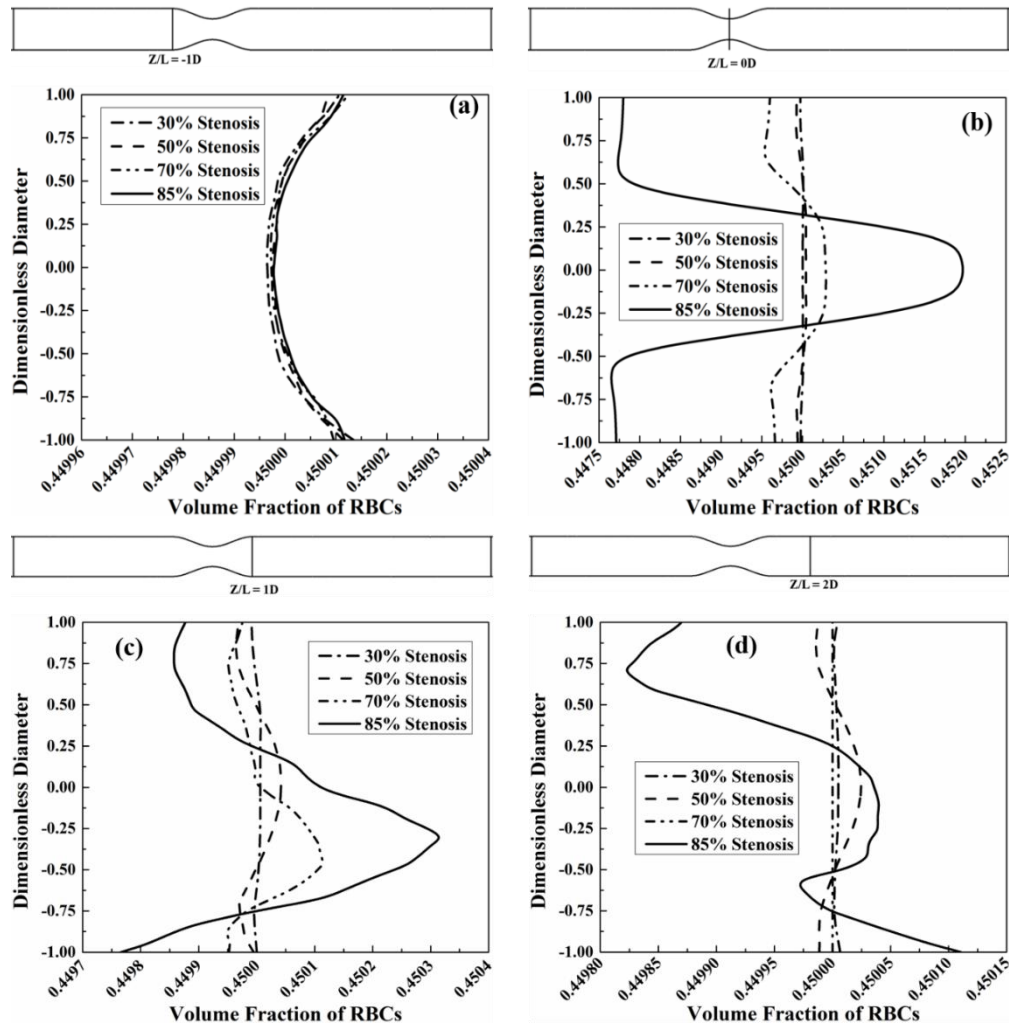


Figure 5.9 Comparison of the RBCs VF profiles at different axial positions (a) $Z/L=-1D$, (b) $Z/L=0D$, (c) $Z/L=1D$, and (d) $Z/L=2D$ for different DOS

Figures 5.9 (c) and (d) shows the distribution of RBC concentration in the downstream region at distances 1D and 2D from the centre of the stenosis. From Fig. 5.9 (c) and (d) it is evident that the RBC concentration is fully disturbed and asymmetric due to the presence of low velocities, large flow disturbance and the presence of turbulence in flow mainly for the models having stenosis above 50%. The lateral changes in RBC VF at the stenosis and in stenosis distal region alter the viscosity of blood and may result in the initiation of a sequence of biological actions such as NO scavenging by RBC hemoglobin and the distribution of oxygen in the arterial lumen (Liu et al. 2012). This altered NO transport by RBC hemoglobin in blood vessels has been claimed to be the precursor for atherogenesis (Liu et al. 2012). Hypoxia at vessel wall has been anticipated to be a subsidizing cause to intimal hyperplasia and atherosclerosis (Crawford et al. 1980, Crawford and Blankenhorn, 1991).

5.4.3 WSS Distribution

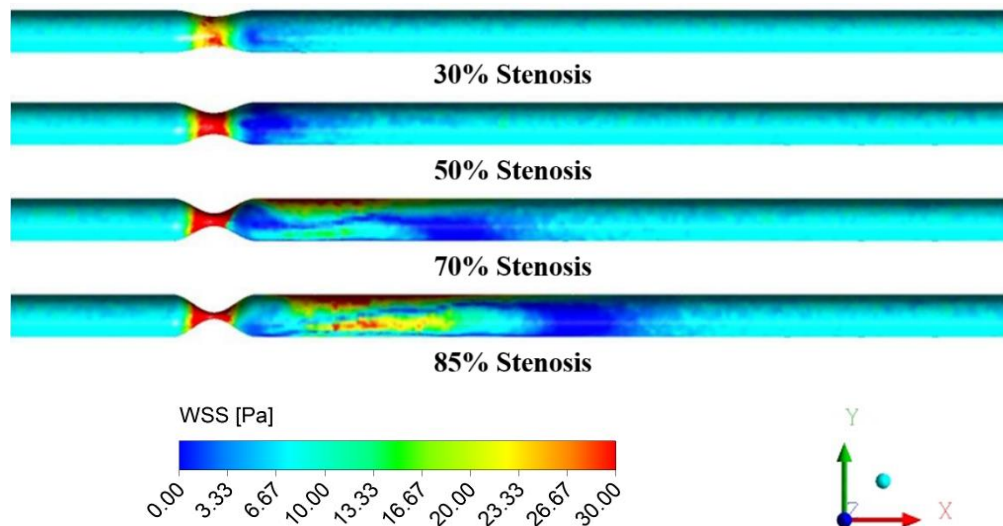


Figure 5.10 Wall shear stress contour for different DOS severities obtained at maximum blood flow at the beginning of diastole ($t=0.55s$)

The WSS is a significant hemodynamic measure that is widely studied in blood flow through arteries. The WSS at the arterial wall induces biological factors that dictate the platelet and vascular behaviour. In arteries, the risk of thrombosis is increased with high WSS. In spite of its significance, the role of SID on WSS in CAs with

different DOS severities has not received sufficient consideration in earlier studies. At the artery wall, the product of velocity gradient and blood viscosity is defined as the WSS. The blood viscosity is a function of RBCs VF and velocity gradient.

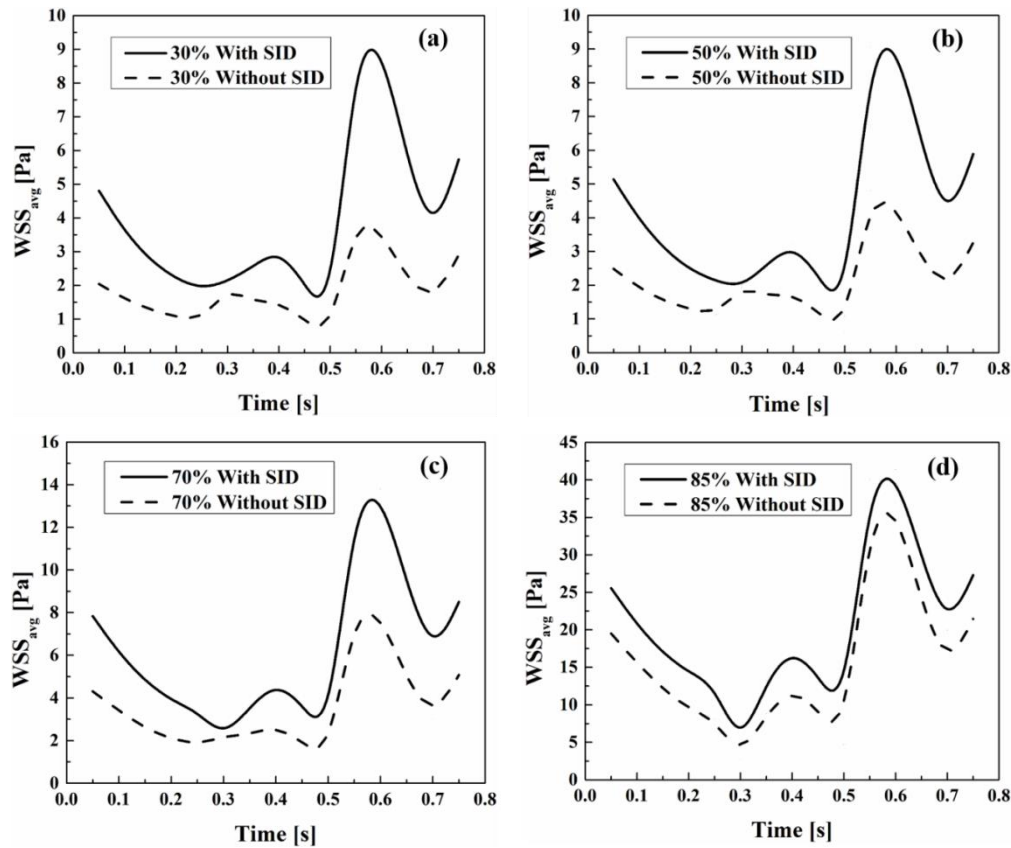


Figure 5.11 Average WSS (WSS_{avg}) versus time for one cardiac cycle with and without SID model, (a) 30%, (b) 50%, (c) 70% and (d) 85% DOS

The WSS contour maps for all DOS severity models at the maximum blood flow at the beginning of diastole are shown in Fig. 5.10. In all DOS severity models, it is observed that the maximum value of WSS befalls at the throat of stenosis and as the DOS severity increases the value of peak WSS increases. Comparing the WSS contour maps between different DOS models in Fig. 5.10, the stenosis formation had a strong influence on the WSS distributions. Especially, large areas of the low and oscillating WSS on arterial wall surface are visible in the distal section of the stenosis for DOS 70% and above. These areas are prone to EC dysfunction and lead to thrombosis and atherogenesis (Chiu and Chien, 2011). The flow recirculation and presence of secondary flow in the downstream region increases as the DOS severity

increases (c.f. Fig. 5.7). This flow recirculation in the downstream region alters the WSS and leads to low and oscillating WSS (Attia et al. 2018). The value of WSS increases exponentially as the DOS severity increases above 50% stenosis.

The comparison of WSS_{avg} between non-Newtonian blood flow model with and without consideration of SID for different DOS severities are shown in Fig. 5.11. It can be observed that for all DOS models the WSS_{avg} is consistently more for the non-Newtonian blood flow model considering SID. Aforesaid, WSS is a product of local effective viscosity of blood and velocity gradient at the wall. The SID of RBCs towards the centre reduces the RBC concentration near the artery wall thus reducing the blood viscosity. Reduction in viscosity near the wall on the other hand increases the velocity gradient (shear rate) near the wall. Given that the WSS considering the SID is always higher than without considering SID indicates that the velocity increase due to reduction in viscosity is more than the decrease in WSS due to viscosity reduction. The velocity gradient is more at the stenosis and in distal wall regions which increases the WSS. The maximum difference in WSS_{avg} between models with and without SID is 55.45%, 53.26%, 41.89% and 10.70% for DOS 30%, 50%, 70% and 85% respectively. Though the maximum difference decreases with increase in DOS as a percentage of WSS_{avg} calculated without SID, the increase in absolute value of WSS_{avg} by including SID is in the range of 4-6 Pa irrespective of DOS. Under-prediction of WSS_{avg} by the model without SID highlights the importance of including SID phenomenon in calculating the hemodynamic parameters and hence can provide a more accurate hemodynamic model.

5.5 SUMMARY

To study the effects of DOS on SID of RBCs in blood flow through idealized stenosed CAs, numerical simulations were conducted and the following conclusions were drawn.

The multiphase mixture model with SID coupled with Quemada non-Newtonian viscosity model is fitted with an improved boundary condition and was found to provide better velocity and concentration profiles compared to the analytical

data of Phillips. The influence of DOS on the velocity profiles in the proximal region of stenosis is insignificant. However, the DOS has a substantial influence on the blood velocity profile in the distal regions and becomes asymmetric for 70% and above stenosis severity. The migration of RBCs towards the centre at the stenosis throat increases exponentially as the DOS severity increases. At the stenosis throat, the wall concentration decreases as the DOS increases and the concentration at the centre of artery increases with the DOS.

Among all DOS models, 85% DOS had the lowest concentration of RBCs near the wall and highest concentration at the centre. The DOS severity has a profound effect on platelet wall concentration at the stenosis throat as the inward migration of RBCs might aid platelets margination towards the wall. This eventually increases the thrombosis formation in the event of plaque rupture. For the stenosis models with 70% and 85% DOS it is observed that the inhomogeneties in RBC wall concentration increases at the distal section of stenosis. This is due to flow becoming turbulent behind the stenosis for DOS above 70%. It is observed that with the increase in DOS severity, the peak velocity increases drastically at the stenosis throat and RBC migration towards the centre increases strengthening hypoxic conditions at the stenotic area. Further, the accumulation of RBCs at the centre results in a substantial increase in blood viscosity at the centre and reduces near the wall due to a reduction in RBC concentration.

In all the DOS severity models higher values of WSS is observed in the stenosis region and the maximum value of WSS increases drastically as the DOS severity increases. The maximum difference in WSS_{avg} between models with and without SID is 55.45%, 53.26%, 41.89% and 10.70% for DOS 30%, 50%, 70% and 85% respectively. However, the predicted WSS_{avg} considering SID increase consistently by 4-6 Pa irrespective of DOS. The wall regions with low WSS and low RBC concentration correlate well with the atherosclerosis sites observed clinically. In the arteries with 70% DOS and above large areas of the low and oscillating WSS on arterial wall surface were observed in the distal section of the stenosis which is mainly

due to low velocity and large flow disturbance in that region. This may have pathological consequences resulting in EC dysfunction leading to atherogenesis.

CHAPTER 6

SUMMARY, CONCLUSIONS AND FUTURE SCOPE

6.1 SUMMARY

Researchers in fluid dynamics have proposed various relationships between plaque growth and WSS in the arterial wall. Both low and high WSS areas have been suggested as being preferential sites for the progression and development of atherosclerosis. The understanding of HDs such as WSS and WSS based HDs within the walls of tortuous and stenotic coronary arteries is of great significance for detailed clinical diagnosis and pathological research. Studies on effect of tortuosity and stenosis on the biomechanical hemodynamic parameters by considering the blood as a multiphase fluid is still limited.

It is well known that HDs constitute a key role in the diagnosis of the local distribution of atherosclerosis plaque. The main purpose of this study was to obtain the multiphase blood flow characteristics through tortuous and stenotic coronary arteries. This can be utilized to determine the effects of stenosis severity and tortuosity morphological indices on the progression and development of the disease in order to find the regions of arteries at risk of atherosclerosis development.

Also, the multiphase blood flow model is successfully applied to study the effect of stenosis severity on shear induced diffusion of red blood cells in stenosed coronary arteries. The multiphase mixture theory model used in the present study is validated successfully and it was found that the results were in good agreement with experimental data and performed better than single phase model.

The multiphase mixture blood flow model used in this work is able to forecast the main features of the physiological blood flow in idealized artery geometries. The study also helps in understanding how the stenosis severity and coronary tortuosity via various HDs contributes to the progression and pathology of the disease.

6.2 CONCLUSIONS

In this study, to the best of our knowledge, it is addressed for the first time a multiphase blood flow study using mixture-theory to investigate the effect of stenosis severity and coronary tortuosity on WSS and WSS based HDs in idealized stenosed and tortuous coronary arteries. The following conclusions were drawn.

- Simulation of RBC velocity distribution in a rectangular microchannel using single phase and multiphase mixture model were carried out and compared with experimental results. It is observed that, multiphase mixture model results were in good agreement with experimental data and performed better than single phase model.
- If the stenosis severity is more than 50%, the WSS is very high at the stenosis throat and the formation of recirculation zone is higher in post-stenosis region. This could lead to further progression of stenosis and may promote a higher risk of atherogenesis and plaque buildup in the flow-disturbed area. It can be concluded that WSS and WSS based hemodynamic indicators were significantly affected by the presence of stenosis and increases with DOS.
- Our findings suggest that all the tortuosity morphological indices, CR, DBB and AoB have significant influence on the distributions of various HDs and artery hemodynamics. Artery wall regions with the high OSI, low TAWSS, high RRT, high TAWSSG and high ECAP which are widely accepted as sites vulnerable for atherogenesis and plaque progression has been identified and quantified for various tortuosity morphological indices. These sites were witnessed at the inner artery wall downstream regions of the bends in all the tortuous artery models studied and found to increase as the CR and DBB were reduced. However, potential zones were found to increase as the AoB is increased.
- The multiphase mixture model with shear induced diffusion (SID) coupled with Quemada non-Newtonian viscosity model is fitted with an improved boundary condition and was found to provide better velocity and concentration profiles compared to the analytical data of Phillips. The influence of DOS on the velocity

profiles in the proximal region of stenosis is insignificant. However, the DOS has a substantial influence on the blood velocity profile in the distal regions and becomes asymmetric for 70% and above severity.

- The migration of RBCs towards the centre at the stenosis throat increases exponentially as the DOS severity increases. At the stenosis throat, the wall concentration decreases as the DOS increases. Among all DOS models, 85% DOS had the lowest concentration of RBCs near the wall and highest concentration at the centre. For the stenosis models with 70% and 85% DOS it is observed that the inhomogeneity in RBC wall concentration increases at the distal section of stenosis.

6.3 SCOPE OF FUTURE WORK

The flow of blood in stenotic and tortuous coronary arteries reveals a very complex interaction of biological and mechanical activities, which, despite its significance, is still poorly understood. There is a strong need for advanced computational models and experimental data to supplement these.

Even though in the present study a considerable understanding was gained into the multiphase blood flow phenomena in tortuous and stenotic coronary arteries, a few number of questions still continue to be answered for future research. Such questions arise as numerical simulations of blood flow through idealized stenotic and tortuous arteries are not fully physiologically representative of what happens in the patient specific blood flow field.

In future scope, this multiphase mixture theory blood flow model with components of blood in addition to RBCs comprising WBCs, lipoproteins and platelets can be applied to different patient-specific arterial geometries in the human body and examine the biomechanical and HDs in real patient-specific models. The mass transfer of these blood components and the HDs affecting the progression and initiation of CVDs can be more clearly understood.

The effect of wall circumferential deformation and dynamic heart motion on the HDs is neglected in the present study. In reality, the CAs during each cardiac cycle is

subjected to contraction, dilation, repetitive flexion and relaxation motion. It is true that the above have some effect on HDs. Hence, it will be worth of studying these effects on the hemodynamics. It is presumed that the numerical blood flow simulations considering the above conditions, in combination with appropriate experiments, may play a critical role in future disease diagnosis and in understanding the pathophysiology of disease, better-quality design of surgical devices, and surgical planning.

REFERENCES

- Aarts, P. A., van den Broek, S. A., Prins, G. W., Kuiken, G. D., Sixma, J. J. and Heethaar, R. M. (1988). "Blood Platelets Are Concentrated Near the Wall and Red Blood Cells, In The Center in Flowing Blood." *Arterioscler. Thromb. Vasc. Biol.*, 8(6), 819-824.
- Aayani, R., Shahidian, A. and Ghassemi, M. (2016). "Numerical Investigation of Non-Newtonian Blood Effect on Acoustic Streaming." *J. Appl. Fluid. Mech.*, 9(1), 173-176.
- Abbott, J. R., Tetlow, N., Graham, A. L., Altobelli, S. A., Fukushima, E., Mondy, L. A. and Stephens, T. S. (1991). "Experimental Observations of Particle Migration in Concentrated Suspensions: Couette Flow." *J. Rheol.*, 35(5), 773-795.
- Ahmed, G. Y. and Singh, A. (2011). "Numerical Simulation of Particle Migration in Asymmetric Bifurcation Channel." *J. Nonnewton. Fluid. Mech.*, 166(1-2), 42-51.
- Ahmed, S. A. and Giddens, D. P. (1983). "Flow Disturbance Measurements Through a Constricted Tube at Moderate Reynolds Numbers." *J. Biomech.*, 16(12), 955-963.
- Aidun, C. K. and Clausen, J. R. (2010). "Lattice-Boltzmann Method for Complex Flows." *Annu. Rev. Fluid. Mech.*, 42, 439-472.
- ANSYS, Inc. (2012). "ANSYS User and Theory Guide." ANSYS Fluent, Release 14.5.
- Arp, A. P. and Mason, S. G. (1977). "The Kinetics of Owing Dispersions. IX. Doublets of Rigid Spheres (Experimental)." *J. Colloid. Interface. Sci.*, 61, 44-61.
- Atkin, R. J. and Craine, R. E. (1976a). "Continuum Theories of Mixtures: Applications." *IMA J. Appl. Math.*, 17(2), 153-207.
- Atkin, R. J. and Craine, R. E. (1976b). "Continuum Theories of Mixtures: Basic Theory and Historical Development." *Q. J. Mech. Appl. Math.*, 29(2), 209-244.

Attia, R. M., Eldosoky, M. A. and Darwish, R. R. (2018). "A Numerical Study of the Blood Flow Behavior in Coronary Artery Anomalies for Normal and Diabetic Persons." *J. Mech. Med. Biol.*, 18(05), 1850051.

Bagchi, P. (2007). "Mesoscale Simulation of Blood Flow in Small Vessels." *Biophys. J.*, 92(6), 1858-1877.

Bao, X., Lu, C. and Frangos, J. A. (1999). "Temporal Gradient in Shear but Not Steady Shear Stress Induces PDGF-A and MCP-1 Expression in Endothelial Cells: Role of NO, Nfkb, And Egr-1." *Arterioscler. Thromb. Vasc. Biol.*, 19(4), 996-1003.

Başkurt, O. K. (2003). "Pathophysiological Significance of Blood Rheology." *Turk. J. Med. Sci.*, 33(6), 347-355.

Bassiouny, H. S., White, S., Glagov, S., Choi, E., Giddens, D. P. and Zarins, C. K. (1992). "Anastomotic Intimal Hyperplasia: Mechanical Injury or Flow Induced." *J. Vasc. Surg.*, 15(4), 708-717.

Bedford, A. and Drumheller, D. S. (1983). "Theories of Immiscible and Structured Mixtures." *Int. J. Eng. Sci.*, 21(8), 863-960.

Beech-Brandt, J. J., Easson, W. J. and Hoskins, P. R. (2005). "Large Eddy Simulation of Flow in A Tube with an Axisymmetric Stenosis." In *Proc. Third IASTED Int. Conf. on Biomechanics*, 145-150.

Beg, O. A., Rashidi, M. M., Akbari, M. and Hosseini, A. (2014). "Comparative Numerical Study of Single-Phase and Two-Phase Models for Bio-Nanofluid Transport Phenomena." *J. Mech. Med. Biol.*, 14(01), 1450011.

Berger, S. and Jou, L. (2000). "Flows in Stenotic Vessels." *Annu. Rev. Fluid. Mech.*, 32, 347-382.

Berne, R. M. and Levy, M. N. (1967). *Cardiovascular physiology*. Mosby, United States.

- Berthier, B., Bouzerar, R. and Legallais, C. (2002). "Blood Flow Patterns in an Anatomically Realistic Coronary Vessel: Influence of Three Different Reconstruction Methods." *J. Biomech.*, 35(10), 1347-1356.
- Bharadvaj, B. K., Mabon, R. F. and Giddens, D. P. (1982). "Steady Flow in A Model of the Human Carotid Bifurcation. Part I—Flow Visualization." *J. Biomech.*, 15(5), 349-362.
- Biasetti, J., Spazzini, P. G., Hedin, U. and Gasser, T. C. (2014). "Synergy Between Shear-Induced Migration and Secondary Flows On Red Blood Cells Transport in Arteries: Considerations On Oxygen Transport." *J. Royal. Soc. Interface.*, 11(97), 20140403.
- Bowen, R. M. (1976). *Theory of Mixtures in Continuum Physics III.*" Ed. AC Eringen, Academic Press: New York. 11-32.
- Bronzino, J. D. (1999). *Biomedical Engineering Handbook.* (Vol. 2). CRC press.
- Brooks, D. E., Goodwin, J. W. and Seaman, G. V. (1970). "Interactions Among Erythrocytes Under Shear." *J. Appl. Physiol.*, 28(2), 172-177.
- Buchanan Jr, J. R., Kleinstreuer, C. and Comer, J. K. (2000). "Rheological Effects On Pulsatile Hemodynamics in A Stenosed Tube." *Comput. Fluids.*, 29(6), 695-724.
- Buchanan, J. R., Kleinstreuer, C., Hyun, S. and Truskey, G. A. (2003). "Hemodynamics Simulation and Identification of Susceptible Sites of Atherosclerotic Lesion Formation in A Model Abdominal Aorta." *J. Biomech.*, 36(8), 1185-1196.
- Buradi, A. and Mahalingam, A. (2018). "Effect of Stenosis Severity on Wall Shear Stress Based Hemodynamic Descriptors using Multiphase Mixture Theory." *J. Appl. Fluid. Mech.*, 11(6), 1497-1509.
- Burton, A. (1965). "Physiology and Biophysics of the Circulation." *Acad. Med.*, 40 (8).

Butler, A. R., Megson, I. L. and Wright, P. G. (1998). "Diffusion of Nitric Oxide and Scavenging by Blood in The Vasculature." *Biochim. Biophys. Acta. Gen. Subj.*, 1425(1), 168-176.

Caro, C. G. (1978). *The Mechanics of the Circulation*. Oxford, Oxford University Press.

Caro, C. G. (2009). "Discovery of The Role of Wall Shear in Atherosclerosis." *Arterioscler. Thromb. Vasc. Biol.*, 29(2), 158-161.

Caro, C. G., Fitz-Gerald, J. M. and Schroter, R. C. (1969). "Arterial Wall Shear and Distribution of Early Atheroma in Man." *Nature.*, 223(5211), 1159-1161.

Caro, C. G., Fitz-Gerald, J. M. and Schroter, R. C. (1971). "Atheroma and Arterial Wall Shear-Observation, Correlation and Proposal of a Shear Dependent Mass Transfer Mechanism for Atherogenesis." *Proc. R. Soc. Lond. B. Biol. Sci.*, 177(1046), 109-133.

Caro, C. G., Pedley, T. J. and Schroter, R. C. (2012). *The Mechanics of the Circulation*. Cambridge University Press, United Kingdom.

Carty, G., Chatpun, S. and Espino, D. M. (2016). "Modeling Blood Flow Through Intracranial Aneurysms: A Comparison of Newtonian and Non-Newtonian Viscosity." *J. Med. Biol. Eng.*, 36(3), 396-409.

Chatzizisis, Y. S., Baker, A. B., Sukhova, G. K., Koskinas, K. C., Papafaklis, M. I., Beigel, R. and Shi, G. P. (2011). "Augmented Expression and Activity of Extracellular Matrix-Degrading Enzymes in Regions of Low Endothelial Shear Stress Colocalize with Coronary Atheromata with Thin Fibrous Caps in Pigs." *Circulation.*, 123(6), 621-630.

Chatzizisis, Y. S., Coskun, A. U., Jonas, M., Edelman, E. R., Feldman, C. L. and Stone, P. H. (2007). "Role of Endothelial Shear Stress in The Natural History of Coronary Atherosclerosis and Vascular Remodeling: Molecular, Cellular, And Vascular Behavior." *J. Am. Coll. Cardiol.*, 49(25), 2379-2393.

Cheng, C., Helderman, F., Tempel, D., Segers, D., Hierck, B., Poelmann, R. and & van Haperen, R. (2007). "Large Variations in Absolute Wall Shear Stress Levels Within One Species and Between Species." *Atherosclerosis.*, 195(2), 225-235.

Cheng, C., Tempel, D., van Haperen, R., van der Baan, A., Grosveld, F., Daemen, M. J. and de Crom, R. (2006). "Atherosclerotic Lesion Size and Vulnerability Are Determined by Patterns of Fluid Shear Stress." *Circulation.*, 113(23), 2744-2753.

Chesnutt, J. K. and Han, H. C. (2011). "Tortuosity Triggers Platelet Activation and Thrombus Formation in Microvessels." *J. Biomech. Eng.*, 133(12), 121004.

Chien, S. (1970). "Shear Dependence of Effective Cell Volume as A Determinant of Blood Viscosity." *Science.*, 168(3934), 977-979.

Chien, S., Usami, S. H. U. N. I. C. H. I., Taylor, H. M., Lundberg, J. L. and Gregersen, M. I. (1966). "Effects of Hematocrit and Plasma Proteins On Human Blood Rheology at Low Shear Rates." *J. Appl. Physiol.*, 21(1), 81-87.

Chiu, J. J. and Chien, S. (2011). "Effects of Disturbed Flow On Vascular Endothelium: Pathophysiological Basis and Clinical Perspectives." *Physiol. Rev.*, 91(1), 327-387.

Cho, Y. I. and Kensey, K. R. (1991). "Effects of The Non-Newtonian Viscosity of Blood On Flows in A Diseased Arterial Vessel. Part 1: Steady Flows." *Biorheology.*, 28(3-4), 241-262.

Chow, A. W., Sinton, S. W., Iwamiya, J. H. and Stephens, T. S. (1994). "Shear-Induced Particle Migration in Couette and Parallel-Plate Viscometers: NMR Imaging and Stress Measurements." *Phys. Fluids.*, 6(8), 2561-2576.

Cokelet, G. R. (1986). "The Rheology and Tube Flow of Blood." *Handbook of Biomechanics*, McGraw-Hill, New York.

Cokelet, G. R. (1999). "Viscometric, In Vitro and in Vivo Blood Viscosity Relationships: How Are They Related?". Lecture given 20 July, 1999 at the 10th

International Congress of Biorheology, Pécs, Hungary. *Biorheology.*, 36(5, 6), 343-358.

Crawford, D. W. and Blankenhorn, D. H. (1991). "Arterial Wall Oxygenation, Oxyradicals, and Atherosclerosis." *Atherosclerosis.*, 89(2-3), 97-108.

Crawford, D. W., Back, L. H. and Cole, M. A. (1980). "In Vivo Oxygen Transport in The Normal Rabbit Femoral Arterial Wall." *J. Clin. Invest.*, 65(6), 1498-1508.

Cunningham, K. S. and Gotlieb, A. I. (2005). "The Role of Shear Stress in The Pathogenesis of Atherosclerosis." *Lab. Invest.*, 85(1), 9-23.

Davies, P. F. (1995). "Flow-Mediated Endothelial Mechanotransduction." *Physiol. Rev.*, 75(3), 519-560.

De Siqueira, I. R. and da Carvalho, M. S. (2018). "Shear-Induced Particle Migration in The Flow of Particle Suspensions Through a Sudden Plane Expansion." *J. Braz. Soc. Mech. Sci. & Eng.*, 40(4), 228.

Dekker, R. J., Boon, R. A., Rondaij, M. G., Kragt, A., Volger, O. L., Elderkamp, Y. W. and Horrevoets, A. J. (2006). "KLF2 Provokes a Gene Expression Pattern That Establishes Functional Quiescent Differentiation of the Endothelium." *Blood.*, 107(11), 4354-4363.

DePaola, N., Gimbrone Jr, M. A., Davies, P. F. and Dewey Jr, C. F. (1992). "Vascular Endothelium Responds to Fluid Shear Stress Gradients." *Arterioscler. Thromb. Vasc. Biol.*, 12(11), 1254-1257.

Di Achille, P., Tellides, G., Figueroa, C. A. and Humphrey, J. D. (2014). "A Haemodynamic Predictor of Intraluminal Thrombus Formation in Abdominal Aortic Aneurysms." *Proc, Math, Phys, Eng, Sci.*, 470(2172), 20140163.

Dupin, M. M., Halliday, I., Care, C. M., Alboul, L. and Munn, L. L. (2007). "Modeling The Flow of Dense Suspensions of Deformable Particles in Three Dimensions." *Phys. Rev. E.*, 75(6), 066707.

Easthope, P. L. and Brooks, D. E. (1980). "A Comparison of Rheological Constitutive Functions for Whole Human Blood." *Biorheology*, 17(3), 235-247.

Egorov, V. A., Regirer, S. A. and Shadrina, N. K. (1994). "Properties of Pulsating Blood Flow Through Resistive Blood Vessels." *Fluid. Dynam.*, 29(2), 221-226.

Ellwein, L. M., Otake, H., Gundert, T. J., Koo, B. K., Shinke, T., Honda, Y. and LaDisa, J. F. (2011). "Optical Coherence Tomography for Patient-Specific 3D Artery Reconstruction and Evaluation of Wall Shear Stress in A Left Circumflex Coronary Artery." *Cardiovasc. Eng. Technol.*, 2(3), 212.

Ethier, C. R. and Simmons, C. A. (2007). *Introductory Biomechanics: From Cells to Organisms*. Cambridge University Press.

Fang, Z. and Phan-Thien, N. (1995). "Numerical Simulation of Particle Migration in Concentrated Suspensions by A Finite Volume Method." *J. Nonnewton. Fluid. Mech.*, 58(1), 67-81.

Ferziger, J. H. and Peric, M. (2012). *Computational Methods for Fluid Dynamics*. Springer Science & Business Media.

Fry, D. L. (1968). "Acute Vascular Endothelial Changes Associated with Increased Blood Velocity Gradients." *Circ. Res.*, 22(2), 165-197.

Fry, D. L. (1976). "Hemodynamic Forces in Atherogenesis." *Cerebrovasc. Dis.*, 77-95.

Fung, Y. C. (1993). *Biomechanics: Mechanical Properties of Living Tissues*. 2nd edition, Springer-Verlag, New York Inc. (USA), 433.

Gadala-Maria, F. and Acrivos, A. (1980). "Shear-Induced Structure in A Concentrated Suspension of Solid Spheres." *J. Rheol.*, 24(6), 799-814.

Gaibazzi, N., Rigo, F. and Reverberi, C. (2011). "Severe Coronary Tortuosity or Myocardial Bridging in Patients with Chest Pain, Normal Coronary Arteries, And Reversible Myocardial Perfusion Defects." *Am. J. Cardiol.*, 108(7), 973-978.

Gidaspow, D. (1994). *Multiphase Flow and Fluidization: Continuum and Kinetic Theory Descriptions*. Academic press.

Gidaspow, D. and Huang, J. (2009). “Kinetic Theory Based Model for Blood Flow and Its Viscosity.” *Ann. Biomed. Eng.*, 37(8), 1534-1545.

Gijsen, F. J. H., Allanic, E., Van de Vosse, F. N. and Janssen, J. D. (1999). “The Influence of the Non-Newtonian Properties of Blood On the Flow in Large Arteries: Unsteady Flow in A 90 Curved Tube.” *J. Biomech.*, 32(7), 705-713.

Gijsen, F. J., van de Vosse, F. N. and Janssen, J. D. (1998). “The Influence of the Non-Newtonian Properties of Blood On the Flow in Large Arteries: Steady Flow in A Carotid Bifurcation Model.” *J. Biomech.*, 32(6), 601-608.

Han, H. C. (2012). “Twisted Blood Vessels: Symptoms, Etiology and Biomechanical Mechanisms.” *J. Vasc. Res.*, 49(3), 185-197.

Hasan, A. B. M. and Das, D. K. (2008). “Numerical Simulation of Sinusoidal Fluctuated Pulsatile Laminar Flow Through Stenotic Artery.” *J. Appl. Fluid. Mech.*, 1(2), 25-35.

Hasan, M., Rubenstein, D. A. and Yin, W. (2013). “Effects of Cyclic Motion On Coronary Blood Flow.” *J. Biomech. Eng.*, 135(12), 121002.

Haynes, R. H. (1960). “Physical Basis of the Dependence of Blood Viscosity On Tube Radius.” *Am. J. Physiol –Legacy. Content.*, 198(6), 1193-1200.

He, X. and Ku, D. N. (1996). “Pulsatile Flow in The Human Left Coronary Artery Bifurcation: Average Conditions.” *J. Biomech. Eng.*, 118(1), 74-82.

Hellums, J. D. (1994). “1993 Whitaker Lecture: Biorheology in Thrombosis Research.” *Ann. Biomed. Eng.*, 22(5), 445-455.

Helmlinger, G., Berk, B. C. and Nerem, R. M. (1995). "Calcium Responses of Endothelial Cell Monolayers Subjected to Pulsatile and Steady Laminar Flow Differ." *Am. J. Physiol. Cell. Physiol.*, 269(2), C367-C375.

Himabindu A. (2018). "Coronary Tortuosity and Its Clinical Significance." *Paripex-Indian J. Res.*, 7(7), 42-43.

Himburg, H. A., Grzybowski, D. M., Hazel, A. L., LaMack, J. A., Li, X. M. and Friedman, M. H. (2004). "Spatial Comparison Between Wall Shear Stress Measures and Porcine Arterial Endothelial Permeability." *Am. J. Physiol. Heart. Circ. Physiol.*, 286(5), H1916-H1922.

Hofer, M. and Perktold, K. (1997). "Computer Simulation of Concentrated Fluid-Particle Suspension Flows in Axisymmetric Geometries." *Biorheology.*, 34(4-5), 261-279.

Hoi, Y., Meng, H., Woodward, S. H., Bendok, B. R., Hanel, R. A., Guterman, L. R. and Hopkins, L. N. (2004). "Effects of Arterial Geometry On Aneurysm Growth: Three-Dimensional Computational Fluid Dynamics Study." *J. Neurosurg.*, 101(4), 676-681.

Hoi, Y., Zhou, Y. Q., Zhang, X., Henkelman, R. M. and Steinman, D. A. (2011). "Correlation Between Local Hemodynamics and Lesion Distribution in A Novel Aortic Regurgitation Murine Model of Atherosclerosis." *Ann. Biomed. Eng.*, 39(5), 1414-1422.

Hookham, P. A. (1986). "*Concentration and Velocity Measurements in Suspensions Flowing Through a Rectangular Channel.*" PhD Thesis, California Institute of Technology, USA.

Hosseinzadegan, H. and Tafti, D. K. (2017). "Prediction of Thrombus Growth: Effect of Stenosis and Reynolds Number." *Cardiovasc. Eng. Technol.*, 8(2), 164-181.

Hsiai, T. K., Cho, S. K., Wong, P. K., Ing, M., Sevanian, A., Navab, M. and HO, C. M. (2003). "Monocyte Recruitment to Endothelial Cells in Response to Oscillatory Shear Stress." *FASEB. J.*, 17(12), 1648-1657.

Huang, J., Lyczkowski, R. W. and Gidaspow, D. (2009). "Pulsatile Flow in A Coronary Artery Using Multiphase Kinetic Theory." *J. Biomech.*, 42(6), 743-754.

Hyun, S., Kleinstreuer, C., Longest, P. W. and Chen, C. (2004). "Particle-Hemodynamics Simulations and Design Options for Surgical Reconstruction of Diseased Carotid Artery Bifurcations." *J. Biomech. Eng.*, 126(2), 188-195.

Ishii, M. (1975). *Thermo-Fluid Dynamic Theory of Two-Phase Flow*. volume 22 of Direction des études et recherches d'électricité de France. Eyrolles, Paris.

Ishii, M. and Hibiki, T. (2010). *Thermo-Fluid Dynamics of Two-Phase Flow*. Springer Science & Business Media.

Ishikawa, T., Guimaraes, L. F., Oshima, S. and Yamane, R. (1998). "Effect of Non-Newtonian Property of Blood On Flow Through a Stenosed Tube." *Fluid. Dyn. Res.*, 22(5), 251.

Johnston, B. M., Johnston, P. R., Corney, S. and Kilpatrick, D. (2004). "Non-Newtonian Blood Flow in Human Right Coronary Arteries: Steady State Simulations." *J. Biomech.*, 37(5), 709-720.

Jung, J. and A. Hassanein (2008). "Three-Phase CFD Analytical Modeling of Blood Flow." *Med. Eng. Phys.*, 30(1), 91-103.

Jung, J., Hassanein, A. and Lyczkowski, R. W. (2006b). "Hemodynamic Computation Using Multiphase Flow Dynamics in A Right Coronary Artery." *Ann. Biomed. Eng.*, 34(3), 393-407.

Jung, J., Lyczkowski, R.W., Panchal, C.B. and Hassanein, A. (2006a). "Multiphase Hemodynamic Simulation of Pulsatile Flow in A Coronary Artery." *J. Biomech.*, 39, 2064-2073.

- Karino, T. and H. L. Goldsmith (1977). "Flow Behavior of Blood-Cells and Rigid Spheres in an Annular Vortex." *Philos. Trans. R. Soc. London. B. Biol. Sci.*, 279(967), 415-445.
- Karnis, A., Goldsmith, H. L. and Mason, S. G. (1966). "The Kinetics of Flowing Dispersions: I. Concentrated Suspensions of Rigid Particles." *J. Colloid. Interface. Sci.*, 22(6), 531-553.
- Kastrati, A., Mehilli, J., Dirschinger, J., Pache, J., Ulm, K., Schühlen, H. and Schömig, A. (2001b). "Restenosis After Coronary Placement of Various Stent Types." *Am. J. Cardiol.*, 87(1), 34-39.
- Kizilova, N. N., Logvenkov, S. A. and Stein, A. A. (2012). "Mathematical Modeling of Transport-Growth Processes in Multiphase Biological Continua." *Fluid. Dynam.*, 47(1), 1-9.
- Kleinstreuer, C., Hyun, S., Buchanan, J. R., Longest, P. W., Archie Jr, J. P. and Truskey, G. A. (2001). "Hemodynamic Parameters and Early Intimal Thickening in Branching Blood Vessels." *Crit. Rev. Biomed. Eng.*, 29(1), 1-64.
- Koh, C. J., Hookham, P. and Leal, L. G. (1994). "An Experimental Investigation of Concentrated Suspension Flows in A Rectangular Channel." *J. Fluid. Mech.*, 266, 1-32.
- Kohler, T. R., Kirkman, T. R., Kraiss, L. W., Zierler, B. K. and Clowes, A. W. (1991). "Increased Blood Flow Inhibits Neointimal Hyperplasia in Endothelialized Vascular Grafts." *Circ. Res.*, 69(6), 1557-1565.
- Kojima, M., Irie, K., Ikeda, S., Fukuda, T., Arai, F., Hirose, Y. and Negoro, M. (2012). "The Hemodynamic Study for Growth Factor Evaluation of Rupture Cerebral Aneurysm Followed Up for Five Years." *J. Biomed. Sci. Eng.*, 5(12), 884.
- Krieger, I. M. (1972). "Rheology of Monodisperse Lattices." *Adv. Colloid. Interface. Sci.*, 3, 111-136.

Krishnan, J. M. (2010). *Rheology of Complex Fluids*. A. P. Deshpande, & P. S. Kumar (Eds.). Springer.

Ku, D. N. (1997). "Blood Flow in Arteries." *Annu. Rev. Fluid. Mech.*, 29(1), 399-434.

Ku, D. N., Giddens, D. P., Zarins, C. K. and Glagov, S. (1985). "Pulsatile Flow and Atherosclerosis in The Human Carotid Bifurcation. Positive Correlation Between Plaque Location and Low Oscillating Shear Stress." *Arterioscler. Thromb. Vasc. Biol.*, 5(3), 293-302.

LaDisa Jr, J. F., Olson, L. E., Guler, I., Hettrick, D. A., Kersten, J. R., Warltier, D. C. and Pagel, P. S. (2005a). "Circumferential Vascular Deformation After Stent Implantation Alters Wall Shear Stress Evaluated with Time-Dependent 3D Computational Fluid Dynamics Models." *J. Appl. Physiol.*, 98(3), 947-957.

LaDisa Jr, J. F., Olson, L. E., Molthen, R. C., Hettrick, D. A., Pratt, P. F., Hardel, M. D. and Pagel, P. S. (2005b). "Alterations in Wall Shear Stress Predict Sites of Neointimal Hyperplasia After Stent Implantation in Rabbit Iliac Arteries." *Am. J. Physiol. Heart. Circ. Physiol.*, 288(5), H2465-H2475.

Lansman, J. B. (1988). "Endothelial Mechanosensors." *Going with the flow. News and Views.*, 331, 481-482.

Lee, S. W., Antiga, L. and Steinman, D. A. (2009). "Correlations Among Indicators of Disturbed Flow at The Normal Carotid Bifurcation." *J. Biomech. Eng.*, 131(6), 061013.

Leighton, D. and Acrivos, A. (1986). "Viscous Resuspension." *Chem. Eng. Sci.*, 41(6), 1377-1384.

Leighton, D. and Acrivos, A. (1987a). "The Shear-Induced Migration of Particles in Concentrated Suspensions." *J. Fluid. Mech.*, 181, 415-439.

Leighton, D. and Acrivos, A. (1987b). "Measurement of Shear-Induced Self-Diffusion in Concentrated Suspensions of Spheres." *J. Fluid. Mech.*, 177, 109-131.

Levesque, M. J., Nerem, R. M. and Sprague, E. A. (1990). "Vascular Endothelial Cell Proliferation in Culture and The Influence of Flow." *Biomaterials.*, 11(9), 702-707.

Levick, J. R. (2003). *An Introduction to Cardiovascular Physiology*. London, Arnold.

Li, G., Hu, R. and Gao, F. (2015). "Numerical Simulation of Coronary Artery Stenosis Before and After Stenting." *J. Med. Biol. Eng.*, 35(4), 528-534.

Li, Y., Shen, C., Ji, Y., Feng, Y., Ma, G. and Liu, N. (2011). "Clinical Implication of Coronary Tortuosity in Patients with Coronary Artery Disease." *PloS one.*, 6(8), e24232.

Li, Y., Shi, Z., Cai, Y., Feng, Y., Ma, G., Shen, C. and Liu, N. (2012). "Impact of Coronary Tortuosity On Coronary Pressure: Numerical Simulation Study." *PloS one.*, 7(8), e42558.

Lima, R., Ishikawa, T., Imai, Y., Takeda, M., Wada, S. and Yamaguchi, T. (2008). "Radial Dispersion of Red Blood Cells in Blood Flowing Through Glass Capillaries: The Role of Hematocrit and Geometry." *J. Biomech.*, 41(10), 2188-2196.

Liu, Q., Mirc, D. and Fu, B. M. (2008). "Mechanical Mechanisms of Thrombosis in Intact Bent Microvessels of Rat Mesentery." *J. Biomech.*, 41(12), 2726-2734.

Liu, X., Fan, Y., Xu, X. Y. and Deng, X. (2012). "Nitric Oxide Transport in an Axisymmetric Stenosis." *J. Royal. Soc. Interface.*, 9(75), 2468-2478.

Longest, P. W. and Kleinstreuer, C. (2003a). "Comparison of Blood Particle Deposition Models for Non-Parallel Flow Domains." *J. Biomech.*, 36(3), 421-430.

Longest, P. W. and Kleinstreuer, C. (2003b). "Numerical Simulation of Wall Shear Stress Conditions and Platelet Localization in Realistic End-To-Side Arterial Anastomoses." *J. Biomech. Eng.*, 125(5), 671-681.

Longest, P. W., Kleinstreuer, C. and Buchanan, J. R. (2004). "Efficient Computation of Micro-Particle Dynamics Including Wall Effects." *Comput. Fluids.*, 33(4), 577-601.

Loscalzo, J. and Schafer, A. I. (Eds.). (2003). *Thrombosis and Hemorrhage*. Lippincott Williams & Wilkins. Philadelphia.

Lowe, G. D. O., Fowkes, F. G. R., Dawes, J., Donnan, P. T., Lennie, S. E. and Housley, E. (1993). "Blood Viscosity, Fibrinogen, and Activation of Coagulation and Leukocytes in Peripheral Arterial Disease and The Normal Population in The Edinburgh Artery Study." *Circulation.*, 87(6), 1915-1920.

Lyon, M. K. and Leal, L. G. (1998). "An Experimental Study of the Motion of Concentrated Suspensions in Two-Dimensional Channel Flow. Part 1. Monodisperse Systems." *J. Fluid. Mech.*, 363, 25-56.

Mahalingam, A., Gawandalkar, U. U., Kini, G., Buradi, A., Araki, T., Ikeda, N. and Suri, J. S. (2016). "Numerical Analysis of the Effect of Turbulence Transition On the Hemodynamic Parameters in Human Coronary Arteries." *Cardiovasc. Diagn. Ther.*, 6(3), 208.

Malek, A. M., Alper, S. L. and Izumo, S. (1999). "Hemodynamic Shear Stress and Its Role in Atherosclerosis." *Jama.*, 282(21), 2035-2042.

Manninen, M., Taivassalo, V. and Kallio, S. (1996). *On The Mixture Model for Multiphase Flow*. VTT Publications, Technical Research Centre of Finland

Mansour, M. H., Bressloff, N. W. and Shearman, C. P. (2010). "Red Blood Cell Migration in Microvessels." *Biorheology.*, 47(1), 73-93.

Markl, M., Bredecke, S. M., Simon, J., Barker, A. J., Weiller, C. and Harloff, A. (2013). "Co-Registration of the Distribution of Wall Shear Stress and 140 Complex Plaques of the Aorta." *J. Magn. Reson. Imaging.*, 31(7), 1156-1162.

Massoudi, M. (2002). "On The Importance of Material Frame-Indifference and Lift Forces in Multiphase Flows." *Chem. Eng. Sci.*, 57(17), 3687-3701.

Massoudi, M. (2008). "A Note On the Meaning of Mixture Viscosity Using the Classical Continuum Theories of Mixtures." *Int. J. Eng. Sci.*, 46(7), 677-689.

- Massoudi, M. (2010). "A Mixture Theory Formulation for Hydraulic or Pneumatic Transport of Solid Particles." *Int. J. Eng. Sci.*, 48(11), 1440-1461.
- Massoudi, M. and Antaki, J. F. (2008). "An Anisotropic Constitutive Equation for The Stress Tensor of Blood Based On Mixture Theory." *Math. Probl. Eng.*, 1-30.
- Massoudi, M., Kim, J. and Antaki, J. F. (2012). "Modeling and Numerical Simulation of Blood Flow Using the Theory of Interacting Continua." *Int. J. Nonlinear. Mech.*, 47(5), 506-520.
- Mesri, Y., Niazmand, H. and Deyranlou, A. (2017). "Numerical Study on Fluid-Structure Interaction in a Patient-Specific Abdominal Aortic Aneurysm for Evaluating Wall Heterogeneity and Material Model Effects on its Rupture." *J. Appl. Fluid. Mech.*, 10(6), 1699-1709.
- Miller, R. M. and Morris, J. F. (2006). "Normal Stress-Driven Migration and Axial Development in Pressure-Driven Flow of Concentrated Suspensions." *J. Nonnewton. Fluid. Mech.*, 135(2-3), 149-165.
- Miller, R. M., Singh, J. P. and Morris, J. F. (2009). "Suspension Flow Modeling for General Geometries." *Chem. Eng. Sci.*, 64(22), 4597-4610.
- Mondy, J. S., Lindner, V., Miyashiro, J. K., Berk, B. C., Dean, R. H. and Geary, R. L. (1997). "Platelet-Derived Growth Factor Ligand and Receptor Expression in Response to Altered Blood Flow in Vivo." *Circ. Res.*, 81(3), 320-327.
- Moore Jr, J. E., Xu, C., Glagov, S., Zarins, C. K. and Ku, D. N. (1994). "Fluid Wall Shear Stress Measurements in A Model of the Human Abdominal Aorta: Oscillatory Behavior and Relationship to Atherosclerosis." *Atherosclerosis.*, 110(2), 225-240.
- Moore, J. A. and Ethier, C. R. (1997). "Oxygen Mass Transfer Calculations in Large Arteries." *J. Biomech. Eng.*, 119(4), 469-475.

Murphy, J. and Boyle, F. (2010). "Predicting Neointimal Hyperplasia in Stented Arteries Using Time-Dependent Computational Fluid Dynamics: A Review." *Comput. Biol. Med.*, 40(4), 408-418.

Myers, J. G., Moore, J. A., Ojha, M., Johnston, K. W. and Ethier, C. R. (2001). "Factors Influencing Blood Flow Patterns in The Human Right Coronary Artery." *Ann. Biomed. Eng.*, 29(2), 109-120.

Nagel, T., Resnick, N., Dewey Jr, C. F. and Gimbrone Jr, M. A. (1999). "Vascular Endothelial Cells Respond to Spatial Gradients in Fluid Shear Stress by Enhanced Activation of Transcription Factors." *Arterioscler. Thromb. Vasc. Biol.*, 19(8), 1825-1834.

National Heart, Lung, and Blood Institute (NHLB). (2011) "What Is Atherosclerosis." <http://www.nhlbi.nih.gov/health/health-topics/topics/atherosclerosis/>,

Neofytou, P. (2004). "Comparison of Blood Rheological Models for Physiological Flow Simulation." *Biorheology.*, 41(6), 693-714.

Neofytou, P. and Drikakis, D. (2003). "Non-Newtonian Flow Instability in A Channel with A Sudden Expansion." *J. Nonnewton. Fluid. Mech.*, 111(2-3), 127-150.

Nerem, R. M. (1992). "Vascular Fluid Mechanics, The Arterial Wall, And Atherosclerosis." *J. Biomech. Eng.*, 114(3), 274-282.

Nerem, R.M. (1993). "Hemodynamics and The Vascular Endothelium." *J. Biomech. Eng.*, 115, 510-514.

Nichols, W. W. and M. F. O'Rourke (2005). *McDonald's Blood Flow in Arteries*. Hodder Arnold.

Nosovitsky, V. A., Ilegbusi, O. J., Jiang, J., Stone, P. H. and Feldman, C. L. (1997). "Effects of Curvature and Stenosis-Like Narrowing On Wall Shear Stress in A Coronary Artery Model with Phasic Flow." *Comput. Biomed. Res.*, 30(1), 61-82.

Nott, P. R. and Brady, J. F. (1994). "Pressure-Driven Flow of Suspensions: Simulation and Theory." *J. Fluid. Mech.*, 275, 157-199.

O'Callaghan, S., Walsh, M. and McGloughlin, T. (2006). "Numerical Modelling of Newtonian and Non-Newtonian Representation of Blood in A Distal End-To-Side Vascular Bypass Graft Anastomosis." *Med. Eng. Phys.*, 28(1), 70-74.

Ojha, M. (1994). "Wall Shear Stress Temporal Gradient and Anastomotic Intimal Hyperplasia." *Circ. Res.*, 74(6), 1227-1231.

Oka, S. (1981). *Cardiovascular Hemorheology*. CUP Archive.

Pal, R. (2003). "Rheology of Concentrated Suspensions of Deformable Elastic Particles Such as Human Erythrocytes." *J. Biomech.*, 36(7), 981-989.

Papaioannou, T. G. and Stefanadis, C. (2005). "Vascular Wall Shear Stress: Basic Principles and Methods." *Hellenic. J. Cardiol.*, 46(1), 9-15.

Papanastasiou, T. C. (1987). "Flows of Materials with Yield." *J. Rheol.*, 31(5), 385-404.

Patrick, M. J., Chen, C. Y., Frakes, D. H., Dur, O. and Pekkan, K. (2011). "Cellular-Level Near-wall Unsteadiness of High-Hematocrit Erythrocyte Flow Using Confocal μ PIV." *Exp. Fluids.*, 50(4), 887-904.

Peiffer, V., Sherwin, S. J. and Weinberg, P. D. (2013). "Does Low and Oscillatory Wall Shear Stress Correlate Spatially with Early Atherosclerosis? A Systematic Review." *Cardiovasc Res.*, 99(2), 242-250.

Phillips, R. J., Armstrong, R. C., Brown, R. A., Graham, A. L. and Abbott, J. R. (1992). "A Constitutive Equation for Concentrated Suspensions That Accounts for Shear-Induced Particle Migration." *Phys. Fluids. A: Fluid Dynamics.*, 4(1), 30-40.

Pohl, U., Holtz, J., Busse, R. and Bassenge, E. (1986). "Crucial Role of Endothelium in The Vasodilator Response to Increased Flow in Vivo." *Hypertension.*, 8(1), 37-44.

Pries, A. R., Neuhaus, D. and Gaehtgens, P. (1992). "Blood Viscosity in Tube Flow: Dependence On Diameter and Hematocrit." *Am. J. Physiol. Heart. Circ. Physiol.*, 263(6), H1770-H1778.

Qiao, A. K., Guo, X. L., Wu, S. G., Zeng, Y. J. and Xu, X. H. (2004). "Numerical Study of Nonlinear Pulsatile Flow in S-Shaped Curved Arteries." *Med. Eng. Phys.*, 26(7), 545-552.

Quemada, D. (1977). "Rheology of Concentrated Disperse Systems and Minimum Energy Dissipation Principle." *Rheol. Acta.*, 16(1), 82-94.

Quemada, D. (1978). "Rheology of Concentrated Disperse Systems II. A Model for Non-Newtonian Shear Viscosity in Steady Flows." *Rheol. Acta.*, 17(6), 632-642.

Quemada, D. (1981). "A Rheological Model for Studying the Hematocrit Dependence of Red Cell-Red Cell and Red Cell-Protein Interactions in Blood." *Biorheology.*, 18(3-6), 501-516.

Rabby, M. G., Shupti, S. P., & Molla, M. (2014). Pulsatile non-Newtonian laminar blood flows through arterial double stenoses. *Journal of Fluids*, 2014.

Rajagopal, K. R. (2007). "On A Hierarchy of Approximate Models for Flows of Incompressible Fluids Through Porous Solids." *Math. Models. Methods. Appl. Sci.*, 17(02), 215-252.

Rajagopal, K. R. and Tao, L. (1995). "Mechanics of Mixtures." *Series on Advances in Mathematics for Applied Sciences*, vol. 35. *World Scientific, Singapore*.

Rajagopal, K. R., Troy, W. and Massoudi, M. (1992). "Existence of Solutions to The Equations Governing the Flow of Granular Materials." *Eur. J. Mech. B/Fluids.*, 11(3), 265-276.

Ramstack, J. M., Zuckerman, L. and Mockros, L. F. (1979). "Shear-Induced Activation of Platelets." *J. Biomech.*, 12(2), 113-125.

- Razavi, A., Shirani, E. and Sadeghi, M. R. (2011). "Numerical Simulation of Blood Pulsatile Flow in A Stenosed Carotid Artery Using Different Rheological Models." *J. Biomech.*, 44(11), 2021-2030.
- Reddy, M. M. and Singh, A. (2014). "Flow of Concentrated Suspension Through Oblique Bifurcating Channels." *AIChE. Journal.*, 60(7), 2692-2704.
- Reinke, W., Gaehtgens, P. and Johnson, P. C. (1987). "Blood Viscosity in Small Tubes: Effect of Shear Rate, Aggregation, And Sedimentation." *Am. J. Physiol. Heart. Circ. Physiol.*, 253(3), H540-H547.
- Ren, X., Qiao, A., Song, H., Song, G. and Jiao, L. (2016). "Influence of Bifurcation Angle on In-Stent Restenosis at the Vertebral Artery Origin: A Simulation Study of Hemodynamics." *J. Med. Biol. Eng.*, 36(4), 555-562.
- Rikhtegar, F., Knight, J. A., Olgac, U., Saur, S. C., Poulikakos, D., Marshall Jr, W. and Kurtcuoglu, V. (2012). "Choosing The Optimal Wall Shear Parameter for The Prediction of Plaque Location-A Patient-Specific Computational Study in Human Left Coronary Arteries." *Atherosclerosis.*, 221(2), 432-437.
- Ross, R. and Glomset, J. A. (1976). "The Pathogenesis of Atherosclerosis." *N. Engl. J. Med.*, 295(7), 369-377.
- Ryou, H. S., Kim, S., Kim, S. W. and Cho, S. W. (2012). "Construction of Healthy Arteries Using Computed Tomography and Virtual Histology Intravascular Ultrasound." *J. Biomech.*, 45(9), 1612-1618.
- Samady, H., Eshtehardi, P., McDaniel, M. C., Suo, J., Dhawan, S. S., Maynard, C. and Giddens, D. P. (2011). "Coronary Artery Wall Shear Stress Is Associated with Progression and Transformation of Atherosclerotic Plaque and Arterial Remodeling in Patients with Coronary Artery Disease." *Circulation.*, 124(7), 779-788.

Sankar, D. S. and Lee, U. (2010). "Two-Fluid Casson Model for Pulsatile Blood Flow Through Stenosed Arteries: A Theoretical Model." *Commun. Nonlinear. Sci. Numer. Simul.*, 15(8), 2086-2097.

Sharan, M. and Popel, A. S. (2001). "A Two-Phase Model for Flow of Blood in Narrow Tubes with Increased Effective Viscosity Near the Wall." *Biorheology.*, 38(5, 6), 415-428.

Soulis, J. V., Lampri, O. P., Fytanidis, D. K. and Giannoglou, G. D. (2011). "Relative Residence Time and Oscillatory Shear Index of Non-Newtonian Flow Models in Aorta." *10th Int. Workshop on Biomed Eng, IEEE*, 1-4.

Stadler, A. A., Zilow, E. P. and Linderkamp, O. (1990). "Blood Viscosity and Optimal Hematocrit in Narrow Tubes." *Biorheology.*, 27(5), 779-788.

Steinman, D. A. (2002). "Image-Based Computational Fluid Dynamics Modeling in Realistic Arterial Geometries." *Ann. Biomed. Eng.*, 30(4), 483-497.

Stone, P. H., Coskun, A. U., Kinlay, S., Clark, M. E., Sonka, M., Wahle, A. and Kuntz, R. E. (2003a). "Effect of Endothelial Shear Stress On the Progression of Coronary Artery Disease, Vascular Remodeling, And In-Stent Restenosis in Humans: In Vivo 6-Month Follow-Up Study." *Circulation.*, 108(4), 438-444.

Stone, P. H., Coskun, A. U., Yeghiazarians, Y., Kinlay, S., Popma, J. J., Kuntz, R. E. and Feldman, C. L. (2003b). "Prediction of Sites of Coronary Atherosclerosis Progression: In Vivo Profiling of Endothelial Shear Stress, Lumen, And Outer Vessel Wall Characteristics to Predict Vascular Behavior." *Curr. Opin. Cardiol.*, 18(6), 458-470.

Stone, P. H., Saito, S., Takahashi, S., Makita, Y., Nakamura, S., Kawasaki, T. and Hirohata, A. (2012). "Prediction of Progression of Coronary Artery Disease and Clinical Outcomes Using Vascular Profiling of Endothelial Shear Stress and Arterial Plaque Characteristics: The Prediction Study." *Circulation.*, 112(126), 172-181.

Stroev, P. V., Hoskins, P. R. and Eason, W. J. (2007). "Distribution of Wall Shear Rate Throughout the Arterial Tree: A Case Study." *Atherosclerosis.*, 191(2), 276-280.

Suess, T., Anderson, J., Danielson, L., Pohlson, K., Remund, T., Blears, E. and Kelly, P. (2016). "Examination of Near-Wall Hemodynamic Parameters in The Renal Bridging Stent of Various Stent Graft Configurations for Repairing Visceral Branched Aortic Aneurysms." *J. Vasc. Surg.*, 64(3), 788-796.

Sugiyama, S. I., Niizuma, K., Nakayama, T., Shimizu, H., Endo, H., Inoue, T. and Tominaga, T. (2013). "Relative Residence Time Prolongation in Intracranial Aneurysms: A Possible Association with Atherosclerosis." *Neurosurg.*, 73(5), 767-776.

Takabe, W., Jen, N., Ai, L., Hamilton, R., Wang, S., Holmes, K. and Li, R. (2011). "Oscillatory Shear Stress Induces Mitochondrial Superoxide Production: Implication of NADPH Oxidase and C-Jun NH₂-Terminal Kinase Signaling." *Antioxid. Redox. Signal.*, 15(5), 1379-1388.

Tang, A. Y. S., Chung, W. C., Liu, E. T. Y., Qu, J. Q., Tsang, A. C. O., Leung, G. K. K. and Chow, K. W. (2015). "Computational Fluid Dynamics Study of Bifurcation Aneurysms Treated with Pipeline Embolization Device: Side Branch Diameter Study." *J. Med. Biol. Eng.*, 35(3), 293-304.

Tarbell, J. M. (2003). "Mass Transport in Arteries and The Localization of Atherosclerosis." *Annu. Rev. Biomed. Eng.*, 5(1), 79-118.

Tardy, Y., Resnick, N., Nagel, T., Gimbrone Jr, M. A. and Dewey Jr, C. F. (1997). "Shear Stress Gradients Remodel Endothelial Monolayers in Vitro Via a Cell Proliferation-Migration-Loss Cycle." *Arterioscler. Thromb. Vasc. Biol.*, 17(11), 3102-3106.

Thurston, C. B. (1994). "Non-Newtonian Viscosity of Human Blood: Flow-Induced Changes in Microstructure." *Biorheology.*, 31(2), 179-192.

Thurston, G. B. (1979). "Rheological Parameters for The Viscosity Viscoelasticity and Thixotropy of Blood." *Biorheology.*, 16(3), 149-162.

Thury, A., Wentzel, J. J., Vinke, R. V., Gijssen, F. J., Schuurbiers, J. C., Krams, R. and Slager, C. J. (2002). "Focal In-Stent Restenosis Near Step-Up." *Circulation.*, 105(23), e185-e187.

Topper, J. N., Cai, J., Falb, D. and Gimbrone, M. A. (1996). "Identification of Vascular Endothelial Genes Differentially Responsive to Fluid Mechanical Stimuli: Cyclooxygenase-2, Manganese Superoxide Dismutase, And Endothelial Cell Nitric Oxide Synthase Are Selectively Up-Regulated by Steady Laminar Shear Stress." *Proc. Natl. Acad. Sci.*, 93(19), 10417-10422.

Torii, R., Wood, N. B., Hadjiloizou, N., Dowsey, A. W., Wright, A. R., Hughes, A. D. and Thom, S. A. M. (2009). "Fluid–Structure Interaction Analysis of a Patient-Specific Right Coronary Artery with Physiological Velocity and Pressure Waveforms." *Commun. Numer. Meth. En.*, 25(5), 565-580.

Traub, O. and Berk, B. C. (1998). "Laminar Shear Stress: Mechanisms by Which Endothelial Cells Transduce an Atheroprotective Force." *Arterioscler. Thromb. Vasc. Biol.*, 18(5), 677-685.

Truesdell, C. (1984). *Thermodynamics of Diffusion*. In *Rational Thermodynamics*. Springer, New York, NY., 219-236.

Van Weert, K. (1996). "Numerical and Experimental Analysis of Shear-Induced Migration in Suspension Flow." Report no. WFW, 96, Master thesis, Eindhoven University of Technology (EUT), Eindhoven, Netherlands.

Vlachopoulos, C., O'Rourke, M. and Nichols, W. W. (2011). *McDonald's Blood Flow in Arteries: Theoretical, Experimental and Clinical Principles*. CRC press.

Vorobtsova, N., Chiastra, C., Stremmer, M. A., Sane, D. C., Migliavacca, F. and Vlachos, P. (2016). "Effects of Vessel Tortuosity On Coronary Hemodynamics: An

Idealized and Patient-Specific Computational Study.” *Ann. Biomed. Eng.*, 44(7), 2228-2239.

Walburn, F. J. and Schneck, D. J. (1976). “A Constitutive Equation for Whole Human Blood.” *Biorheology.*, 13(3), 201-210.

Wang, K., Zhou, X. R., Verbeken, E., Ping, Q. B., Yanming, H., Jianhua, H. and De Scheerder, I. (2000b). “Overlapping Coronary Stents Result in an Increased Neointimal Hyperplasia: Insight from A Porcine Coronary Stent Model.” *J. Interv. Cardiol.*, 13(3), 173-177.

Wells, R. E. and E. W. Merrill (1962). “Influence of Flow Properties of Blood Upon Viscosity-Hematocrit Relationships.” *J. Clin. Invest.*, 41(8), 1591-1598.

Wentzel, J. J., Gijssen, F. J., Stergiopoulos, N., Serruys, P. W., Slager, C. J. and Krams, R. (2003). “Shear Stress, Vascular Remodeling and Neointimal Formation.” *J. Biomech.*, 36(5), 681-688.

White, C. R., Haidekker, M., Bao, X. and Frangos, J. A. (2001). “Temporal Gradients in Shear, But Not Spatial Gradients, Stimulate Endothelial Cell Proliferation.” *Circulation.*, 103(20), 2508-2513.

Wilson, G. J., Polovick, J. E., Huibregtse, B. A. and Poff, B. C. (2007). “Overlapping Paclitaxel-Eluting Stents: Long-Term Effects in A Porcine Coronary Artery Model.” *Cardiovasc. Res.*, 76(2), 361-372.

Wolberg, A. S., Aleman, M. M., Leiderman, K. and Machlus, K. R. (2012). “Procoagulant Activity in Hemostasis and Thrombosis: Virchow’s Triad Revisited.” *Anesth Analg.*, 114(2), 275-285.

World Health Organization (WHO). (2016). Cardiovascular Disease. https://www.who.int/cardiovascular_diseases/en/,

Wu, W. T., Aubry, N. and Massoudi, M. (2014b). "On The Coefficients of the Interaction Forces in A Two-Phase Flow of a Fluid Infused with Particles." *Int. J. Nonlinear. Mech.*, 59, 76-82.

Wu, W. T., Aubry, N., Massoudi, M., Kim, J. and Antaki, J. F. (2014a). "A Numerical Study of Blood Flow Using Mixture Theory." *Int. J. Eng. Sci.*, 76, 56-72.

Xie, X., Wang, Y. and Zhou, H. (2013a). "Impact of Coronary Tortuosity On the Coronary Blood Flow: A 3D Computational Study." *J. Biomech.*, 46(11), 1833-1841.

Xie, X., Wang, Y., Zhu, H. and Zhou, J. (2014). "Computation of Hemodynamics in Tortuous Left Coronary Artery: A Morphological Parametric Study." *J. Biomech. Eng.*, 136(10), 101006.

Xie, X., Wang, Y., Zhu, H. and Zhou, J. (2015). "Shear-Induced Platelet Activation in Tortuous Coronary Artery: A Numerical Study." *J. Mech. Med. Biol.*, 15(03), 1550031.

Xie, X., Wang, Y., Zhu, H., Zhou, H. and Zhou, J. (2013b). "Impact of Coronary Tortuosity On Coronary Blood Supply: A Patient-Specific Study." *PloS one.*, 8(5), e64564.

Yadav, S., Reddy, M. M. and Singh, A. (2015). "Shear-Induced Particle Migration in Three-Dimensional Bifurcation Channel." *Int. J. Multiph. Flow.*, 76, 1-12.

Yan, F., Jiang, W. T., Dong, R. Q., Wang, Q. Y., Fan, Y. B. and Zhang, M. (2017). "Blood Flow and Oxygen Transport in Descending Branch of Lateral Femoral Circumflex Arteries After Transfemoral Amputation: A Numerical Study." *J. Med. Biol. Eng.*, 37(1), 63-73.

Yang, L. I., Liu, N. F., Gu, Z. Z., Yong, C. H. E. N., Jun, L. U., Yi, F. E. N. G. and Shen, C. X. (2012). "Coronary Tortuosity Is Associated with Reversible Myocardial Perfusion Defects in Patients Without Coronary Artery Disease." *Chin. Med. J.*, 125(19), 3581-3583.

Zarins, C. K., Giddens, D. P., Bharadvaj, B. K., Sottiurai, V. S., Mabon, R. F. and Glagov, S. (1983). "Carotid Bifurcation Atherosclerosis. Quantitative Correlation of Plaque Localization with Flow Velocity Profiles and Wall Shear Stress." *Circ. Res.*, 53(4), 502-514.

Zarins, C. K., Zatina, M. A., Giddens, D. P., Ku, D. N. and Glagov, S. (1987). "Shear Stress Regulation of Artery Lumen Diameter in Experimental Atherogenesis." *J. Vasc. Surg.*, 5(3), 413-420.

Zegers, E. S., Meursing, B. T. J., Zegers, E. B. and Ophuis, A. O. (2007). "Coronary Tortuosity: A Long and Winding Road." *Neth. Heart. J.*, 15(5), 191-195.

Zeng, D., Ding, Z., Friedman, M. H. and Ethier, C. R. (2003). "Effects of Cardiac Motion On Right Coronary Artery Hemodynamics." *Ann. Biomed. Eng.*, 31(4), 420-429.

Zhang, J. M., Chua, L. P., Ghista, D. N., Yu, S. C. M. and Tan, Y. S. (2008). "Numerical Investigation and Identification of Susceptible Sites of Atherosclerotic Lesion Formation in A Complete Coronary Artery Bypass Model." *Med. Biol. Eng. Comput.*, 46(7), 689-699.

Zhang, J., Johnson, P. C. and Popel, A. S. (2009). "Effects of Erythrocyte Deformability and Aggregation On the Cell Free Layer and Apparent Viscosity of Microscopic Blood Flows." *Microvasc Res.*, 77(3), 265-272.

Zhao, H. and Shaqfeh, E. S. (2011). "Shear-Induced Platelet Margination in A Microchannel." *Phys. Rev. E.*, 83(6), 061924.

Ziegler, T., Silacci, P., Harrison, V. J. and Hayoz, D. (1998). "Nitric Oxide Synthase Expression in Endothelial Cells Exposed to Mechanical Forces." *Hypertension.*, 32(2), 351-355.

NATIONAL INSTITUTE OF TECHNOLOGY KARNATAKA, SURATHKAL

List of Publications based on Ph.D. Research Work

Sl. No.	Title of the paper	Authors (in the same order as in the paper. Underline the Research Scholar's name)	Name of the Journal/ Conference, Vol., No., Pages, DOI	SCIE, SCOPUS Indexed	Month, Year of Publication	Category*
1	Effect of Stenosis Severity on Wall Shear Stress Based Hemodynamic Descriptors using Multiphase Mixture Theory	Abdulrajak Buradi and Arun Mahalingam	Journal of Applied Fluid Mechanics, 11(6), pp.1497-1509. DOI: 10.18869/acadpub.jafm.73.249.29062	SCIE, SCOPUS	November 2018	1
2	Effect of Stenosis Severity On Shear Induced Diffusion of Red Blood Cells in Coronary Arteries	Abdulrajak Buradi , Sumant Morab and Arun Mahalingam	Journal of Mechanics in Medicine and Biology, 19(5), p.1950034, DOI: 10.1142/S0219519419500349	SCIE, SCOPUS	July, 2019	1
3	Impact of Coronary Tortuosity on the Artery Hemodynamics	Abdulrajak Buradi and Arun Mahalingam	Biocybernetics and Biomedical Engineering DOI: 10.1016/j.bbe.2019.02.005	SCIE, SCOPUS	April, 2019	1
4	Numerical analysis of the effect of turbulence transition on the hemodynamic parameters in human coronary arteries	Mahalingam, Arun, Udhav Ulhas Gawandalkar, Girish Kini, Abdulrajak Buradi , Tadashi Araki, Nobutaka Ikeda, Andrew Nicolaides, John R. Laird, Luca Saba, and Jasjit S. Suri.	Cardiovascular Diagnosis and Therapy, 6(3), pp.208-220. DOI: 10.21037/cdt.2016.03.08	SCIE, SCOPUS, PubMed, PubMed Central	June 2016	1
5	Numerical Analysis of Wall Shear Stress Parameters of Newtonian Pulsatile Blood Flow Through Coronary Artery and Correlation to Atherosclerosis	Abdulrajak Buradi and Arun Mahalingam	Advances in Mechanical Engineering, Lecture Notes in Mechanical Engineering, Book Chapter, DOI: 10.1007/978-981-15-0124-1_12	SCOPUS	September 2019 (In Press)	5
6	Numerical Simulation of Pulsatile Blood Flow in an Idealized Curved Section of a Human Coronary Artery	Abdulrajak Buradi and Arun Mahalingam	International Journal of Mechanical and Production Engineering, Special Issue, pp. 15-19.	-	September 2016	1
7	Numerical Analysis of the Effect of Turbulence Transition on the Hemodynamic Parameters in Human Coronary Arteries	Abdulrajak Buradi , Arun Mahalingam and Jasjit S. Suri	42 nd National Conference on Fluid Mechanics and Fluid Power (FMFP-2015), NITK, Surathkal, Karnataka, India.	-	December 14-16, 2015	4

8	Pulsatile Laminar Newtonian Blood Flows through an Idealized Coronary Artery: A Numerical Hemodynamic Study	Abdulrajak Buradi and Arun Mahalingam	2 nd International Conference on Frontiers in Engineering, Applied Sciences and Technology (FEAST-2018), NIT , Trichy, Tamilnadu, India	-	April 27-28, 2018	3
9	Numerical Analysis of Wall Shear Stress Parameters of Newtonian Pulsatile Blood Flow Through Coronary Artery and Correlation to Atherosclerosis	Abdulrajak Buradi and Arun Mahalingam	International Conference on Recent Innovations and Developments in Mechanical Engineering (IC-RIDME-2018), NIT , Meghalaya, India	-	November 08-10, 2018	4
10	Numerical Analysis of Pulsatile Blood Flow Through an Idealized Axisymmetric Stenosis in Coronary Artery	Abdulrajak Buradi and Arun Mahalingam	7 th International and 45 th National Conference on Fluid Mechanics and Fluid Power (FMFP-2018), IIT , Bombay, Mumbai, Maharashtra, India.	-	December 10-12, 2018	3
11	Numerical Simulation of Pulsatile Newtonian Laminar Blood Flows through an Idealized Non-Stenosis Curved Coronary Artery: A Hemodynamic Study	Abdulrajak Buradi and Arun Mahalingam	International Conference on Recent Trends in Electrical Sciences and Medical Engineering (ICRTESME-2017), MIT , Manipal, Karnataka, India.	-	August 8-10, 2017	4
12	Hemodynamic Modelling of Pulsatile Newtonian Laminar Blood Flows through an Idealized Curved Coronary Artery: A Hemodynamic Study	Abdulrajak Buradi and Arun Mahalingam	4 th International Conference on Computational Methods in Engineering and Health Sciences (ICCMEH-2017), MIT , Manipal, Karnataka, India.	-	December 19-20, 2017	4
13	Numerical Simulation of Pulsatile Blood Flow in an Idealized Curved Section of a Human Coronary Artery	Abdulrajak Buradi and Arun Mahalingam	International Conference on Mechanical, Civil, Electronics & Communications and Computer Science Engineering (ICMCECE-2016), BTI , Bangalore, Karnataka, India.	-	April 23 rd , 2016	3

*Category: 1: Journal paper, full paper reviewed 2: Journal paper, Abstract reviews 3: Conference/Symposium paper, full paper reviewed
4: Conference/Symposium paper, abstract reviewed 5: Others (including papers in Workshops, NITK Research Bulletins, Short notes etc.)

Abdulrajak Buradi
Research Scholar
Name & Signature, with Date

Dr. Arun M
Research Guide
Name & Signature, with Date

BIODATA

Name: ABDULRAJAK BURADI

Date of Birth: 12-06-1987

Mobile No.: +91 9036268639

Email: arbnitk@gmail.com, aminburadi@gmail.com



ADDRESS:

S/o Moulasab A. Buradi, Konnur Post, Nargund Taluk, Gadag district, Karnataka State INDIA-582206.

EDUCATIONAL QUALIFICATION:

Qualification	Institute	University/Board	Year of Passing	% age /CGPA
PhD in Mechanical Engineering (Course work)	NITK Surathkal	NITK Surathkal	2015	7.25 CGPA
MTech in Thermal Power Engineering	BLDEA's VP Dr. PG Halakatti CET Vijaypur	VTU Belagavi	2013	70.62%
BE in Mechanical Engineering	BLDEA's VP Dr. PG Halakatti CET Vijaypur	VTU Belagavi	2009	65.06%
Diploma in Automobile Engineering	Govt. Polytechnic Vijaypur	DTE Bangalore	2006	73.72%
SSLC (10 th)	MDMR School Mulgund, Gadag	KSEEB Bangalore	2003	61.28%

EXPERIENCE:

Sr. No	Name of the college/Institute	Department	Designation	From	To
1.	Jain University, School of Engineering and Technology, Jakkasandra Post, Kanakapura Taluk, Ramanagara Dist.	Mechanical Engineering	Assistant Professor	July 2019	Till Date
2.	SECAB Institute of Engineering and Technology Vijaypur	Mechanical Engineering	Assistant Professor	July 2013	June 2014
3.	SECAB Institute of Engineering and Technology Vijaypur	Mechanical Engineering	Lecturer	October 2010	July 2011
4.	K.L.E. Society's Polytechnic Mahalingpur	Mechanical Engineering	Lecturer	June 2010	October 2010
5.	Government Polytechnic Rabkavi-Banhatti	Mechanical Engineering	Guest Lecturer	July 2009	May 2010

I hereby declare that above information is true and correct to best of my knowledge and belief.

Abdulrajak Buradi